5^{th} International Workshop on Functional and Nanostructured Materials

31 August – 6 September, 2008, L'viv, Ukraine

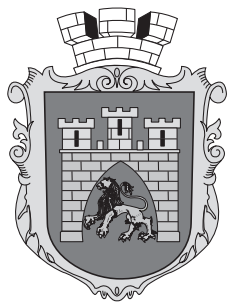

ABSTRACT BOOK

TITLE
5th International Workshop on Functional and Nanostructured Materials: Abstract Book

EDITOR
Jarosław Rybicki

TYPESETTING using TEX
BOP s.c., www.bop.com.pl

PRINTING
DP "Skhid Sontsya" TzOV "Splayn"
15 Dudaev Blvd., L'viv, Ukraine

TASK PUBLISHING 2008
GDANSK, POLAND

ISBN 978-83-908112-5-3

5th International Workshop
on Functional and Nanostructured Materials

31 August – 6 September, 2008, L'viv, Ukraine

ORGANIZED BY

Ivan Franko National University of L'viv, Ukraine

Mathematical Modelling Center of NAS of Ukraine

Karpenko Physico-Mechanical Institute of NAS of Ukraine

Academic Computer Centre TASK
Gdansk University of Technology, Poland

Department of Solid State Physics
Faculty of Technical Physics and Applied Mathematics
Gdansk University of Technology, Poland

University of Zielona Gora, Poland

Poznan Supercomputing and Networking Centre, Poland

Institute of Molecular Physics
Polish Academy of Sciences, Poland

IN COOPERATION WITH

INTEL Technology, Poland

COMMITTEES

Scientific Committee

Sir Sam Edwards (Cambridge, England) – Honorary Chairman
J. T. Devreese, (Antwerp, Belgium) – Honorary Chairman
G. J. Papadopoulos, (Athens, Greece) – Honorary Chairman

A. Di Cicco (Paris, France)
Yu. Feldman (Jerusalem, Israel)
S. Glenis (Athens, Greece)
M. Grinberg (Gdansk, Poland)
R. Gunnella (Camerino, Italy)
N. Guskos (Athens, Greece) – Chairman
W. G. Hoover (Livermore & UCD, CA, USA)
S. Kaczmarek (Szczecin, Poland)
T. Kanaya (Kyoto, Japan)
T. Klimczuk (Los Alamos NL, USA)
R. Lakes, (Wisconsin, USA)
V. Machulin (Kiev, Ukraine)
B. Maruszewski (Poznan, Poland)
S. Mudry (L'viv, Ukraine)
R. Reisfeld (Jerusalem, Israel)
J. Rybicki (Gdansk, Poland) – Co-Chairman
W. Sadowski (Gdansk, Poland)
J. Savula (L'viv, Ukraine)
A. Sherman (Tartu, Estonia)
A. Shpak (Kiev, Ukraine)
K. W. Wojciechowski, (Poznan, Poland) – Co-Chairman

Industrial Advisory Board

A. Banaszkiewicz (ALSTOM, Poland)
P. Gepner (INTEL Technology, Poland)

Organizing Committee

E. Chapla (L'viv, Ukraine)
M. Doerffer (Gdansk, Poland)
M. Dudek, (Zielona Gora, Poland) – Co-Chairman
M. Nakonieczny (Gdansk, Poland)
B. Padlyak (L'viv, Ukraine)
J. Rybicki (Gdansk, Poland) – Chairman
M. Stroiński (Poznan, Poland)
A. Torskiy (L'viv, Ukraine)

SPONSORS

Poznan Supercomputing
and Networking Centre,
Poznan, Poland

TASK Computer Centre
Gdansk, Poland

University of Zielona Gora
Zielona Gora, Poland

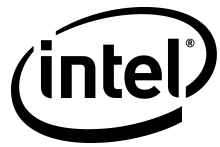

INTEL Technology Poland

CONTENTS

Lectures

Oral communications

Posters

In memoriam Andreas Papadopoulos

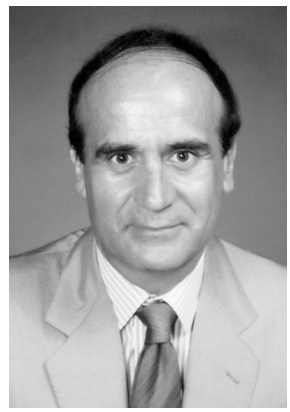

Andreas Papadopoulos (1934–2007) was born in Limassol, Cyprus. He studied Civil Engineering at Athens Polytechnic (Greece) and the University of Birmingham (UK).

Andreas was a highly respected civil servant working for the Cyprus Government. He served as an Operative Engineer for the Department of Public Works and was made Senior Operative Engineer for Port and Airport Works before reaching the position of Top Administrator for the Ministry of Public Transport and Works. In addition, he served as advisor to government officials and a representative of Cyprus on development issues at conferences abroad.

Andreas was a talented entrepreneur. He had the ability to take an idea and realise its business potential. He established Ypsonas Ltd in Cyprus which manufactures prefabricated concrete products.

Further to his business pursuits Andreas also had a vivid interest in philosophy and art being an active member of the Cyprus Philosophical Society and an enthusiastic and knowledgeable collector of art works as well as an amateur painter. He also had an interest in physical science and its historical evolution.

Andreas served as a member on the Advisory Board for the 4^{th} Conference on Functional and Nanostructured Materials, FNMA'07.

Andreas is survived by his wife Olga and two daughters, Eleni and Anna.

LECTURES

Monte Carlo Study of Complex Nanostructures in Sulfonated Block Copolymers

M. Banaszak

Institute of Physics, A. Mickiewicz University
Umultowska 85, 61-614 Poznan, Poland

Phase behavior of poly(styrenesulfonate-b-methylbutylene) (PSS-b-PMB) block copolymers has been recently studied by varying the molecular weight and the sulfonation level. In this study we perform Monte Carlo lattice simulations of model block copolymers with the corresponding microarchitectures. We show some thermodynamic and structural properties of the simulated copolymer melts, as the reduced dimensionless temperature is lowered. We identify the low-temperature nanostructures. In particular, we demonstrate that the symmetric PSS-b-PMB diblock self-assembles into a gyroid phase.

Propagation Technique for Ultrashort Pulses in a Nonlinear Medium

V. Cao Long

Institute of Physics, University of Zielona Góra
Podgórna 50, 65-246 Zielona Góra, Poland

In our presentation, we investigate the propagation of ultrashort laser pulses in dispersive nonlinear media. We derive a general propagation equation of pulses which includes linear and nonlinear effects to all orders. We study a specific case of Kerr media and obtain an ultrashort pulse propagation which is called the Generalized Nonlinear Schrodinger Equation. The impact of the third order dispersion, the higher-order nonlinear terms self-steepening and stimulated Raman scattering are explicitly analyzed. We also present a numerical technique to solve approximately the pulse propagation equation. Two efficient methods for this problem, the Split-Step Fourier and the fourth order Runge-Kutta methods are considered. Our numerical experiments are implemented for soliton propagation and interacting high order solitons. We also investigate numerically an important technique to create ultrashort pulses which is known as the pulse compression. The pulse splitting dynamics will be considered.

Magnetic-Elastic Coupling Dynamics in Ferromagnetic Resonance Experiment

M. R. Dudek[1], N. Guskos[2,3], M. Maryniak[3], R. Szymczak[4], J. Jóźwik[1], E. Senderek[5], Z. Rosłaniec[5]

[1] *Institute of Physics, University of Zielona Góra ul. Szafrana 4a, 65-069 Zielona Góra, Poland*

[2] *Solid State Physics Section, Department of Physics, University of Athens, Panepistimiopolis, 15 784 Athens, Greece*

[3] *Institute of Physics, Szczecin University of Technology Al. Piastów 17, 70-310 Szczecin, Poland*

[4] *Institut of Physics, Polish Academy of Sciences Al. Lotników 36/42, 02-668 Warsaw, Poland*

[5] *Institute of Materials Science and Engineering, Szczecin University of Technology Al. Piastów 17, 70-310 Szczecin, Poland*

A Ferromagnetic Resonance (FMR) spectrum of carbon coated magnetic nanoparticles in a non-magnetic elastic polymer matrix is investigated for a single cluster consisting of N magnetic nanoparticles. The Bloch law

$$M_s(T) = M_0(0)\left(1 - \left(\frac{T}{T_0}\right)^{\alpha}\right)$$

for the saturation magnetization of the magnetic nanoparticles is assumed, where T is temperature and $\alpha = 1/3$. The Arrhenius law for the viscosity parameter, ν,

$$\nu(T) = Ae^{E/kT}$$

of magnetic nanograins within a polymer matrix is also assumed, where E is the activation energy.

The experimental absorption data are compared with analogous data obtained with the help of the stochastic Landau-Lifshitz equation [1, 2] for the magnetic moment of a ferromagnetic single-domain nanoparticle and stochastic equations describing rotational oscillations of the polymer region containing a magnetic nanoparticle [3] We show that the absorption lines in the FMR experiment strongly depend on the direction of the magnetic easy axis with respect to the applied external DC magnetic field. A similar observation, but for fixed directions of the anisotropy axes, can be found in [4]. These results are discussed for different viscosities of the non-magnetic polymer matrix.

References

[1] L. Landau and E. Lifshitz, *Phys. Z. Sovjetunion* (1953) **8**, 153

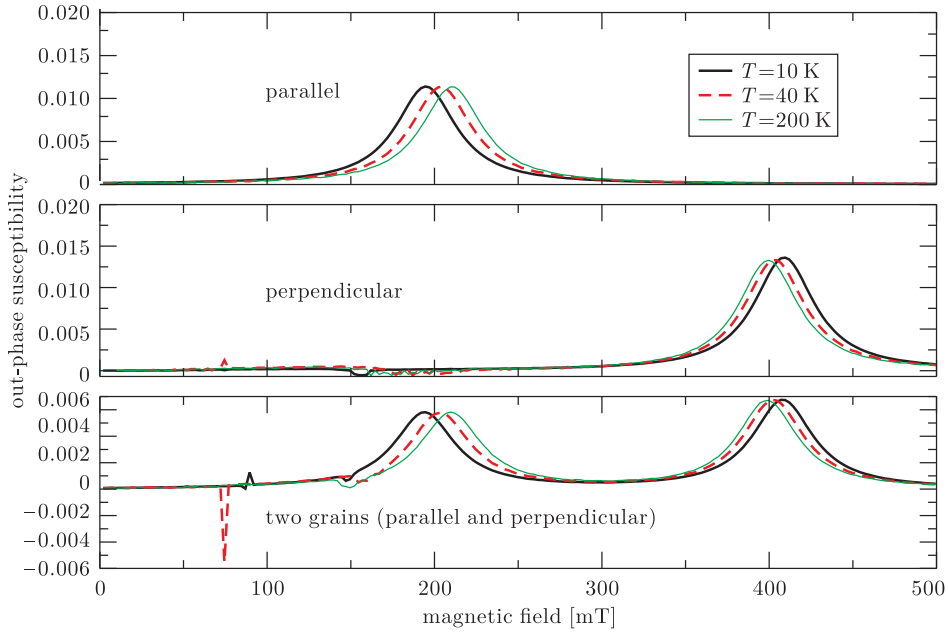

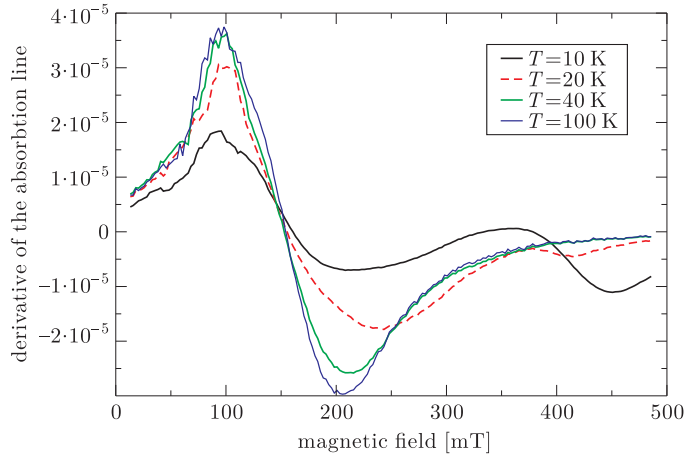

Figure 1: Top diagram: the effect of a different orientation of magnetic anisotropies with respect to the direction of the external DC magnetic field on the absorption lines; upper panel – a single magnetic nanoparticle with the anisotropy axis initially parallel to the DC magnetic field; middle panel – a single magnetic nanoparticle with the anisotropy axis initially perpendicular to the DC magnetic field, bottom panel – a cluster consisting of two magnetic nanoparticles (a) and (b). Bottom diagram: derivatives of the absorption lines, $d\chi''/dH_{\rm dc}$ for different temperatures; the results come from computer simulations.

[2] T. L. Gilbert, *Phys. Rev.* (1955) **100** 1243
[3] M. R. Dudek, N. Guskos, B. Grabiec, and M. Maryniak, to appear in *J. Non-Crystalline Solids* (2008)
[4] A. Sukhov, K. D. Usadel, U. Nowak, *JMMM* (2008) 320, 31–35

Combining Molecular Dynamics and Tight Binding to Study the Nanoindentation Process

J. Dziedzic[1a], J. Rybicki[1,2,3]

[1] *Faculty of Technical Physics and Applied Mathematics, Gdansk University of Technology*
Narutowicza 11/12, 80-952 Gdansk, Poland
[a] *jaca@kdm.task.gda.pl, 0048 58 3472095*

[2] *TASK Computer Centre, Gdansk University of Technology*
Narutowicza 11/12, 80-952 Gdansk, Poland

[3] *Institute of Mechatronics, Nanotechnology and Vacuum Techniques*
Koszalin University of Technology
Racławicka 15–17 F, 75-620 Koszalin, Poland

Nanoindentation and ultra-precision machining of metals belong to the class of technologically important processes which are difficult and costly to investigate experimentally [1, 2]. Because of this, they are often simulated numerically, typically employing the molecular-dynamics (MD) method (e.g. [3], in which the system is treated classically. However, substantial electronic effects involved in heavy bond-breaking and bond-reconstruction require the utilization of more involved, quantum-based methods such as density functional theory (DFT) or the tight-binding (TB) approximation. With these, however, the computational demand rises prohibitively as the number of atoms exceeds a few hundred.

For this reason, the so-called cross-scaling methods are developed, which aim to treat the important part of the system with a quantum-based method, and the remaining part with the cruder molecular-dynamics. Unfortunately, devising a physically sound interface between the two parts of the system is usually difficult, especially in the case of metallic systems. What is more, computer codes that allow for cross-scaling simulations are lacking.

We present a multiscale method targeted at non-equilibrium simulation of metals, in which the energetically active region is modelled using a robust TB scheme developed at the Naval Research Laboratory (NRL-TB) [4, 5] and the rest of the system is treated with MD employing (in this case) the Sutton-Chen many-body interaction potential.

Apart from the presentation of the method and implementation in computer code, we discuss the results of a series of simulations of nanoindentation of copper with an infinitely rigid tool, where the immediate region of contact between the tool and the workpiece is treated with the TB method. Stress fields, the nature of dislocations and the force experienced by the indenter are investigated.

Acknowledgements
The work has been sponsored by the Polish Ministry of Science and Information Technology, under grant number 3 T11F 026 29, and the Ministry of Science and

Higher Education, under grant number N519 019 31/3498. Our calculations were performed at the TASK Computer Centre (Gdansk, Poland).

References

[1] Komanduri R, Chandrasekaran N and Raff L 2000 *Wear* **242** 60
[2] da Silva EZ, da Silva AJ and Fazzio A 2001 *Phys. Rev. Lett.* **87** 256102
[3] Maekawa K, Itoh A 1995 *Wear* **188** 115–122
[4] Broughton JQ, Abraham FF, Bernstein N, Kaxiras E 1999 *Phys. Rev.* **B 60** 2391
[4] Kirchhoff F, Mehl M, Papanicolaou NI, Papaconstantopoulos D, Khan F 2001, *Phys. Rev.* **B 63** 195101

Negative Materials and Structures

J. N. Grima[a], R. Gatt, D. Attard, R. N. Cassar

Department of Chemistry, Faculty of Science, University of Malta,
Msida MSD 2080, Malta
[a]*joseph.grima@um.edu.mt*

Most materials we encounter tend to get thinner when stretched (i.e. exhibit a positive Poisson's ratio), expand when heated (i.e. exhibit a positive thermal expansion coefficient) or shrink in size when subjected to an increase in the external hydrostatic pressure (positive compressibility). Nevertheless, not all materials and structures behave like this and examples which defy such common expectations are known to exist: example the silicate α-cristobalite which gets fatter when stretched in various crystallographic directions (i.e. exhibits negative Poisson's ratio, or as commonly known 'auxetic behaviour'). Such negative systems are generally found to have various enhanced characteristics with the result of having many potential practical applications. For example, auxetics exhibit improved indentation resistance, enhanced acoustic properties, etc. which make them ideal for use as protective materials whilst NTE materials are very useful in applications involving the manufacture of composite materials which can be tailor made to exhibit pre-desired thermal expansion properties.

Here we discuss some of the recent developments in this field by discussing mechanisms which can lead to negative properties and how such systems behave under various pressure / stress / temperature conditions.

Acknowledgments
The financial support of the Malta Council of Science and Technology, the University of Malta and the Government of Malta is gratefully acknowledged.

Self-Assembly of Nanostructured Materials

B. A. Grzybowski

Dept. of Chemical and Biological Engineering and Dept. of Chemistry
Northwestern University
tel. 847.491.3024 or 847.491.3969, fax: 847.491.3728

Self-assembly of nanoscopic components into higher-order architectures defines the forefront of fundamental nanoscience research and is important for the development of new materials with potential applications in optoelectronics, high-density data storage, catalysis, and biological sensing. My talk will focus on how electrostatic and photoinduced dipole-dipole forces acting between nanoscale components can mediate their self-assembly into various superstructures. I will show how the interactions underlying self-assembly can be studied and understood in quantitative detail, and how they can be tailored to synthesize bulk materials exhibiting unusual optical, electrical and mechanical properties. Discussion of experimental results will be accompanied by theoretical analyses combining elements of thermodynamics, statistical and quantum mechanics, electrodynamics and elasticity.

References

[1] *Science* (2006) **312** 420
[2] *Science* (2007) **316** 261

Ion Beam Rubbed Poly(3hexil)thiophene Thin Films Grown by Electro-spray under Illumination Conditions

R. Gunnella, F. D'Amico[a], M. Abbas

Dipartimento di Fisica, CNISM, Università di Camerino
62032 Camerino (MC), Italy
[a]*francesco.damico@unicam.it*

Poly(3-hexyl)thiophene (P3HT) is one of the most used organic semiconductors in the photovoltaic field. The reasons can be found in its relatively high mobility and its ability to crystallize in a wide range of temperatures [1]. Recently a new procedure of polymer sample rubbing has been discovered and developed to increase the conjugation length in the rubbing direction with a consequent improvement of the conductivity in such a direction. It consists of low energy ion beam sputtering of the film surface. In order to understand how the rubbing influences the P3HT film characteristics we have performed a systematic study on P3HT samples prepared at room temperature (RT) and at 70°C by electro-spin coating. The samples were characterized with ultra-violet photoemission spectroscopy (UPS), UV-Visible absorption and photocurrent measurements. By the absorption and photocurrent measurements we discovered, as expected, an increase in the conjugation length along the rubbing direction. Moreover, variations in the photoconductivity current due to both local and global order effects of the P3HT film were observed.

In subsequent measurements the behavior of a rubbed P3HT sample under the illumination of a halogen lamp (in order to simulate sunlight) was analyzed. The purpose was to investigate the local order effects of the rubbing through the valence band spectra variation on different samples. The sample prepared at RT shows a reversible change of the ionization potential (IP) during the illumination (from 4.3 to 4.5 eV) accompanied by a homogeneous accumulation of negative localized charges on the whole sample. On the contrary, the sample prepared at 70°C shows the charge accumulation, but the ionization potential remains stable (about 4.8 eV). All these changes occur in a temporal scale of several minutes (time constant about 20 min).

For what regards the IP variation, a correlation between the negative charge accumulation in a polymer and the IP increase has been proved recently [4]. This result is particularly intriguing because it shows how the accumulation of a localized negative charge on the P3HT samples can modify the film properties when P3HT is exposed to illumination. This variation must be taken into account for proper modeling of a photovoltaic device.

References

[1] A. Salleo (2007) *Mat. Today* **10** 38-45

[2] M. Barmentlo, N. A. J. M. Van Aerle and R. W. J. Hollering (1993) *J. Appl. Phys.* **74** 3111-3120
[3] A. Bolognesi, C. Botta, C. Mercogliano, W. Porzio, P. C. Jukes, M. Geoghegan, M. Grell, M. Durell, D. Trolley, A. Das, and J. E. Macdonald (2004) *Polymer* **45** 4133-4138
[4] D. Sainova, S. Janietz, U. Asawapirom, L. Romaner, E. Zojer, N. Koch, A. Vollmer (2007) *Chem. Mater.* **19** 1472-1481

Photoacoustic Response of Sea Urchin Tissue

N. Guskos[1,2], J. Majszczyk[2], J. Typek[2], J. Rybicki[3],
A. Guskos[2], I. Kruk[2], C. Aidinis[4], G. Żołnierkiewicz[2]

[1] *Solid State Section, Department of Physics*
University of Athens, Panepistimiopolis
15 784 Zografos, Athens, Greece

[2] *Institute of Physics, Technical University of Szczecin*
Al. Piastów 17, 70-310 Szczecin, Poland

[3] *Department of Solid State Physics*
Faculty of Technical Physics and Applied Mathematics
Gdansk University of Technology
Narutowicza 11/12, 80-952 Gdansk, Poland

[4] *Applied Physics Section, Department of Physics, University of Athens*
Panepistimiopolis, 15 784 Zografos, Athens, Greece

A sea urchin tissue in the form of a thick film has been prepared for a photoacoustic (PA) study. Figure 1 presents a PA spectrum of a sea urchin. A broad absorption bands in the visible region (with a maximum near the yellow color, at about 570 nm) of the electromagnetic PA spectrum is registered.

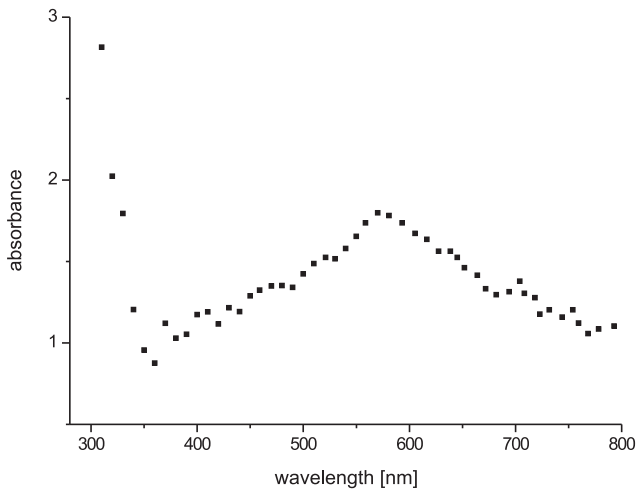

Figure 1: PA spectrum of a sea urchin

A very intense PA band arising from $\pi \rightarrow \pi^*$, $\pi \rightarrow$ n charge transfer transition (Fig. 1) is observed below 350 nm. The visible PA spectra strongly depend on the

decomposition or dehydration processes of organic matter. The obtained PA spectra are very similar to those obtained earlier for other living organisms, Truncullariopis Trunculus and Asterias Rubens [1, 2]. The absorption band near 570 nm is also very similar to that obtained for spermidine copper complexes, important for transferring information to DNA [3]. The obtained results might be experimental evidence of a law stating that evolutionally older living beings, absorb more intensely the part of solar radiation that is transparent in water. The human body is composed mostly of water molecules and the same part of solar radiation penetrating deep inside the body might play a crucial role in many physicochemical processes.

References

[1] N. Guskos, K. Aidnis, G. J. Papadopoulos, J. Majszczyk, J. Typek, J. Rybicki, and M. Majszczyk *Optical Materials* **30** 814 (2008).

[2] International Workshop on Advanced Spectroscopy and Optical Materials, 13–17 July 2008, Gdansk, Poland.

[3] N. Guskos, G. J. Papadopoulos, V. Likodimos, J. Majszczyk, J. Typek, M. Wabia, E. Grech and T. Dziembowska, A. Perkowska, and K. Aidinis, J. Appl. Phys. **90**, 1436 (2001)

Heterogeneous Nucleation in the Melt-spinning Process

S. A. Kostyrya[1], V. I. Tkatch[1], S. G. Rassolov[1], B. Idzikowski[2]

[1] *Donetsk Physics and Engineering Institute, NAS of Ukraine*
R. Luxemburg 72, 83114 Donetsk, Ukraine
[2] *Institute of Molecular Physics, Polish Academy of Sciences*
M. Smoluchowskiego 17, 60-179 Poznan, Poland

Melt quenching techniques including the most common melt-spinning procedure are well established commercial methods for production of materials with metastable structures of superior physical properties. In view of the fact that most of the properties of metastable phases depend on their structure, good control of the structure formation during rapid cooling is of prime importance. However, rapid solidification occurs in very short periods of time and small volumes which makes direct experimental studies very difficult. In such a situation, a computer simulation based on proper physical models is a very useful tool to predict microstructures as a function of the melt composition and processing conditions.

A numerical approach to the description of cooling and crystallization processes in the melt-spinning technique has been proposed. Using the experimentally determined input parameters, controlling both the heat transfer and glass crystallization, the model has correctly predicted the conditions of $Fe_{40}Ni_{40}P_{14}B_6$ melt amorphization for a case of homogeneous nucleation. The dominant contribution of heterogeneous nucleation to this melt crystallization in the majority of experiments has been confirmed and the most probable values of the heterogeneous sites density and wetting angle have been estimated.

Spectral and Magnetic Properties of Macroacyclic and Macrobicyclic Schiff Base RE Complexes as Selective Catalyzers, Contrasts and Enzymes

S. M. Kaczmarek[a], G. Leniec

Institute of Physics, Szczecin University of Technology
Al. Piastów 48, 70-310 Szczecin
[a]*skaczmarek@ps.pl*

Macrocyclic compounds are interesting because of their ability to form complexes with transition metal ions and rare-earths. The coordination chemistry of lanthanide(III) ions has been extensively studied in the recent years because the resulting complexes can be conveniently employed as useful devices or probes in a variety of fields, ranging from solid state to analytical chemistry, hydrometallurgy, biology, medicine, etc. [1–3]. These ions can be used in the design of novel probes of biomedical interest and in the preparation of new kinds of catalysts [4–6]. Their high magnetic moments together with magnetic anisotropy are of particular interest in the field of molecular magnetism. The great interest in synthetic macrocycles and macroacycles and their corresponding metal complexes is related to the fact that they can mimic naturally occurring macromolecules in their structural features, e. g. enzymes. Macroacyclic compounds, such as podands, have higher flexibility of their arms, and their complexation ability grows with the ionic radius of rare-earth ions. The macrobicycle compounds formation significantly depends on the cation's accuracy of fit in the ligand cavity; they are more rigid than macroacyclic compounds. The design and synthesis of macrobicyclic ligands and their lanthanide complexes are important in applied chemistry, biochemistry and technology. These complexes are often applied to separate selected metals, as catalysts and supramolecular devices. Moreover, the related d- and especially 4f-metal ion complexes are used as fluorescent probes in biological systems, as contrast media in medical diagnostics, and as synthetic enzymes to split the nucleic acid chain. They are often applied in the treatment of arteriosclerosis and in radioimmunology [7–10].

Formations of mononuclear acyclic Schiff base complexes have been achieved with d- and f- transition ions. In recent years, considerable attention has been paid to [1+1], [2+1], [1+2] or [3+1] macroacyclic complexes derived from the template condensation of appropriate amine-precursors in the presence of lanthanide(III) salts.

In one of our previous papers we have presented the EPR properties of a gadolinium Schiff base macroacyclic complex (LnL = (Ln = Gd, L = tripodal heptadentate N_4O_3tris [2-(salicylideneamino)ethyl]amine): $C_{27}H_{27}N_4O_3Cl_3Gd$, MaSB-Gd^{3+}) [11]. We have confirmed the [1:1] form of the complex and we have investigated its spectroscopic and magnetic properties. As a continuation of these studies we have also

presented a macroacyclic Schiff base complex with another paramagnetic ion – dysprosium(III) with the formula $C_{27}H_{27}N_4O_3Cl_3Dy$ (MaSB-Dy^{3+}) [12].

The formation of macrobicyclic complexes to act as suitable chelating agents for rare-earth (RE) ions depends significantly on: (a) the internal cavity's dimension and the cation's goodness of fit in the ligand cavity (macrobicycle rigidity); (b) the complexing properties of the counterion; (c) the nature of the donor atoms. These macrobicyclic compounds allow both monometallic (1:1) and bimetallic (1:2) lanthanide cryptates to be formed and the lanthanide ion to be encapsulated into the cavity. Lanthanide cryptates are attractive due to their ability to bind two or more metal ions in close proximity.

In one of our previous papers we have reported a gadolinium cryptate synthesis as a result of Schiff base condensation and w have studied its spectroscopic properties using EPR, IR, TG-DTA and mass spectroscopy [13]. An analysis of the obtained EPR spectra in a wide temperature range has allowed us to draw conclusions on the structure and magnetic properties of the investigated complex.

The properties of both kinds of macrocyclic compounds have been summarized in the paper [14].

On the basis of the performed measurements we have proposed a structure of macrobicycle Schiff base complexes with gadolinium and erbium, giving distances from RE ion to its closest neighboring ion. The results of investigations, showing repletion of gadolinium coordination in gadolinium complexes may be applied by pharmacology manufacturers to fabricate new contrast material to Magnetic Resonance Imaging (MRI) [15].

Very similar results have been obtained for less stable, due to their constitution, macroacyclic compounds of samarium, europium, gadolinium, dysprosium and holmium. These complexes may catalyze reactions of toxic compounds and seem to be better candidates for synthetic enzymes. Their advantage over natural enzymes is their smaller dimension.

RE ions in macrocyclic complexes show low symmetry (in case of gadolinium – monoclinic symmetry). The complexes' magnetic properties strongly depend on the kind of the paramagnetic ion which is sufficiently isolated from the neighboring ion by ligands. Thus, interactions between complexes are negligible.

References

[1] B. Dietrich, et al., *Macrocyclic Chemistry, Aspects of Organic and Inorganic Supramolecular Chemistry*, VCH, Weinheim, 1993
[2] D. Parker, *Macrocyclic Synthesis*, Oxford University Press, Oxford, 1996
[3] W. Radecka-Paryzek, V. Patroniak-Krzyminiewska, *Wiad. Chem.* **50** (1996) 171 (in polish)
[4] A. Roigk, R. Hettich, H. Schneider, *Inorg. Chem.* **37** (1998) 751
[5] P. Guerriero, S. Tamburini, P.A. Vigato, *Coord. Chem. Rev.* **139** (1995) 17
[6] P. Guerriero, P. A. Vigato, D. E. Fenton, P. C. Hallier, *Acta Chem. Scand.* **46** (1992) 1025
[7] C. Platas, F. Avecilla, A. de Blas, T. Rodriguez-Blas, S. F. Geraldes, E. Toth, A. E. Merbach and J.-C. G. Bunzli, *J. Chem. Soc. Dalton Trans.* **4** (2000) 611
[8] P. A. Vigato and S. Tamburini, *Coordinat. Chem. Rev.* **248** (2004) 1717
[9] M. G. B. Drew, O. W. Howarth, Ch. J. Harding, N. Martin and J. Nelson, *J. Chem. Soc. Chem. Commun.* (1995) 903
[10] S. Kobayashi, M. Kawamura, *J. Am. Soc. Chem.* **120** (1998) 5840

[11] G. Leniec, S. M. Kaczmarek, J. Typek, B. Kołodziej, E. Grech, W. Schilf, "Magnetic and spectroscopic properties of gadolinium macroacyclic Schiff base complex", *Solid State Sciences* **9** (2007) 267
[12] G. Leniec, S. M. Kaczmarek, J. Typek, "EPR and IR study of a Dy(III) macroacyclic Schiff base complex", *this conference*
[13] G. Leniec, S. M. Kaczmarek, J. Typek, B. Kołodziej, E. Grech, W. Schilf, "Spectroscopic and magnetic properties of gadolinium macrobicyclic cryptate complex", *J. Phys.: Cond. Matter* **18** (2006) 9871
[14] G. Leniec, S. M. Kaczmarek, J. Typek, B. Kołodziej, E. Grech, W. Schilf, "Spectroscopic and magnetic properties of gadolinium macroacyclic and macrobicyclic complexes", *Solid State Phenomena* **128** (2007) 199
[15] J. C. G. Bunzli, "Benefitting from the unique properties of lanthanide ions", *Acc. Chem. Res.* **39** (2006) 53–61

Physical properties of the noncentrosymmetric superconductor $Mg_{10}Ir_{19}B_{16}$

T. Klimczuk

Condensed Matter and Thermal Physics
Los Alamos National Laboratory
Los Alamos, NM 87545, USA

Specific heat, electrical resistivity and magnetic susceptibility measurements on a high quality sample of $Mg_{10}Ir_{19}B_{16}$ provide a self-consistent determination of its superconducting properties. They indicate that $Mg_{10}Ir_{19}B_{16}$ is a type-II superconductor ($T_c = 4.45$ K, $\kappa(0) \approx 20$), with an electron-phonon coupling constant $\lambda_{ep} = 0.66$. An analysis of the T-dependent specific heat shows that superconducting properties are dominated by an s-wave gap ($\Delta = 0.7$ meV). Point contact tunneling data provides evidence for multiple superconducting gaps, as expected from strong asymmetric spin-orbit coupling.

YAG:Ln(III) Nanocrystals Incorporated into Silica Xerogel as a Luminescent Material

A. M. Kłonkowski[1a], M. Kobus[1], H. J. Meyer[2]

[1] *Faculty of Chemistry, University of Gdansk*
Sobieskiego 18, 80-952 Gdansk, Poland
[a] *aklonk@chem.univ.gda.pl*

[2] *Institute of Inorganic Chemistry, University of Tübingen*
72074 Tübingen, Germany

Inorganic phosphors have been extensively investigated for applications to various types of display panels and highly effective luminescent materials that can transform UV light into visible radiation. New light sources, mainly blue emitting diodes (LEDs), generate new challenges. Commercialized LED lamps need cheap, efficient and chemically stable phosphors that transform UV radiation into white light. Yttrium aluminum garnet, YAG, $Y_3Al_5O_{12}$, is a well known inorganic compound and it is also widely utilized in the optical area. YAGs doped with such lanthanide (Ln) ions as Tb(III) and Eu(III) are employed as phosphors, e.g. on cathode ray tube (CRT) displays [1]. One of the cheapest synthesis methods for of optically active materials consisting of many components is the sol-gel procedure. Multicomponent sol-gel processing allows a large spectrum of materials modified with nanostructures to be prepared [2].

In this study, nanocrystals of YAG:Ln(III) embedded in a silica xerogel matrix have been additionally modified with nobel metal nanoparticles and middle-chain alcohols by the one-pot procedure. A Xerogel matrix minimizes the excitation energy scattering in the materials. On the other hand, silver nanostructures in low concentration enhance the luminescence intensity owing to the surface plasmon resonance (SPR) [3]. Then, alcohols improve the luminescence properties due to the prevention of YAG nanoparticles from agglomeration. Luminescent materials consisting of YAG:Ln(III) in the vicinity of Ag nanostructures incorporated into the silica matrix exhibit higher thermal resistance at higher temperatures.

Acknowledgement
The support of the Ministry of Science and High Education (Grant DBN 3376/T02/ 2007/32 is gratefully acknowledged.

References

[1] J. Nanda, K. S. Narayan, B. A. Murty, D. D. Sarma (1998) *Appl. Phys. Lett.* **72** 1335
[2] V. L. Colvin, M. C. Schlamp, P. A. Alivastos (1994) *Nature* **370** 354
[3] B. O. Dabbousi, M. G. Bawendi, O. Onitsuka, M. F. Robner (1995) *Appl. Phys. Lett.* **66** 1316

Optical Investigations of Germanium Nanocluster-rich SiO_2 Layers Produced by Ion Beam Synthesis

H. Krzyżanowska[1], M. Kulik[1], W. Rzodkiewicz[2], A. P. Kobzev[3], W. Skorupa[4], J. Żuk[1]

[1] *Institute of Physics, Maria Curie-Skłodowska University Pl. M. Curie-Skłodowskiej 1, 20-031 Lublin, Poland*

[2] *Institute of Electron Technology Al. Lotników 32/46, 02-668 Warszawa, Poland*

[3] *Frank Laboratory of Neutron Physics, Joint Institute of Nuclear Research 141980 Dubna, Russia*

[4] *Institute of Ion Beam Physics and Materials Research, Forschungszentrum Rossendorf PO Box 510119, D-01314 Dresden, Germany*

Germanium nanoclusters embedded in silicon dioxide matrices have recently received attention because of their potential for developing integrated optoelectronic devices directly on silicon substrates. Unique properties of SiO_2, including long-term stability and quality of the interface between the oxide and Si substrate are the reasons for the success of silicon as a basic material for microelectronic technology.

The present work is focused on an optical characterization of Ge^+-implanted SiO_2 layers. Two techniques: spectroscopic ellipsometry and photoluminescence were used. Additionally, Rutherford Backscattering Spectroscopy (RBS) was applied for determination of Ge post-implantation depth profiles in SiO_2.

The samples consisted of 500 nm thick supported SiO_2 layers produced by thermal oxidation on a flat-surface, single-crystalline Si substrate in a wet ambient at the temperature of 1000°C. Subsequently, they were doubly implanted with Ge^+ ions at the energies of 480 keV (fluence, $F = 4.2 \cdot 10^{16}$ cm^{-2}) and 280 keV ($F = 1.7 \cdot 10^{16}$ cm^{-2}) at room temperature. Immediately after ion implantation the structures were annealed for 60 min. at temperatures ranging from 700 to 1100°C in a dry N_2 ambient.

Variable Angle Spectroscopic Ellipsometry (VASE) investigations were carried out. Optical constants (refractive indices and extinction coefficients) were computed from experimentally taken ellipsometric angles Ψ and Δ in the range of 250–1000 nm. The spectra revealed the characteristic band with a maximum at 500–600 nm, shifting to shorter wavelengths with an increase in the annealing temperature. as observed Photoluminescence spectra of the same samples showed a band at about 700 nm as the main source of light emission under the argon laser excitation. The origin of the extinction coefficient and photoluminescence spectral features, as well as their correlation are discussed using models of quantum confinement and ion implantation-induced creation of defect centers in Si dioxide layers and their temperature transformation.

Statistical Description of Ferromagnetic and Ferroelectric Domains in Thin Films

K. Lukierska-Walasek[1], K. Topolski[2]

[1] *Institute of Physics, University of Zielona Góra*
ul. Z. Szafrana 4a, 65-516 Zielona Góra, Poland

[2] *Institute of Mathematics, Wroclaw University*
pl. Grunwaldzki 2/4,50-384 Wroclaw, Poland

The Mandelbrot-Zipf's power law is used to describe the system's inhomogenity. Statistical distributions of the domain masses are described using Ising-like models, near the phase transition induced by the temperature. The statistical distribution near the critical point appears to be of the Pareto type.

Steady states for a Hybrid Quantum-classical Hydrodynamic Model for Semiconductors

F. Di Michele, P. Marcati, B. Rubino

Department of Pure and Applied Mathematics, University of L'Aquila
I-67100 L'Aquila Italy

The recent reduction of device dimensions requires the use of more and more accurate models which include quantum effects. Generally, these quantum effcts are important in a limited region, e.g. around the double barrier in resonant tunneling diodes, whereas the rest of the device is adequately described by classical models. For this reason, the hybrid strategy has been introduced. We will apply the strategy to a pair of equations, namely, a classical hydrodynamical equation (HD)

$$(J_c)_t + \left(\frac{J_c^2}{n_c} + T\, n_c\right)_x - n_c\, V_x = -\frac{Jc}{\tau} \tag{1}$$

and a quantum hydrodynamical equation (QHD)

$$(J_q)_t + \left(\frac{J_q^2}{n_q} + T\, n_q\right)_x - n_q\, V_x\, \delta^2 \big(n_q (\ln n_q)_{xx}\big)_x = -\frac{J_q}{\tau}\,. \tag{2}$$

We discuss the transmission conditions between the classical and the quantum regions, and use them to recover the existence of steady states. Preliminary results concerning their stability will be shown.

Electrical and Thermal Properties of Nanowires in a Quantum Regime

W. Nawrocki

Poznan University of Technology
Piotrowo 3A, 60-965 Poznan, Poland
nawrocki@et.put.poznan.pl

1. Theory of conductance quantization

We have analyzed the quantization of electrical and thermal conductance in nanowires formed between two macroscopic metallic electrodes. According to the theory proposed by Landauer [1] the quantization phenomenon in nanowires occurs because of the formation of a nanometer-sized sample (nanowire) between macroscopic contacts. We have measured the electrical conductance in nanowires formed by metals (Au, Cu, W, Ni, Co). We have built a measuring system for investigating electrical conductance in nanowires. The investigation has been performed outdoors at room temperature.

We consider a constriction with length L and width W between two wide metallic conductors, which have been called "electron reservoirs" after Landauer. An average free path in the conductor is equal to λ, and the Fermi level E_{F}. On applying a potential difference V to the ends of the constriction, a flux of electrons will flow through it. The transport of electrons is ballistic, i.e. it is realised without collisions, if the constriction length is less than the average free path: $L < \lambda$. If the conductor width W is comparable with the Fermi wave λ_{F} length, then such system is regarded as quasi-one-dimensional, an electron is regarded as a wave, and effects showing directly the quantum character of electrons are to be expected. A certain number of current carrying channels is formed for such conditions in the constriction which has been called a nanowire.

The channels are connected with the existence of discrete energy levels of electrons in metal, located below the Fermi level and "delivering" electrons for charge transport.

Conductance G_j for channel j in the conditions of spin degeneration is defined by (1) [1].

$$G_j = \frac{dI_j}{dV} = \frac{2e^2 T_j}{h}, \tag{1}$$

where: I_j – the electrical current in the channel j, V – the voltage on a constriction, e – electron charge, h – Planck's constant, T_j – total probability of carriers transmission over channel j.

For ideal ballistic transport of electrons, i.e. for the motion of electrons without scattering on impurities and contaminations, probability T_j is equal to 1. In such case, conductance G_j of one transport channel is defined exclusively by the fundamental

constants of physics, e and h:

$$G_0 = \frac{2e^2}{h}. \tag{2}$$

It is worth noticing that the quantum of conductance G_0 is equal to the inverse of twice the von Klitzing constant: $G_0 = 2/R_K$. According to the Büttiker-Landauer theory, electrical conductance is transmission between two reservoirs of electrons. In a constriction of a nonmagnetic metal with nanometer dimensions, called a nanowire, the ballistic transport of electrons occurs in conductive channels. The number of channels is proportional to the nanowire width. The conductance of such nanowire is described by Landauer's formula (3):

$$G = \frac{2e^2}{h} \sum_{n=1}^{N} T_n, \tag{3}$$

where: T_n – transmission of electrons in channel number n.

2. Measurement results on electrical conductance in metallic nanowires

The quantization of electric conductance depends neither on the kind of metal nor on temperature. However, the purpose of studying the quantization for different metals has been to observe how the metal properties affect the contacts between wires. We have investigated the conductance quantization of nanowires for three nonmagnetic metals (gold, copper and tungsten) and for magnetic metals (cobalt and nickel). All measurements have been carried out at room temperature. For nonmagnetic metals, the conductance quantization in units of $G_0 = 2e^2/h = (12.9\ \mathrm{k\Omega})^{-1}$ has been observed in the nanowires. All characteristics have shown the same steps equal to $2e^2/h$. The characteristics are only partially reproducible; they differ in the number and height of steps, and in the time length. The steps can correspond to 1, 2, 3 or 4 quanta. It should be emphasised that quantum effects have been observed only for some of the characteristics recorded. The conductance quantization has been so far more pronouncedly observable for gold contacts. Figure 1a shows an example plot of conductance vs. time during the process of drawing of a gold nanowire [2]. Figure 1b shows the conductance histogram obtained from 6000 consecutive characteristics in the conductance range from $0.5G_0$ to $4G_0$, for the bias voltage $V_{\mathrm{bias}} = 0.420$ V.

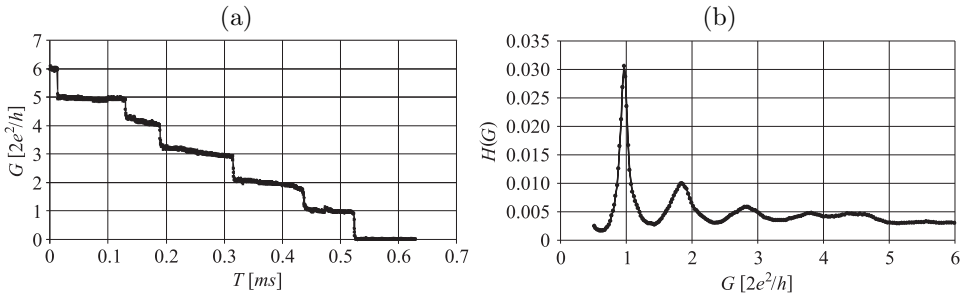

Figure 1: Conductance quantization in gold nanowires (formation of nanowires during breaking contact)

The quantization of electric conductance depends neither on the kind of metal nor on temperature. However, the purpose of studying the quantization for differ-

ent metals has been to observe how the metal properties affect the contacts between wires. For nonmagnetic metals, the conductance quantization in units of $G_0 = 2e^2/h = 7.75 \cdot 10^{-5}$ [A/V] = $(12.9\ \mathrm{k\Omega})^{-1}$ has been previously observed for the following nanowires: Au-Au, Cu-Cu, Au-Cu, W-W, W-Au, W-Cu.

3. Thermal problems in nanowires

Both electrical G_E and thermal G_T conductance of a nanostructure are related to the same process: electron transport. Therefore, there are several analogies between the two physical quantities. In addition to the observations of electrical conductance quantization in nanowires, thermal conductance quantization can be expected, as well. The electron transport in a nanowire has two effects: electrical current I and heat flux density Q_D:

$$I = G_E\,\Delta V, \quad Q_D = G_T\,\Delta T,$$

where: G_E – electrical conductance of a sample, ΔV – difference of electrical potentials, G_T – thermal conductance of a sample, ΔT – temperature difference.

$$G_E = \sigma\,A/l, \quad G_T = \lambda\,A/l \tag{4}$$

where: σ – electrical conductivity, λ – thermal conductivity, l – sample length (e.g. nanowire), A – sample cross-section area.

Quantized thermal conductance in one-dimensional systems (e.g. nanowires) has been predicted theoretically by Rego [3] using the Landauer theory. The thermal conductance is considered in a similar way like the electrical conductance. Conductive channels are formed in one-dimension systems. Each channel contributes to total thermal conductance with the quantum of thermal conductance G_{T_0}. Quantized thermal conductance and its quantum (unit) G_{T_0} has been confirmed experimentally by Schwab [4]. The quantum of thermal conductance

$$G_{T_0}\ [\mathrm{W/K}] = (\pi^2 k_B^2/3h)\,T = 9.5 \cdot 10^{-13}\,T \tag{5}$$

depends on the temperature. At $T = 300$ K the value of $G_{T_0} = 2.8 \cdot 10^{-10}$ [W/K]. This value is determined for ideal ballistic transport (without scattering) in a nanowire, with the transmission coefficient $T_{ij} = 100\%$. It means that the thermal conductance in all practical cases (for $T_{ij} < 100\%$ is below the limit given by the formula (6). A single nanowire should be considered together with its terminals (Figure 2), which are reservoirs of electrons.

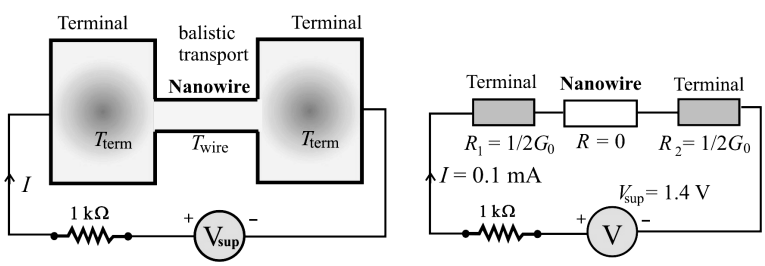

Figure 2: Conductance distribution in a nanowire with ballistic transport

Electron transport in a nanowire is ballistic, it means transport without scattering of electrons and without energy dissipation. The energy dissipation occurs in terminals. Due to the energy dissipation, the local temperature T_{term} in terminals is higher than the temperature T_{wire} of nanowires Figure 2). The heat distribution in terminals of a nanostructure should be analyzed.

In small structures the dissipated energy is quite large. For the first step of conductance quantization, $G_E = G_{E_0} = 7.75 \cdot 10^{-5}$ [A/V], and at the supply voltage of $V_{\mathrm{sup}} = 1.4$ V the current in the circuit $I = 100$ μA ($I = 190$ μA for the second step of quantization). The power dissipation in the terminals of nanowires is $P = I^2/G_{E_0} = 130$ μW for the first step and $P = 230$ μW for the second step. It should be noticed that the electric current density in nanowires is extremely high. The diameter of the gold nanowire at the first step of quantization can be estimated as $D = 0.4$ nm, hence, the current density $J \approx 8 \cdot 10^{10}$ [A/cm^2] for $I = 100$ μA.

References

[1] Landauer R., "Conductance determined by transmission: probes and quantised constriction resitance", *J. Phys.: Cond. Matter 1* (1989) 8099

[2] Susła B., Wawrzyniak M., Barnaś J., Nawrocki W., "Conductance quantization in magnetic and nonmagnetic metallic nanowires", *Materials Science* (2007) **25** (2) 305–312

[3] Rego L.G. C., Kirczenow G., "Quantized thermal conductance of dielectric quantum wires", *Phys. Rev. Lett.* (1998) 81, 232–235

[4] Schwab K., Henriksen E. A., Worlock J. M., Roukes M. L., "Measurement of the quantum of thermal conductance", *Nature* (2000) 404, 974–977

I-V characteristic of a single parabolic barrier

G. J. Papadopoulos

Department of Physics, Solid State Physics Section
University of Athens, Panepistimiopolis, Athens 157 84, Greece

Transport in a nanostructure across a truncated parabolic barrier located along the width of a thin layer sandwiched by semiconductor reservoirs is examined. Contrary, to the case of a square barrier upon application of dc voltage the height of the parabolic barrier diminishes. Prompted by this peculiarity we have chosen the parabolic barrier for our presentation. Utilizing the combined potential energy in the relevant Schrödinger equation we are able to obtain the corresponding scattering solution, enclosed form, and thereby the transmission coefficient in terms of the applied voltage. Furthermore, upon application of the Tsu-Esaki formalism we are led to the required I-V characteristic, which exhibits regions of negative differential resistance. We consider the case whereby the effective carrier masses in the two reservoirs are equal, but differing from the corresponding mass in the barrier layer. The influence of parameters such as temperature and effective masses is obtained, as well as the corresponding peak to valley ratio associated with a given negative differential resistance region. While keeping the same effective masses the location of the various peaks and valleys in terms of the applied bias is not affected while the peak to valley ration diminishes with increasing carrier density.

Tailoring the Nano-structure of Magnetic Micro-wires for Multifunctional Macro-composites

Hua-Xin Peng[1a], Faxiang Qin[1], Manh-Huong Phan[2]

[1] *Advanced Composites Centre for Innovation and Science*
Department of Aerospace Engineering
Bristol University, University Walk, Bristol, BS8 1TR, UK
[a] *H.X.Peng@bristol.ac.uk*

[2] *PHY 221, Department of Physics, University of South Florida*
4202 E. Fowler Ave., Tampa FL 33620, USA

The recent invention of metallic glasses produced in the form of thin ribbons (∼25 μm thick) and amorphous microwires (1∼30 μm diameter) using rapid quenching techniques such as amorphous and nanocrystallined Fe- and Co-based micro-ribbons and micro-wires including glass coated microwires offers exciting new opportunities in the development of new magnetic sensing devices owning mainly to their excellent magnetic properties such as the giant magnetoimpedance (GMI) effect [1–2]. Our recent efforts have therefore been focused on improving the GMI effect in such materials through tailoring their nano-structures via (i) novel field treatment method and (ii) fine tuning the composition such as partially substituting Al for Fe, which has been found to increase the GMI effect and its field sensitivity; the substitution of Cu and Nb for B in an initial $Co_{70}Fe_5Si_{15}B_{10}$ composition forming the $Co_{70}Fe_5Si_{15}Nb_{2.2}Cu_{0.8}B_7$ composition improves both giant magnetoimpedance effect and its field sensitivity [3–4] which are desirable properties for magnetic sensing applications.

With the overall aim to add further functionalities to advanced structural composite materials to create multifunctional composites, we have started to develop new composite materials by employing these micro-ribbons and micro-wires. Here, we report two new findings:

(1) The enhancement of GMI effect in a polymer matrix containing Co-based ferromagnetic micro-wires. The composite materials consisting of parallel Co-based ferromagnetic microwires embedded in a polymer matrix. A great enhancement of the GMI effect and its sensitivity are achieved in these composite materials. It has been found that the GMI effect strongly increased with increasing number of ferromagnetic microwires. At a given frequency of 10 MHz, the GMI ratio and its field sensitivity reached the highest values of 450% and 45%/Oe for the composite containing four microwires when compared with those of 14% and 1%/Oe for that containing one microwire. This indicates that the newly developed composite material is very promising for magnetic sensing applications.

(2) Magnetic microwires were embedded into a typical glass fibre reinforced polymer (GFRP) composite material for advanced sensing applications, the results indicate that, the new composite has superior magnetic properties that are ideal for sensing applications; the magnetic property can be controlled by varying the direction of applied magnetic field; the role of stress and wire arrangement are also found important in determining the magnetic behaviour.

The results of this investigation afford new opportunity in developing novel composite materials with added functionality for a wide range of engineering applications.

Acknowledgements
HXP gratefully acknowledges the support from the Engineering and Physical Science Research Council (EPSRC) UK for financial support.

References
[1] Panina LV and Mohri K 1994 *Appl. Phys. Lett.* **65** 1189
[2] Knobel M, Sánchez M L, Marín P, Gómez-Polo C, Vázquez M and Hernando A 1996 *J. Appl. Phys.* **79** 1646
[3] Phan M H, Peng H X, Wisnom M R and Yu S C 2005 *J. Appl. Phys.* **98** 014316
[4] Phan M H and Peng H X 2004 *Phys. Stat. Sol.* **A 201** 1558

Block-Copolymer Micellization in Compressible Solvents: Polystyrene-*block*-Polydiene in Near Critical Propane

Winoto Winoto[1], Sugata Tan[1], Youqing Shen[1], J. Mays[2], M. Radosz[1a]

[1] *Soft Materials Laboratory*
Department of Chemical and Petroleum Engineering
University of Wyoming Laramie, WY 82071-3295
[a] *radosz@uwyo.edu*

[2] *Oak Ridge National Laboratory and University of Tennessee*

Micelles of block polymers, such as polystyrene-*block*-polydiene, can be formed upon decompression and decomposed upon compression of near critical solvent, such as propane, at constant temperature. Experimental and calculated data on model polystyrene, polybutadiene, polyisoprene, and their diblock copolymers in propane are presented to understand the effects of molecular weight, deuteration, impurities, and crystallizability on bulk and micellar phase transitions. Such understanding is needed to develop novel processes of making polymeric nanoparticles for medical applications, illustrated, for example, with real nanoparticles for cancer-drug delivery.

Computer Simulation of Stress-Strain State of Elastic Body with Thin Inclusion

Ya. Savula, L. Vynnyts'ka

Faculty of Applied Mathematics and Informatics
Ivan Franko National University of L'viv,
Universytets'ka 1, 79000 L'viv, Ukraine

Thin layers are essential elements of modern structures such as buildings and different types of machines. They are also important components of composite materials. It is worth mentioning that inclusions can be nano-dimensional in this case. In general, the presence of a thin inclusion has a strong influence on distributions of displacements, strains and stresses.

Numerical methods, especially the finite elements method, are rarely used for investigation of models with thin inclusions because a small thickness of the layer produces difficulties in implementation of numerical methods. Reduced dimension models can be used for a thin inclusion as a way to overcome these problems. Within the bounds of such approach, the stress-strain state of a thin layer is described by models of plates and shells.

A computer simulation of an elastic body model with a thin inclusion is carried out for the plane elastic problem. Numerical experiments are performed for a model in which a thin inclusion is considered as one-dimensional and the membrane theory of shells is used for describing its stress-strain state. At the same time the stress-strain state of a matrix is described by equations of the classical theory of elasticity. Junction conditions are obtained with the assumption of perfect bonding on the surface of contact.

The finite elements method is used for a numerical investigation. A one-dimensional hierarchical basis of "bubble"-functions and a corresponding two-dimensional hierarchical basis on a triangle are chosen as approximation functions.

EPR Study of Magnetic Interactions in $FeSbVO_6$

J. Typek[1], N. Guskos[1,2], E. Filipek[3]

[1] *Institute of Physics, Szczecin University of Technology, Al. Piastów 17, 70-310 Szczecin, Poland*

[2] *Solid State Physics, Department of Physics, University of Athens, Panepistimiopolis, 15 784 Zografos, Athens, Greece*

[3] *Department of Inorganic and Analytical Chemistry, Szczecin University of Technology, Al. Piastów 42, 70-065 Szczecin, Poland*

Powder samples of $FeSbVO_6$ have been synthesized from a mixture of appropriate oxides by the solid state reaction technique and investigated by the electron paramagnetic resonance (EPR) in the 4–300 K temperature range. At room temperature the EPR spectrum consists of two widely differing components: a narrow (12 mT) line centered at $g_{\mathrm{na}} = 1.966$ and an intense, almost Lorentzian broad (200 mT) line at $g_{\mathrm{br}} = 1.974$. The EPR spectral parameters (linewidth, g-factor, amplitude, integrated intensity) of both components have displayed a marked thermal dependence. At low temperature, below 100 K, the broad line has been analysed in terms of three components. The temperature dependence of integrated intensity for the main component of the broad line has shown very interesting behaviour reaching a maximum at 65 K. The narrow line in EPR spectrum of $FeSbVO_6$ has been attributed to strongly interacting V^{4+} monomers, while the broad line is due to the iron and vanadium spin clusters. A comparison of the magnetic properties of $FeSbVO_6$ is made with the recently studied isostructural compound $CrSbVO_6$ [1].

References

[1] J. Typek, N. Guskos, E. Filipek *to be published in J. Non-Cryst. Solids* (2008)

A Few Models of Anomalous Mechanical Properties

K. W. Wojciechowski

Institute of Molecular Physics, Polish Academy of Sciences
M. Smoluchowskiego 17, 60-179 Poznań, Poland
kww@ifmpan.poznan.pl

One of most important characteristics of materials, crucial for their applications, are mechanical properties. Despite they have been studied for a very long time and many of our intuitions are based on those studies (additionally supported by everyday experience), some of the mechanical properties we find in real materials are still counterintuitive. The examples are:

- negative Poisson's ratio [1–4],
- negative thermal expansion [5–10],
- negative bulk modulus or compressibility [9, 11].

It should be stressed that materials with the above mentioned anomalous properties are not only interesting from the point of view of fundamental research but also various practical applications have been designed for them [4, 12–14]. For these reasons, it is important to understand such surprising properties and to reveal the mechanisms (both on the micro- and macroscopic scale) responsible for them. This can be done by studying well defined models.

In this lecture, a few models exhibiting either the above mentioned anomalies or other mechanical anomalies are discussed. Some possible connections between various effects are pointed out.

Acknowledgements
The Author acknowledges with gratitude support of his travel and stay at the conference by the Poznan Supercomputing and Networking Center (PCSS, Poland) where also most of the the simulations were performed. Part of this work was supported by the Ministry of Science and Higher Education (Poland) grants N202 07032/1512 and NN 202 1353 33.

References

[1] R. S. Lakes 1987 "Negative Poisson's Ratio Materials" *Science* **235** 1038–40
[2] K. E. Evans, M. A. Nkansah, I. J. Hutchinson, and S. C. Rogers 1991 "Molecular Network Design" *Nature* **353** 124
[3] R. H. Baughman, "Avoiding the shrink" 2003 *Nature* **425** 667
[4] Ch. W. Smith and K. W. Wojciechowski 2006 1st Conference on Auxetics and Other Unusual Materials, Exeter, UK – Preface; 2008 *Physica Status Solidi (b)* **245** 486–488 (see also other papers and references there)

[5] R. S. Lakes 1996 "Cellular Solid Structures with Unbounded Thermal Expansion" *J. Mater. Sci. Lett.* **15** 475–477
[6] C. W. Smith, W. Miller, D. S. Mackenzie, K. E. Evans 2005 "Mechanism for Negative Thermal Expansion and Its Links to Negative Poisson's Ratio" (presented at the 2^{nd} Int. Workshop on Auxetic and Related Systems, Poznan, Poland)
[7] J. Grima, P. S. Farrugia, R. Gatt, and V. Zammit 2007 "A System with Adjustable Positive or Negative Thermal Expansion" *Proc. R. Soc. London A* **463** 1585–1596 (see also references therein)
[8] R. S. Lakes 2007 "Solids with Tunable Positive or Negative Thermal Expansion of Unbounded Magnitude" *Appl. Phys. Lett.* **90** 221905
[9] R. S. Lakes and K. W. Wojciechowski 2008 "Negative Compressibility, Negative Poisson's Ratio, and Stability" *Physica Status Solidi (b)* **245** 545–551
[10] J. W. Grima and K. W. Wojciechowski 2007 "4th Workshop on Auxetics and Related Systems, Msida, Malta – Preface; 2008 *Physica Status Solidi (b)* **246** (in print, see also other papers and references there)
[11] R. S. Lakes 2006 "Negative Incremental Bulk Modulus in Foams" *Philos. Mag. Lett.* **86** 651–659
[12] "Advances in Negative Poisson's Ratio Materials" 1993 *Advanced Materials (Weinheim, Germany)* **5** 293–296
[13] K. E. Evans and K. L. Alderson 2000 "Auxetic Materials: the Positive Side of Being Negative" *Engineering Science and Education Journal* **9** (4) 148–54
[14] D. A. Konyok, K. W. Wojciechowski, J. M. Pleskaczewski, and S. W. Szylko 2004 "Materials With a Negative Poisson's Ratio" *Mechanics of Composite Materials and Structures* **10** 35–69 (in Russian)

Collective Diffusion in the Presence of Defects and Interactions

M. A. Załuska-Kotur[1], Z. W. Gortel[2], F. Krzyżewski[1]

[1] *Institute of Physics, Polish Academy of Sciences*
Al.Lotników 32/46, Poland

[2] *Department of Physics, University of Alberta*
Edmonton, T6G 2J1 Alberta, Canada

Diffusional flow controls various physical phenomena in many particle systems, such as building of nanostructures, crystal growth, or efficiency of chemical reactions. This collective process depends on the particle density, the substrate's potential energy landscape, and particle-particle interactions. From a theorist's perspective a collective diffusion is a complicated multi-body problem to which a variety of approaches is being applied ranging from analytic ones based on master, Fokker-Planck, or Kramers equations, to numerical Monte Carlo or molecular dynamics simulations [1]. We have recently proposed a novel variational analytic approach allowing the density dependent diffusion coefficient to be calculated for systems modeled by a lattice gas with kinetics given by site and local occupancy configuration dependent transition rates [2, 3]. The approach is quite versatile and makes it possible to investigate diffusion in adsorbed systems with or without short or long range interactions, on homogeneous or inhomogeneous crystalline substrates [2–6, 8]. The choice of variational parameters is especially important in the case of inhomogeneous systems, where they have to take into account the differences in equilibrium occupation probabilities of different sites. Using this approach we derive the density dependence of the diffusion coefficient for a variety of model systems that agrees very well with the results of the numerical MC simulations for these systems. The method applied to 2D systems yields dynamical correlations between two main symmetry directions on the lattices for which a single particle diffusion is known to proceed independently in each direction. Such density dependent behavior of the collective diffusion in these 2D systems is confirmed by the simulations. The correlations between the directions in the collective particle transport makes it also possible to account for the finite particle size effects in confined geometries. The variational approach to collective diffusion is applicable in all interacting systems whose static correlations can be calculated exactly or, at least, approximately. Selected theoretical results for interacting 1D and 2D systems will be presented and confronted with the results of numerical simulations for these systems.

Acknowledgments
This work was supported by Poland's Ministry of Science and Higher Education Grant No. N202 042 32/1171.

References
[1] T. Ala–Nissila, R. Ferrando, and S. C. Ying (2002) *Adv. Phys.* **51** 949

[2] Z. W. Gortel and M. A. Załuska-Kotur (2004) *Phys. Rev.* **B 70** 125431
[3] M. A. Załuska-Kotur and Z. W. Gortel (2007) *Phys. Rev.* **B 76** 245401
[4] M. A. Załuska-Kotur and Z. W. Gortel (2005) *Phys. Rev.* **B 72** 235425
[5] L. Badowski, M. A. Załuska-Kotur, and Z. W. Gortel (2005) *Phys. Rev.* **B 72** 245413
[6] M. A. Załuska-Kotur, L. Badowski, and Z. W. Gortel (2005) *Physica* **A 357** 305
[7] M. A. Załuska-Kotur and Z. W. Gortel (2006) *Phys. Rev.* **B 74** 045405
[8] M. Yakes, M. Hupalo, M. A. Załuska-Kotur, Z. W. Gortel, and M. C. Tringides (2007) *Phys. Rev. Letters* **98** 135504

ORAL COMMUNICATIONS

"Learn on the Fly" Fitting for Quantum-Classical Hybrid Particle Methods for Metals

M. Bobrowski[1,2], J. Dziedzic[1], J. Rybicki[1,2,3]

[1] *Department of Solid State Physics, Gdansk University of Technology Narutowicza 11/12, 80-952 Gdansk, Poland*

[2] *TASK Computer Centre, Gdansk University of Technology, Narutowicza 11/12, 80-952 Gdansk, Poland*

[3] *Institute of Mechatronics, Nanotechnology and Vacuum Techniques Koszalin University of Technology Racławicka 15–17 F, 75-620 Koszalin, Poland*

Many engineering processes and phenomena such as cutting, materials fracture or surface oxidation involve chemical reactions. Classical Molecular Dynamics (MD) simulations based on empirical inter-atomic potentials often fail to describe such processes since the potentials are usually fitted only to the equilibrium properties of bulk materials. Instead, the interactions need to be calculated by means of quantum-mechanical methods which are able to describe the breaking and formation of bonds.

The "Learn on the Fly" (LOTF) fitting scheme was first proposed by Csanyi et al. [1] and applied successfully for vacancy diffusion as well as for crack propagation in silicon simulated with MD methods. In the LOTF scheme, classical forces acting on atoms selected to be treated quantum mechanically (and flagged as such) are fitted to forces calculated quantum mechanically, considered to be exact. At first, the forces originating from atoms surrounding the central (flagged) atom and acting thereon, are calculated quantum-mechanically. Then, the parameters of a classical potential function are tuned to reproduce quantum mechanical forces with the nonlinear Levenberg-Marquardt procedure.

In this work the LOTF scheme is applied to metallic systems using Tight-Binding (TB) algorithms of Papconstantopoulos et al. [2] as the quantum-mechanical method and our own program with the Sutton-Chen force-field for MD simulations. The method is adapted for various defects in cuprum and gold as well as for cuprum nanocutting by means of a metallic rigid nano-edge.

Acknowledgements
The work has been sponsored by the Polish Ministry of Science and Information Technology, under grant number 3 T11F 026 29, and the Ministry of Science and Higher Education, under grant number N519 019 31/3498. Our calculations were performed at the TASK Computer Centre (Gdansk, Poland).

References

[1] Csanyi G. et al, *Phys. Rev. Lett.*, **93**, 175503 (2004)
[2] M. J. Mehl and D. A. Papaconstantopoulos, *Phys. Rev.*, **B 54**, 4519 (1996)

Influence of Tm Codopant on Magnetic Properties of Er-doped Lithium Niobate Single Crystals

T. Bodziony[1,2], S. M. Kaczmarek[1], R. Kruk[2]

[1] *Institute of Physics, Szczecin University of Technology*
Al. Piastów 17, 70-310 Szczecin, Poland

[2] *Institute of Nanotechnology, Forschungszentrum Karlsruhe GmbH*
P.O. Box 3640, D-76021 Karlsruhe, Germany

The results of magnetic susceptibility measurements of lithium niobate weakly doped with erbium and codoped with thulium, $LiNbO_3$:Er (0.2 wt. %), Tm (0.3 wt. %) single crystals are reported for the first time. The dependence of magnetic susceptibility versus temperature fulfils the Curie-Weiss law. The estimated Curie-Weiss constant is $\Theta = 0.37 \pm 0.13$ K for an $LiNbO_3$:Er, Tm single crystal. This estimated Curie-Weiss constant is in good agreement with the temperatures obtained from earlier measurements of the intensity of EPR lines. Magnetic susceptibility measurements detect the presence of ferromagnetic interactions between Er^{3+} ions in a weakly doped $LiNbO_3$:Er, Tm single crystal. These results are an independent confirmation of the presence of ferromagnetic interactions between Er^{3+} ions in a weakly doped $LiNbO_3$:Er and $LiNbO_3$:Er, Tm single crystal which we have previously recorded on the basis of EPR measurements. The EPR intensity measurements indicate that the codopant (Tm^{3+}) plays an important role in substitute Er^{3+} ions in an $LiNbO_3$ host crystal. The effects of stoichiometry and codoping in a lithium niobate host crystal are also considered.

Phase Transformations in $La_{1-x}Nd_xNi_{3.5}Al_{1.5}$-$H_2$ ($x = 0.1$; 0.2) Systems

A. M. Trostianchyn[1], I. I. Bulyk[1], I. V. Trostianchyn[2], S. I. Mudry[2]

[1] *Karpenko Physico-Mechanical Institute of National Academy of Sciences of Ukraine*
5 Naukova str., 79601 L'viv, Ukraine

[2] *Department of Physics, Ivan Franko National University of L'viv*
8 Kyrylo and Mephodii str., 79005 L'viv, Ukraine

Interactions in $La_{1-x}Nd_xNi_{3.5}Al_{1.5}$-$H_2$ ($x = 0.1$ and 0.2) systems were studied at temperatures from room temperature up to 950°C at the initial hydrogen pressure 5 MPa by means of differential thermal (DTA) and *X*-ray phase analyses. The heating of two-phase alloys ($x = 0.1$ and 0.2) under hydrogen results in their disproportionation (at 530 and 560°C respectively) with the formation of NiAl and unidentified amorphous products. The single-phase $La_{0.9}Nd_{0.1}Ni_{3.5}Al_{1.5}$ alloy decomposes under hydrogen at 900°C into a rare-earth metal hydride and a Ni_3Al intermetallic; traces of NiAl and a hydride of a phase with $CaCu_5$-type structure were also observed. The heating of disproportionated samples in vacuum up to 520–550°C leads to their recombination into a homogenized phase with a $CaCu_5$-type structure. In other words, the increase of neodymium content shifts the reaction equilibrium of $La_{1-x}Nd_xNi_{3.5}Al_{1.5}$ alloys with hydrogen towards recombination.

Dynamical and Structural Properties of 4-cyano-4-n-pentylbiphenyl (5CB) Molecules Adsorbed on Zigzag Carbon Nanotubes of Different Chiralities: Computer Simulation Study

A. Dawid[a], W. Gwizdała

University of Silesia, Institute of Physics
Uniwersytecka 4, Katowice 40-007, Poland
[a] *dawid@us.edu.pl*

Small aggregates of mesogenic molecules adsorbed on a single walled carbon nanotube (CN) surface exhibit many interesting properties [1–2]. The main subject of this work is the influence of carbon nanotube chiralities [3] on the liquid crystal dynamics. We have taken different zigzag CNs. We have studied the system at several temperatures.

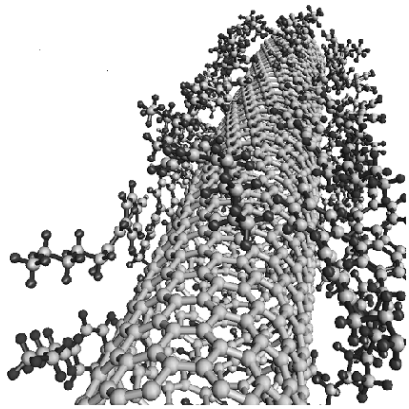

Figure 1: Zigzag carbon nanotube covered with 5CB molecules.

We have chosen the Lennard-Jones potential to calculate the forces between atoms. All molecules have been simulated with a constant bond length (rigid bodies). The equation of motion has been calculated using the Verlet algorithm. The system has been treated as a cluster, no extra conditions have been applied. The angular and linear velocity autocorrelation functions and their Fourier transforms have been calculated and discussed. The 5CB layer structure has been studied calculating the

orientational and radial distribution functions. We have found a dependency between the carbon nanotube chirality and the mesogene layer structure. We have shown that the ultra-thin mesogene layer structure strongly depends on temperature.

References

[1] A. Dawid and Z. Gburski *J. Non-Cryst. Solid.* **353**, 4339 (2007)
[2] Z. Dendzik, M. Kośmider, P. Raczyński and A. Piątek *J. Non- Cryst. Solid.* **353**, 4586 (2007)
[3] Z. Dendzik, M. Kośmider, A. Dawid and Z. Gburski *J. Mol. Struct.* **744**, 577 (2004)

Analytic Bond Order Potential Parametrization for Atomistic Simulations of Tungsten Trioxide

Z. Dendzik[1,3], D. Chrobak[2,3], R. Nowak[3]

[1] *Institute of Physics, University of Silesia*
Uniwersytecka 4, 40-007 Katowice, Poland

[2] *Institute of Materials Science, University of Silesia*
Bankowa 12, 40-007 Katowice, Poland

[3] *Nordic Hysitron Laboratory, Helsinki University of Technology*
Vuorimiehentie 2A, 02015 Espoo, Finland

Tungsten trioxide (WO_3) is an exciting material for electrochromic devices, such as large area displays, windows with controlled light transmission or variable reflectance mirrors [1]. Alkali-doped tungsten trioxide shows surprisingly interesting physical properties, such as surface superconductivity at 91 K which has been reported in sodium-doped tungsten trioxide [2]. A special case of tungsten oxide applications are one-dimensional nanostructures (nanowires) that have been found attractive for solid state gas sensors [3] due to their high surface-volume ratio as well as radial stress relaxation that prevents generation of dislocations due to the lattices mismatch [4].

We have derived a parametrization of the analytical potential for tungsten trioxide, based on the analytical bond-order scheme proposed by Albe et al. [5] which provides a good description of a number of tungsten trioxide properties, including the lattice constant, bulk modulus and elastic constants.

References

[1] Broclawik E, Gora A, Liguzinski P, Petelenz P and Witek H A 2006 *J. Chem. Phys.* **124** 054709
[2] Reich S and Tsabba Y 1999 *Eur. Phys. J.* **B 9** 1
[3] Kim Y S et al. 2005 *Appl. Phys. Lett.* **86** 213105
[4] Klinke C, Hannon J B, Gignac L, Reuter K and Avouris P 2005 *J. Phys. Chem.* **B 109** 17787
[5] Albe K, Nordlund K, Nord J and Averback R S 2002 *Phys. Rev.* **B 65** 195124

Auxetic Properties of Cubic Polycrystals

A. J. Duda[1], K. W. Wojciechowski[2]

[1] *Institute of Theoretical Physics, Wrocław University, pl. Maksa Borna 9, 50-204 Wrocław, Poland*

[2] *Institute of Molecular Physics, Polish Academy of Sciences M. Smoluchowskiego 17, 60-179 Poznań, Poland*

The Poisson's ratio and the transverse compliance of isotropic polycrystals composed of cubic crystallites as a function of monocrystal's materials constants is investigated. Reuss's and Voigt's estimates, orientational averaging and several other methods are used to calculate it. A comparison with experimental data is made for several polycrystals. A similar analysis is applied to an orthorhombic aggregate of cubic crystallities and additionally the areal Poisson's ratio for such aggregate is investigated.

Determination of the Diameter Distribution of Confined Metallic Nanogranules from XAS measurements

S. Frigio[1], G. Cosimi[1], A. Witkowska[1,2], J. Rybicki[2,3,4]

[1] *Istituto di Matematica e Informatica, Universita di Camerino via Madonna delle Carceri, Camerino (MC), Italia*

[2] *Faculty of Technical Physics and Applied Mathematics Gdansk University of Technology Narutowicza 11/12, 80-952 Gdansk, Poland*

[3] *TASK Computer Centre, Gdansk University of Technology Narutowicza 11/12, 80-952 Gdansk, Poland*

[4] *Institute of Mechatronics, Nanotechnology and Vacuum Techniques Koszalin University of Technology Racławicka 15–17 F, 75-620 Koszalin, Poland*

During the first order phase transition a significant changes in the X-ray absorption coefficient are observed (especially close to the absorption edge) related to a change of structural and electronic properties. Thus, performing Single Energy X-ray Absorption Detection (SEXAD) experiment [1], i.e. measuring the X-ray absorption coefficient at a fixed, suitably chosen energy as a function of temperature, one can determine the phase transition temperature and many other related physical quantities.

Since a melting temperature of metallic nanogranules depends on their diameter, the temperature variations of the absorption coefficient follows the temperature variations of liquid-to-solid volume ratio. Assuming a suitable model of melting [2] (e.g. homogeneous or liquid-skin melting models), the diameter distribution of nanogranules can be determined or at least estimated.

In the paper, we propose an original numerical scheme of extracting information on the distribution of diameters of metallic nanogranules embedded in a glassy matrix using SEXAD data. Preliminary results for lead and bismuth nanogranules confined in a silica matrix are presented.

References

[1] Filipponi A et al. 1998 *J. Phys.* **CM 10** 235
[2] Peters K F, Cohen J B and Chung Y-W 1998 *Phys. Rev.* **B 57** 13430

The Influence of Carbon Nanotube on the Cholesterol Domain: Molecular Dynamics Simulation

Z. Gburski[a], P. Raczyński

University of Silesia, Institute of Physics
Uniwersytecka 4, Katowice 40-007, Poland
[a] *zgburski@us.edu.pl*

The dynamics of cholesterol molecules embedded between phospholipids in a cell membrane as well as those forming an ultrathin layer (lodgment) around an extracellular domain protein has been studied via molecular dynamics (MD) simulations. We have also investigated the impact of an armchair (10, 10) carbon nanotube on the nanosystems studied. We have shown that the presence of a nanotube even quite close to the cell membrane does not destroy the structure of a cholesterol-phospholipide system i.e. it is neutral for the membrane functions. On the other hand, a carbon nanotube influences the motion of cholesterol molecules forming a layer developed over a protein surface.

EPR Study of Cr_2Te_3 Alloy

I. Stefaniuk, M. Bester, M. Kuźma[a]

Institute of Physics, Rzeszow University
Al. Rejtana 16c, 35-959 Rzeszow, Poland
[a]*kuzma@univ.rzeszow.pl*

AsNi crystals have attracted considerable attention due to a layered crystal structure which determines the peculiar electrical and magnetic properties of such materials (e. g. high temperature FeAs superconductivity [1, 2]). Cr-chalcogenides are a wide class of those crystals with a half-metal ferromagnetism perspective for spintronics. There are many crystal structures of these compounds such as $Cr_{1-x}Te$ [3] with various magnetic properties such as antiferromagnetism, non-colinar spin structures or itinerant ferro- magnetism [4]. Substitution of Cr atoms with Ti or V creates new properties such as spin-glass [5, 6]. Some chalcogenides such as CrTe or Cr Se) exhibit a metastable zinc-blende structure. Owing to that, it is possible to grow zinc-blende solid solution semiconductor compounds with the properties of diluted magnetic semiconductors (DMS), e. g. CrMnTe [7], ZnCrTe [8], ZnCrSe [9]. Recently Ko and Blamire [10, 11] have reported room-temperature ferromagnetism in CrCdTe crystals. We have observed this phenomenon, as well [12]. The origin of this ferromagnetism is not clearly understood yet, and the supposition that it may come from Cr2Te3 inclusions motivates the aim of this paper to study the magnetic resonance properties of this compound. The CrTe alloy was prepared by melting Cr_2Te_3 powder (Alfa Aesar, 99.5%) in evacuated quartz ampulae at the temperature of 1300–1340°C. The heating and cooling parameters are listed in Table 1. The ingot shows a porous, brittle structure consisting of fine grains. The structure of the samples was examined with optical and scanning electron microscopy.

Table 1: Cd_2Te_3 samples

Sample	Crystal	Melting temp. [°C]	Melting time	Cooling time
1	$Cr_{1-x}Te$	1300	1 h	3 h 15 min
2	$Cr_{1-x}Te$	1320	1 h	3 h 45 min
3	$Cr_{1-x}Te$	1340	30 min	4 h
4	Cr_2Te_3 powder	—	—	—

The EPR spectra were recorded using an X-band (9.4 GHz) spectrometer provided with a gas nitrogen cryostat (Oxford Instrument) with the nominally stabilizing temperature of the sample in the range of 77–500 K. The measurements were taken in the temperature range of 150–350 K. The temperature dependence of EPR spectra from samples no. 1 are collected in Figure 1.

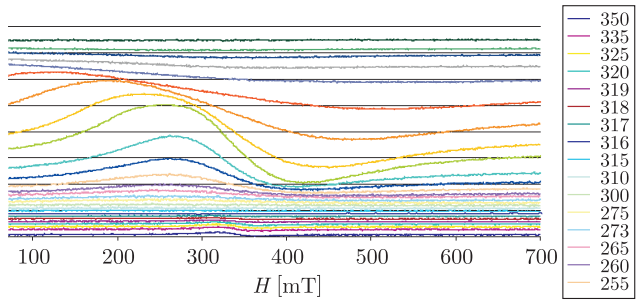

Figure 1: EPR spectra of CdTe for sample no. 1

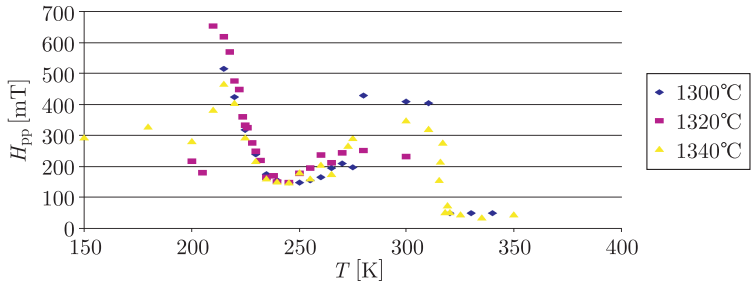

Figure 2: Linewidth dependence on temperature for samples 1, 2 and 3

As can be seen in Figure 1 the EPR line shape depends strongly on the temperature. The line is very wide and weak, and even totally disappears in the room temperature range. At lower temperatures, the shape of the lines approaches the Lorentz function. The asymmetry of the lines is also visible what can be attributed to strong exchange interactions. Above the room temperature, the shape of the spectra is characteristic for a paramagnetic phase. The linewidth dependence on the temperature is presented in Figure 2. There are two temperature ranges where the linewidth is constant: near 220 K and above the room temperature.

The g factor calculated value is 1.92. The factor increases considerably below the room temperature due to the internal field and the change is drastic below 220 K (see Figure 3). In Figure 4 we have compared the spectra of the alloy samples (nos. 1, 2 and 3) with those obtained for the Cr_2Te_3 powder (sample no. 4) which was the initial material for the alloy sample preparation. These spectra were recorded at room temperature. There is a great difference between the EPR line of sample no. 4 and those of samples nos. 1, 2 and 3. It probably indicates various Curie temperatures for these materials. At room temperature Cr_2Te_3 is in a paramagnetic state while the alloy phases exhibit ferromagnetic properties. Comparing the EPR spectra for samples nos. 1, 2 and 3 it can be concluded that the samples preparation technological parameters applied in this study do not have strong influence on the properties of the

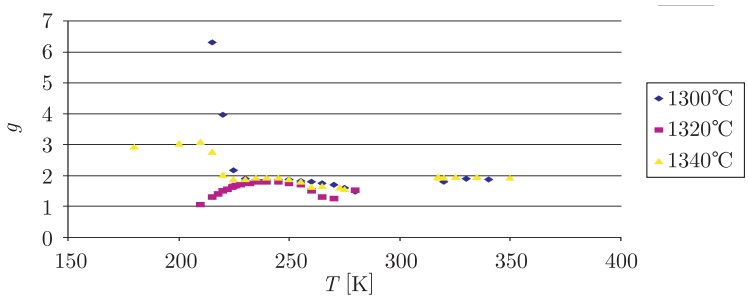

Figure 3: g factor dependence on temperature

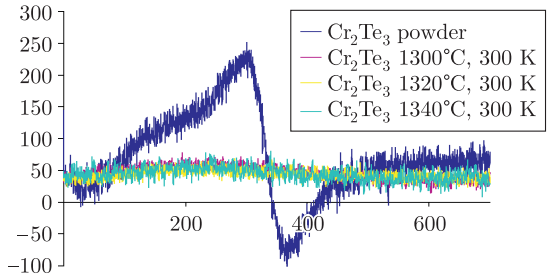

Figure 4: EPR spectra for Cr_2Te_3 powder (sample no. 4)

material. The results presented in the paper contribute to the new design of room temperature DMS materials.

References

[1] Kamihara Y, Watanabe T, Hirano M and Hosono H 2008 *J. Am. Chem. Soc.* **130** 3296
[2] Huang X arXiv:0805.0355v1 [cond-mat.str-el] 3 May 2008
[3] Chattopadhyay 1994 *J. Phase Equlibria and Diffusion* **15** 1547
[4] Shimada K, Saitoh T, Fujimori A, Ishida S, Asano S, Matoba M and Anzai S 1996 *Phys. Rev.* **B 53** 7673
[5] Ohta S 1985 *J. Phys. Soc. Jpn.* **54** 1076
[6] Makovetskii G and Dorofeichik S 2007 *Inorganic Materials* **43** 591
[7] Nakamura K, Freeman A J and Ito T 2005 *Phys. Rev.* **B 72** 064449
[8] Zhao L, Zhang B, Pang Q, Yang S, Zhang X, Ge W and Wang J 2006 *Apl. Phys. Lett.* **89** 092111
[9] Mac W, The Koi N, Twardowski A, Gaj and Demianiuk W 1993 *Phys. Rev. Lett.* **71** 2327
[10] Ko K Y and Blamire M G 2006 *Apl. Phys. Lett.* **88** 172101
[11] Ko K Y and Blamire M G 2006 *J. Korean Phys. Soc.* **49** 591
[12] Stefaniuk I, Bester M and Kuzma M 2008 *J. Phys.: Conf. Ser.* **104** 012010

Studies of Hydrogenation of Nanocarbon Materials

I. Pełech[1a], U. Narkiewicz[1], W. Arabczyk[1], M. Woźniak[2], K. J. Kurzydłowski[2]

[1] *Institute of Chemical and Environment Engineering*
Technical University of Szczecin
Pułaskiego 10, 70-322 Szczecin, Poland
[a] *ipelech@ps.pl*

[2] *Faculty of Materials Science and Engineering*
Warsaw University of Technology
Wołoska 141, 02-507 Warsaw, Poland

Carbon nanotubes can be synthesized by different methods. One of the effective methods is chemical vapor deposition (CVD) [1–12]. The preparation conditions are mild and the process is easy to control. This method can be also promising for industrial relevance. Carburisation of transition metals with hydrocarbons results in formation of carbon nanotubes. In addition to these forms, a significant amount of other carbon products, such as amorphous carbon, graphitic particles or catalyst traces are also formed. Carbon nanotubes are most often separated from catalyst traces using hydrofluoric acid [13, 14], hydrochloric acid [15, 16] or nitric acid [17]. The oxidation method has been applied to purify carbon nanotubes of carbon impurities [13, 14, 16, 18–21]. Amorphous carbon can be eliminated by oxidation in air flow [13, 14, 16, 18] or by oxidation by potassium permanganate [13, 14, 19], hydrogen peroxide [19–21], ozone [19], perchloric acid [19]. Another way of elimination of amorphous carbon is a hydrogenation process [22, 23].

In this work, the nanocarbon materials were obtained by catalytic decomposition of ethylene on nanocrystalline iron at 500°C and 5500°C. The increase in the carbon mass was controlled using the thermogravimetric method. The processes were carried out up to an increase in the carbon mass equal to about 0.7 gC/gFe. The samples after carburisation were analyzed using the HRTEM and X-ray diffraction methods. The samples contained iron carbide (cementite – Fe_3C) and nanocarbon materials (carbon nanofibers, carbon nanotubes and amorphous carbon). Crystallites of cementite were observed at the end of carbon nanofibers and nanotubes.

After the carburisation process the samples were cooled to the room temperature under a nitrogen flow or were reduced under a hydrogen flow and also cooled to the room temperature under a nitrogen flow afterwards. The hydrogenation process was carried out isothermally in the range of temperatures from 450°C to 520°C in order to remove the amorphous carbon and the thick carbon nanofibers. After carburisation followed by hydrogenation the samples were characterized using the X-ray diffraction method (Philips X'Pert) with CuKα radiation (λ = 0.15418 nm) and the HRTEM (High Resolution Transmission Electron Microscopy) method (Jeol JEM 3010). Some

carbon nanofibers were removed in the hydrogenation process. Multiwall carbon nanotubes about 10–30 nm in diameter remained. Iron carbide crystallites at the end of the fibrous carbon structure were not present any longer. Cementite crystallites were decomposed to iron and carbon. Iron crystallites were separated from the nanotubes.

The reduction process rate has been analyzed. At the beginning of hydrogenation an increase in the reaction rate is observed and the local maximum is reached at the carbon content of about 0.67 gC/gFe. After this local maximum, the reaction rate decreases and a second increase in the reaction rate is observed in the next step of the process until a maximum reaction rate is reached.

During a further reduction of the samples a decrease in the reaction rate is observed and the reaction rate drops to zero before complete carbon hydrogenation.

The reaction rate changes are connected probably with hydrogenation of different carbon forms. In the first stage, a total decrease in the carbon mass is equal to 0.07 gC/gFe. This value corresponds to the carbon/iron ratio in the stoichiometric Fe_3C. Then, in the first hydrogenation step, cementite is hydrogenated to metallic iron. After decomposition of cementite, carbon deposit hydrogenation is observed. A decrease in the reaction rate after the maximum in the first stage can be attributed to a decrease in the substrate (cementite) concentration.

The mass decrease growth rate together with a diminution of substrate concentration in the second stage can be explained by a catalytic effect of free iron [21] appearing as a result of carbon removal. Not covered with carbon, free iron atoms on the surface are the active sites for hydrogen dissociative adsorption. Next, hydrogen atoms react with carbon forming methane.

The proposed method of reduction of carbon deposits under a hydrogen flow can be applied for a controlled purification of multiwall carbon nanotubes of other carbon impurities The hydrogenation method could be preferable in comparison with oxidation because of easier process control in the former case.

References

[1] Hernadi K, Fonseca A, Nagy J B, Bernaerts D, Lucas A A 1996 *Carbon* **34** 1249
[2] Venegoni D, Serp P, Feurer R, Kihn Y, Vahlas C, Kalck P 2002 *Carbon* **40** 1799
[3] Zhou Z et al 2003 *Carbon* **41** 337
[4] Louis B, Gulino G, Vieira R, Amadou J, Dinzer T, Galvagno S, Centi G, Ledoux M J, Pham-Huu C 2005 *Catal. Today* **102–103** 23
[5] Gulino G, Vieira R, Amadou J, Nguyen P, Ledoux M J, Galvagno S, Centi G, Pham-Huu C 2005 *Appl. Catal. A: General* **279** 89
[6] Perez-Cabero M, Rodriguez-Ramos I, Guerrero-Ruiz A 2003 *J. Catal.* **215** 305
[7] Qian W, Liu T, Wang Z, Yu H, Li Z, Wei F, Lou G 2003 *Carbon* **41** 2487
[8] Park C, Keane A 2004 *J. Catal.* **221** 386
[9] Hafner J H, Bronikowski M J, Azamian B R, Nikolaev P, Rinzler A G, Colbert D T, Smith K A, Smalley R E 1998 *Chem. Phys. Lett.* **296** 195
[10] Qian W, Liu T, Wei F, Wang Z, Lou G, Yu H, Li Z 2003 *Carbon* **41** 2613
[11] Wang Y, Wu J, Wei F 2003 Carbon 41 2939
[12] Emmenegger C, Bonard J M, Mauron P, Sudan P, Lepora A, Grobety B, Züttel A, Schlapbach L 2003 *Carbon* **41** 539
[13] Colomer J F, Piedigrosso P, Fonseca A, Nagy J B 1999 *Synth. Met.* **103** 2482
[14] Biro L P et al 2002 *Mater. Sci. Eng. C* **19** 9
[15] Jeong T, Kim W, HahnY 2001 *Chem. Phys. Lett.* **344** 18
[16] ZhangY, Shi Z, Gu Z, Iijima S 2000 *Carbon* **38** 2055

[17] Couteau E, Hernadi K, Seo J W, Thien-Nga L, Miko Cs, Gaal R, Forro L 2003 *Chem. Phys. Lett.* **378** 9
[18] Gajewski S, Maneck H E, Knoll U, Neubert D, Dörfel I, Mach R, Strauß B, Friedrich J F 2003 *Diamond Related Mat.* **12** 816
[19] Hernadi K, Siska A, Thien-Nga L, Forro L, Kiricsi I 2001 *Solid State Ionics* **141–142** 203
[20] Ando Y, Zhao X, Inoue S, Iijima S 2002 *J. Cryst. Growth* **237–239** 1926
[21] Choi W K, Park S G, Takahashi H, Cho T H 2003 *Synth. Met.* **139** 39
[22] Hernadi K, Fonseca A, Nagy J B, Bernaerts D, Riga J, Lucas A 1996 *Synth. Met.* **77** 31
[23] Ivanov V, Fonseca A, Nagy J B, Lucas A, Lambin P, Bernaerts D, Zhang X B 1995 *Carbon* **33** 1727

Optical Spectroscopy of $Sr_4B_{14}O_{25}$:Nd^{3+} Single Crystal

B. V. Padlyak[1a], W. Ryba-Romanowski[2], R. Lisiecki[2], Yu. S. Oseledchik[3], A. V. Prosvirnin[3], D. P. Kudryavtcev[3], N. V. Svitanko[3]

[1] *Institute of Physical Optics*
23 Dragomanov Str. 79005 L'viv, Ukraine
[a] *bohdan@mail.lviv.ua*

[2] *Institute of Low Temperatures and Structure Research*
Polish Academy of Sciences
Okólna 2, 50-422 Wroclaw, Poland

[3] *Zaporizhya State Engineering Academy*
226 Lenin Ave., 69006 Zaporizhya, Ukraine

New un-doped and rare-earth doped $Sr_4B_{14}O_{25}$ single crystals have been obtained [1, 2]. According to [2], the structure of $Sr_4B_{14}O_{25}$ crystals can be described by the $Cmc2_1$ space group. Optical absorption, emission and luminescence kinetics of Nd^{3+} centres in the crystal with $Sr_4B_{14}O_{25}$:Nd ($Nd_2O_3 : SrO = 1 : 100$) chemical composition are investigated. The oscillator strengths (P) and phenomenological intensity parameters Ω_t (Ω_2, Ω_4, and Ω_6) for Nd^{3+} centres have been obtained using the standard Judd-Ofelt theory. The calculated Ω_t parameters, radiative transitions rates (W_r), branching ratios (β) and radiative lifetime ($\tau_{\rm rad}$) for Nd^{3+} centres in the $Sr_4B_{14}O_{25} : Nd$ single crystal have been analysed in comparison with the corresponding parameters obtained for Nd^{3+} centres in the glass with the same ($4SrO–7B_2O_3$) composition [3]. The measured lifetime is compared with the calculated one and quantum efficiency (η) for Nd^{3+} luminescence centres from the $^4F_{3/2}$ emitting level in the $Sr_4B_{14}O_{25}$:Nd crystal is estimated. Incorporation peculiarities, spectroscopic parameters and local structure of the Nd^{3+} luminescence centres in the $Sr_4B_{14}O_{25}$ single crystal and the corresponding glass with $4SrO–7B_2O_3$ composition have been considered and discussed on the basis of the obtained results and referenced [2, 3] data.

References

[1] Kudryavtcev D P, Oseledchik Yu S, Prosvirnin A L and Svitanko N V 2003 *J. Cryst. Growth* **254** 456
[2] Lapshin A E, Litovchik E O, Polyakova I G and Shepelev Yu F 2007 *Russian Journal of Inorganic Chemistry* **52** 839
[3] Kudryavtcev D P, Oseledchik Yu S, Prosvirnin A L and Svitanko N V 2003 *Ukr. J. Phys. Opt.* **4** 83

X-ray Study and Simulation of Atomic Structure of Liquid Al−Ni−Co Alloys

O. S. Roik[a], O. V. Samsonnikov, V. P. Kazimirov, V. E. Sokol'skii

Chemical Department, National Taras Shevchenko University of Kyiv
64 Volodymyrska str., Kyiv, UA-01033, Ukraine
[a]*sasha78@univ.kiev.ua*

Modern materials science is directed on preparation and examination of quasicrystalline (QC) metallic alloys, since they possess unique physical, chemical and mechanical properties. The main part of QC materials can be obtained from Al-based liquid binary Al−TM (TM – 3*d* transition metal) and ternary Al−TM_1−TM_2 alloys [1]. A comparison of a local atomic structure of liquid metallic alloys and the corresponding quasicrystalline (QC) phases as well as a systematic study of the structural prerequisites of QC formation are the most prominent directions to develop a scientific base for preparation of QC metallic alloys. The purpose of this work has been to perform a complex analysis of the structure of liquid ternary Al−Ni−Co alloys.

The study of the atomic structure of liquid ternary Al−Ni−Co alloys includes the following steps: a diffraction experiment with maximum possible accuracy, correct calculations of the structure factor ($S(Q)$) and the radial distribution functions of atoms $g(R)$, reconstruction of 3D-models of liquid alloys from the experimental SF using the Reverse Monte Carlo (RMC) method, and an analysis of the local and medium-range atomic ordering by means of Voronoi and Delaunay tessellations.

Liquid ternary $Al_{80}Ni_{10}Co_{10}$, $Al_{72.5}Ni_{13}Co_{14.5}$ and $Al_{65}Ni_{17.5}Co_{17.5}$ alloys have been studied by means of *X*-ray diffraction with a θ-θ diffractometer (MoK_α-radiation, $\lambda = 0.71069$ Å). The liquid $Al_{72.5}Ni_{13}Co_{14.5}$ alloy, the content of which coincides with the concentration range of QC phases formation, has been studied at 1473, 1533 and 1673 K. The X-ray diffraction experiments for liquid $Al_{80}Ni_{10}Co_{10}$ and $Al_{65}Ni_{17.5}Co_{17.5}$ alloys have been carried out at 1473 K. A prepeak in the $S(Q)$ functions at $1.1 < Q/\text{Å}^{-1} < 2.2$ has been found. The prepeak intensity reaches the maximum value for a liquid $Al_{72.5}Ni_{13}Co_{14.5}$ alloy but decreases significantly with increasing temperature.

The prepeaks registered in the structure factor for small Q-values are attributed to a medium-range order for Al-Co and Al-Ni binary liquid alloys [2, 3]. The partial structure factors obtained from the RMC models show that the prepeak has been realized on $a_{\text{NiNi}}(s)$, $a_{\text{NiCo}}(s)$ and $a_{\text{CoCo}}(s)$ curves. The prepeaks in the experimental structure factors for the liquid ternary alloys are caused by a correlated arrangement of TM atoms at a distance ranging from 4.2 to 4.4 Å. To estimate this correlation, we have used the empirical equation proposed by Ehrenfest: $S_\text{p} \cdot R_\text{p} = 1.23 \cdot 2\pi$, where Q_p is the prepeak position in $S(Q)$, R_p is the corresponding distance in $g(R)$. According

to the structure study results, the experimental structure factor prepeaks seem to be caused by a specific arrangement of TM atoms in dense packing polytetrahedral clusters. A detailed analysis of these clusters shows that their quantitative composition depends insignificantly on the stochiometric composition of the melt.

An analysis of partial RDF ($g_{\mathrm{NiNi}}(R)$, $g_{\mathrm{NiCo}}(R)$ and $g_{\mathrm{CoCo}}(R)$) denotes a more ordered local structure in a liquid $Al_{72.5}Ni_{13}Co_{14.5}$ alloy in comparison with liquid $Al_{80}Ni_{10}Co_{10}$, $Al_{65}Ni_{17.5}Co_{17.5}$ alloys. This result allows us to make a conclusion about a competition between Ni and Co atoms in the formation of Al coordination in liquid Al−Ni−Co alloys. A comparative analysis of the local structure in liquid binary Al−Ni, Al−Co and liquid ternary Al−Ni−Co alloys has been also performed.

References

[1] W. Steurer *Z. Kristallogr.* **219** (1) 391
[2] A. S. Roik, A. V. Samsonnikov, V. P. Kazimirov, V. E. Sokolski 2006 *J. Struct. Chem.* **47** (Suppl. 1) S167
[3] A. S. Roik, A. V. Samsonnikov, V. P. Kazimirov, V. E. Sokol'skii 2006 *Russ. Metall.* (*Metally*) (3) 206

Structure Changes in $In_{20.49}Ga_{66.96}Sn_{12.55}$ Eutectic Melt upon Alloying with Ni

S. Mudry, I. Shtablavyi[a]

Physics of Metals Department, Ivan Franko L'viv National University,
8 Kyrylo and Mephodii str., 79005 L'viv, Ukraine
[a]*sihor@ukr.net*

An $In_{20.49}Ga_{66.96}Sn_{12.55}$ eutectic melt shows a low melting point (292 K) and for that reason it is used as a matrix where small magnetic particles are distributed. Materials of this kind are known as ferrocolloidal suspensions whose magnetic properties permit us to use them in various areas of application. Unfortunately the stability of such a composite system is rather low which restricts the working characteristics.

We have carried out X-ray diffraction investigations in order to study structure changes in a liquid $In_{20.49}Ga_{66.96}Sn_{12.55}$ eutectic melt upon mixing with Ni-powder. The structure factors have been obtained for alloys with a different content of Ni (5, 10 and 15 at. % Ni). The main structure parameters estimated from these curves have been analyzed by being compared with the relative parameters for various phases which can be formed upon solidification of a composite system. The structure factors have been also used in calculations of pair correlation functions.

It is also shown that an addition of Ni-powder to an $In_{20.49}Ga_{66.96}Sn_{12.55}$ eutectic melt is accompanied by formation of chemically ordered microdomains on the base of Ga_3Ni_2, GaNi, In_3Ni_2, InNi, Ni_3Sn_2 chemical compounds.

It is the possible aggregation of such structural microdomains that can be responsible for the degradation of the main characteristics with time.

Properties of Star-branched Copolymers. A Monte Carlo Simulation Study

A. Sikorski[a], D. Gront, K. Charmuszko

Department of Chemistry, University of Warsaw
Pasteura 1, 02-093 Warsaw, Poland
[a]*sikorski@chem.uw.edu.pl*

An idealized coarse-grained model of polymer chains has been designed and studied. The chains have consisted of united atoms (segments) which positions have been restricted to a hybrid [310] lattice. The model macromolecules have been star-branched chains consisting of two kinds of polymer segments defined as hydrophilic and hydrophobic. The force field used had consisted of the long-range contact potential between a pair of non-bonded segments and of a local stiffness. In order to study the properties of the model chain we have used some variants of the Monte Carlo method: the Replica Exchange method, the Pruned-Enriched Rosenbluth Method (PERM) and the Wang-Landau method. The static properties and structure of model chains in a wide range of solvent conditions have been studied. A thermodynamic description of the coil-to-globule transition has been made. The influence of the number of arms on the process of their self-assembly has been shown and discussed.

Physical-Chemical Features of Ultrasonic Modification of Porous and Electronic Structures of Carbon Materials

B. Ya. Venhryn[1a], I. I. Grygorchak[1], S. I. Mudry[2b], I. V. Typilo[1]

[1] *L'viv Polytechnic National University*
12 St. Bandera str., L'viv, 79013, Ukraine
[a] *venhryn_b@ukr.net*

[2] *Ivan Franko L'viv National University*
8 Kyrylo and Mephodii str., 79005 L'viv, Ukraine
[b] *mudry@physics.wups.lviv.ua*

It is known that a significant increase in energy accumulation and storage in molecular energy storage devices can be reached by a combination of an optimal porous structure with the corresponding electron distribution resulting in the Helmholtz capacity deblocking by the volume charge capacity. Chemical methods can be useful for the porous structure modification but at the same time the electronic structure is in fact unchangeable. Ultrasonic radiation treatment is proposed in order to achieve accordance between the controlled porous structure and the corresponding electronic distribution.

Different kinds of activated carbon used in experiments were obtained by means of activational carbonization of initial raw materials of a various nature: phenotic resin (PhR), fruit stones (FS), wood coal (WC) and carbon nanotubes (CNT). Ultrasonic treatment at a frequency of 22 kHz was carried out using a special ultrasonic powder distributing device under water and heptan conditions. Aqueous (7.6 m KOH) and unaqueous (1 M $(C_2H_5)_4NBF_4$ in CH_3CN) solutions were used as the electrolyte systems for molecular energy storages.

The precisional porometry method and the small angle X-ray scattering method were applied to investigate their porous structure; ASAP 2000 M porometer and DRON-3 diffractometer were used, respectively. Galvanostatic, potentiodynamic, faradvolt and impedance (within the frequency range of 10^{-2}–10^5 Hz) dependences were determined with the help of an "AUTOLAB" device equipped with FRA-2 and GPES programs manufactured by "ECO CHEMIE" (the Netherlands).

The results, obtained in this work have allowed us to establish the fact that nanoporous carbon modification depends to a significant extent on the ultrasonic irradiation parameters as well as on the nature of the initial raw material. It should be also noted that a specific capacitance change in comparison with the initial material shows significantly different behaviour in aqueous and unaqueous electrolyte solutions. Using the small angle X-ray diffraction data it is confirmed that ultrasonic

irradiation effects mostly the changes of the electronic structure of the near-surface layers in comparison with the material's volume. Other experimental methods such as secondary ion mass spectrometry (SIMS) and impedance spectroscopy (IS), showing the influence of ultrasonic treatment parameters on the Fermi level position, also confirm these suggestions.

The obtained data have allowed us to reveal that a significant improvement in the capacity characteristics in case of PhR, FS and WC is observed when ultrasonic treatment is carried in water. For instance, the most optimal values of specific capacitance for WC can be reached by ultrasonic irradiation during 20 min in 50 ml H_2O. The increase in the specific capacitance in 7.6 m KOH is higher by 2 in comparison with the initial value. Following the ultrasonic treatment of carbon materials obtained from FS, the specific capacitance is in fact unchangeable. An increase in the specific capacitance in an organic electrolyte is observed only upon treatment during 5 min in 100 ml H_2O the 25%, whereas a 20% decrease in the specific capacitance occurs under the same conditions (but treated in heptane). In respect of PhR a reduction of the specific capacitance is observed with various ultrasonic treatment parameters. It should be noted that the behaviour in case of CNT is different. A significant improvement is observed when the dispersive medium is heptane. The modified material obtained in this way shows better properties in an organic electrolyte. The proposed method, used for CNT, permits to increase the specific capacitance by 30%. It should be noted that the mass of the initial material, which was exposed by ultrasonic treatment, was equal to 0.5 g in all the considered cases.

Using the obtained data it can be concluded that ultrasonic irradiation is an effective controlled modification method for porous and electron structures of carbon materials. This method permits to significantly improve the capacitive and other working characteristics of molecular energy storages produced from modified materials.

POSTERS

Tensile Strength of Carbon Nanotubes

M. Białoskórski[1, 2a], J. Rybicki[1, 2b, 3]

[1] *Department of Solid State Physics*
Faculty of Technical Physics and Applied Mathematics
Gdansk University of Technology
Narutowicza 11/12, 80-952 Gdansk, Poland

[2] *TASK Computer Centre, Gdansk University of Technology*
Narutowicza 11/12, 80-952 Gdansk, Poland
[a] *skorka@task.gda.pl,* [b] *ryba@task.gda.pl*

[3] *Institute of Mechatronics, Nanotechnology and Vacuum Techniques*
Koszalin University of Technology
Racławicka 15–17 F, 75-620 Koszalin, Poland

Extensive classical Molecular Dynamics simulations of the tensile strength of single-walled carbon nanotubes have been performed using the AIREBO force field.

About 230 nanotubes with radii ranging from 2.1 Å (a $(0, 5)$ nanotube) to 13.3 Å (a $(20, 20)$ nanotube) have been simulated systematically and the dependence of their tensile strength and stiffness moduli on the nanotubes' radii has been determined. It turns out that (n, n) nanotubes are mechanically more resistant than $(n, 0)$ nanotubes.

Acknowledgements
This work was supported by the Ministry of Science and Higher Education grant no. N519 024 32/3053. The simulations have been performed at the TASK Computer Centre, Gdansk, Poland.

The Structural Self-organization and Electrical Properties of Bicontained Thin Films

V. I. Bilozertseva[1a], H. M. Khlyap[2],
N. L. Dyakonenko[1], D. A. Gaman[1]

[1] *National Technical University "Kharkov Polytechnical Institute", 21 Frunze str., Kharkov, 61002 Ukraine*
[a] *biloz@mail.ru*

[2] *University of Technology, 11 Diestel str. Kaiserslautern, 67657, Germany*

Investigations of multicomponent solid compounds allow us to expand the possibilities of their practical applications in modern electronics as replacements of elemental and binary materials. Amorphous chalcogenide semiconductor thin films containing alkali metals make it possible to vary the physical and chemical properties in a wide range. Bi-contained materials are not only considered to be attractive for structural studies (the question is still almost open), but also as a subject of electric investigations. These properties have not been studied until recently.

The present abstract describes some structural peculiarities of amorphous Li-Bi-Se thin films (40–100 nm thick) grown on glass substrates by the resistive evaporation technique and demonstrates their electric field-induced characteristics for the first time.

Layers were deposited under substrate temperatures of 300 K and 400 K. The deposition rate was estimated to be 0.1–0.5 nm/s. The electron-diffraction investigation demonstrated the layers' amorphous structure. The transmission electron microscopy and diffraction methods applied to study the films showed the crystal structure of films to have a cubic lattice of the bulk compound at $T_s = 400$ K.

The film's surface is sufficiently inhomogeneous, consisting of two structural units: globules and clusters. The surface of the $LiBi_3Se_5$ films is different: apart from the globules and clusters, their relief consists of micro crystals. Diffraction patterns observed in the images indicate the amorphous structure of layers. Polycrystalline $LiBi_3Se_5$ films were obtained under condensation at the substrate temperature of 400 K. Crystallization is connected with increased temperature of the substrate. As Ts increases, the mobility of atoms absorbed on the substrate also increases, resulting in the crystallization energy barrier being overcome. Even a small 3 K increase of the substrate temperature (40–600 K) due to focusing the electron beam causes the growth of separate needle-like crystallites, which means that a self-organization process taking place.

Electrical measurements were carried out under applied electric field of up to $4 \cdot 10^4$ V/m. An analysis of the experimental current-voltage characteristics has exhibited a quasi-tunneling mechanism of carrier transport: a two-step process under

direct applied voltage and one-step transfer under reverse direction. These results suggest a considerable effect of the layer structure on carrier transport.

Thus, amorphous and polycrystalline Li-Bi-Se thin films of various composition were prepared by the resistive evaporation technique from a quasi-closed volume. Condensation on glass substrates at various temperatures of the substrate (300 K and 400 K) made it possible to obtain amorphous $LiBiSe_2$ films and polycrystalline $LiBi_3Se_5$ layers. The amorphous films' surface was globule-and-cluster in character. Room-temperature current-voltage characteristics of the amorphous films demonstrated tunneling and space charge-limited currents due to peculiarities of the film surface.

Wave Function and Spectrum of an Electron in a Two-layer Ellipsoidal Quantum Dot

V. I. Boichuk, V. B. Hols'kyi[a], I. S. Shevchuk, M. M. Romans'kyi

Ivan Franko Drohobych State Pedagogical University
Department of Theoretical Physics
Stryis'ka 3, Drohobych 82100, Ukraine
[a]*hol.wit@gmail.com*

The process of research of low-dimensional structures opens new prospects in creation of semiconductor lasers, memory elements and one-electron transistors. Quantum dots (QDs) in which particles are confined in three directions are most interesting for investigation. Many theoretical studies consider quantum dots modelled by spherical quantum wells [1–2]. In [3], nanocrystal shape-dependent quasiparticle energy levels have been analysed in spherical, cylindrical and cubic QDs. A QD is not always cubic, cylindrical or spherical in real physical situations. An ellipsoidal QD which can be considered spherical or cylindrical occurs more often under certain conditions. A theoretical research of ellipsoidal QDs is completed in [4–5]. The energy spectrum of a charged particle and an exciton is found. The influence of polarization effects on a quasi-particle spectrum is investigated.

An electron energy spectrum in a twolayer ellipsoidal QD in the infinite band mismatch approximation at the separation boundary of the media is found in the report. The heterostructure is modelled with a quantum well confined with two ellipsoids of rotation. The problem is solved in prolate spheroidal coordinates. In the effective mass approximation the Hamiltonian of the system is written:

$$\hat{H} = -\frac{\hbar^2}{2m_e}\nabla^2 + U(\xi),$$

where m_e is the electron effective mass.

The wave function form is found which makes it possible to study the quasiparticle location probability. Also the energies of the ground and excited states in a twolayer ellipsoidal QDs dependent on focal distances and parameters ξ_1, ξ_2 that determine the QD region are investigated. Specific calculations are performed for the structures GaAs/InAs/GaAs and glass/CdSe/glass.

References

[1] Efros Al. L., Efros A. L. *Fiz. I Tekhn. Poupr.* 1982 **16** (1982) 7, 1209–1214
[2] Boxchuk V. I., Hols'kyi V. B. *Journal of Physical Studies* **8** (2004) 3, 122–126
[3] Boichuk V. I., Hols'kyi V. B. *Fiz. i Khim. Tverd. Tila* **1** (2007) 82–87
[4] Cantele G., Ninno D. and Iadonisi G., *Nano Letters* **1** (2001) 3, 121–124
[5] Leon H., Marin J. L., Riera R. *Physica* **E 27** (2005) 385–396

Mathematical Modelling Diffusion of Radioactive Particles in Regular Structures

Ye. Chaplya[1,2], O. Chernukha[1]

[1] *Centre of Mathematical Modelling of Pidstryhach Institute of Applied Problems of Mechanics and Mathematics of Ukrainian NAS J. Dudayev Str. 15, 79005 L'viv, Ukraine*

[2] *Kazimierz Wielki University in Bydgoszcz Chodkiewicza 30, 85-064 Bydgoszcz, Poland*

Decaying admixture diffusion processes in a body of a two-phase periodical stratified structure are studied. An exact solution of the problem is found. Concentration distributions regularities depending on the migrating substance decay intensity coefficient values are studied.

One of the actual problems today is to describe and analyse mass transfer processes in piecewise homogeneous spatially regular systems. Polycrystalline materials or fine-dispersed composite structures are often modelled by such structures. Moreover, diffusing particles in distinct areas of the system are characterized by essentially different diffusion coefficients and there is a mass exchange between the areas [1–3].

Exact solutions of diffusion initial-boundary value problems in bodies with regular structures have been developed for a non-decaying substance in the paper [4, 5]. A similar problem for a decaying admixture is considered in this work. An exact solution of the corresponding contact initial-boundary value problem of diffusion is found. Mass flows in the contacting area are defined. An exact solution of the Fisher problem is also obtained by the limiting process as well as a set of equations of decaying particle diffusion by two ways in the continuum approximation.

Let a layer x_0 in thickness consist of two distinct periodically disposed areas perpendicular to the layer surfaces (Fig. 1a). Let it be assumed that areas with diffusion coefficient D_1 are $2L$ in width and the width of areas with coefficient D_2 is $2l$. As long as such a structure has a family of symmetry planes ($y = \pm n(L + l)$, $n = 0$, 1, 2,...) a diffusion in a body element on the vertical boundaries of which the mass fluxes equal zero in the direction of Oy-axis can be considered (Fig. 1b).

Decaying admixture concentrations $c_1(x, y, t)$ in the area $\Omega_1 =]0; x_0[\times]0; L[$ and $c_2(x, y, t)$ in the area $\Omega_2 =]0; x_0[\times]L; L + l[$ are determined from the equations

$$\frac{\partial c_i}{\partial t} = D_i \left[\frac{\partial^2 c_i}{\partial x^2} + \frac{\partial^2 c_i}{\partial y^2} \right] - \lambda c_i, \qquad x, y \in \Omega_i, \quad i = 1, 2, \tag{1}$$

where λ is the intensity coefficient of the admixture particle decay.

Let assume zero initial conditions be assumed:

$$c_1(x, y, t)|_{t=0} = c_2(x, y, t)|_{t=0} = 0. \tag{2}$$

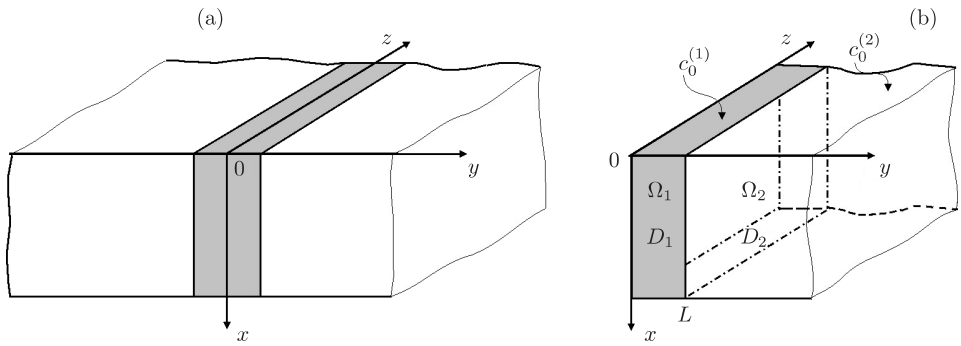

Figure 1: (a) A body structure; (b) a separated body element of such structure

The values of concentrations for $t > 0$ constant are:

$$c_1(x,y,t)|_{x=0} = c_0^{(1)} \equiv const, \qquad c_2(x,y,t)|_{x=0} = c_0^{(2)} \equiv const; \tag{3}$$

$$c_1(x,y,t)|_{x=x_0} = c_2(x,y,t)|_{x=x_0} = 0; \quad \left.\frac{\partial c_1(x,y,t)}{\partial y}\right|_{y=0} = \left.\frac{\partial c_2(x,y,t)}{\partial y}\right|_{y=L+l} = 0. \tag{4}$$

Conditions of non-ideal contact formulated for functions of concentrations

$$k_1 c_1(x,y,t)|_{y=L} = k_2 c_2(x,y,t)|_{y=L}\,; \quad \rho_1 D_1 \left.\frac{\partial c_1(x,y,t)}{\partial y}\right|_{y=L} = \rho_2 D_2 \left.\frac{\partial c_2(x,y,t)}{\partial y}\right|_{y=L}, \tag{5}$$

are imposed on the contact surface $y = L$ where k_1 and k_2 ($k_1 \neq k_2$) are coefficients of the concentrating dependence of chemical potentials in the areas Ω_1 and Ω_2, ρ_1 and ρ_2 are the densities of those areas.

A solution of the problem (1)–(5) is found by integral transformations over space variables outside the contacting areas Ω_1 and Ω_2 [4, 5]. At first the finite Fourier sine transform is applied with respect to variable x ($x \to x_n = n\pi/x_0$, $n = 1, 2, \ldots$; $c_i(x,y,t) \to \tilde{c}_i(n,y,t)$, $i = 1, 2$). Then, the values of mass flows on the contact boundary are redefined by the second contact condition

$$\rho_1 D_1 \left.\frac{\partial \tilde{c}_1(n,y,t)}{\partial y}\right|_{y=L} = \rho_2 D_2 \left.\frac{\partial \tilde{c}_2(n,y,t)}{\partial y}\right|_{y=L} = g(n,L,t) \equiv g(t) \tag{6}$$

and the finite Fourier cosine transform is applied with respect to variable y in the area Ω_1: $y \to y_k = k\pi/L$, $k = 0, 1, 2, \ldots$; $\tilde{c}_1(n,y,t) \to \hat{c}_1(n,k,t)$ and cosine transform with a shift $(y - L)$ is applied in the area Ω_2: $y \to y_m = m\pi/l$, $m = 0, 1, 2, \ldots$; $\tilde{c}_2(n,y,t) \to \hat{c}_2(n,m,t)$. Having obtained solutions of ordinary differential equations, the unknown function $g(t)$ is found from the first contact condition of the concentration jump on the interphase.

Finally,

$$c_1(x,y,t) = c_0^{(1)} \left(1 - \frac{x}{x_0}\right) - \frac{2}{x_0} \sum_{n=1}^{\infty} \sin(x_n x) e^{-D_1(x_n^2+\lambda)t} \left\{ \frac{c_0^{(1)}}{x_n} D_1 -\right.$$

$$-\frac{1}{\rho_1 L}\int_0^t g(t')e^{D_1(x_n^2+\lambda)t'}dt' + \frac{2}{\rho_1 L}\sum_{k=1}^{\infty}(-1)^k e^{-D_1 y_k^2 t}\cos(y_k y)\int_0^t g(t')e^{D_1(x_n^2+y_k^2+\lambda)t'}dt'\Bigg\}, \tag{7a}$$

$$c_2(x,y,t) = c_0^{(2)}\left(1-\frac{x}{x_0}\right) - \frac{2}{x_0}\sum_{n=1}^{\infty}\sin(x_n x)e^{-D_2(x_n^2+\lambda)t}\left\{\frac{c_0^{(2)}}{x_n}D_2 -\right.$$

$$\left.-\frac{1}{\rho_2 l}\int_0^t g(t')e^{D_2(x_n^2+\lambda)t'}dt' + \frac{2}{\rho_2 l}\sum_{m=1}^{\infty}(-1)^m e^{-D_2 y_m^2 t}\cos(y_m y)\int_0^t g(t')e^{D_2(x_n^2+y_m^2+\lambda)t'}dt'\right\}, \tag{7b}$$

are obtained where

$$g(t') = \frac{x_n\left\{k_2 c_0^{(2)}D_2 e^{-D_2(x_n^2+\lambda)(t-t')} - k_1 c_0^{(1)}D_1 e^{-D_1(x_n^2+\lambda)(t-t')}\right\}}{k_1 e^{-D_1(x_n^2+\lambda)(t-t')}/(\rho_1 L) + k_2 e^{-D_2(x_n^2+\lambda)(t-t')}/(\rho_2 l) + 2S_n(t-t')}, \tag{8}$$

$$S_n(t-t') = \sum_{j=1}^{\infty}\left[\frac{k_1}{\rho_1 L}e^{-D_1\left(x_n^2+\lambda+(j\pi/L)^2\right)(t-t')} - \frac{(-1)^j k_2}{\rho_2 l}e^{-D_2\left(x_n^2+\lambda+(j\pi/l)^2\right)(t-t')}\right]$$

and $L_1 = L$, $L_2 = l$.

The obtained analytical expressions (7) and (8) give an opportunity to find admixture mass flows through the layer.

It should be noted that when the functions of concentration $c_i(x,y,t)$ are averaged over the whole width of the body element $[0; L+l]$ and certain physically justified dependences are assumed between mass fluxes and chemical potentials on a contact surface, a set of mass transfer equations is obtained by two ways in the continuum approximation [6].

Moreover the following natural dimensionless variables can be used with respect to the problem (1)–(5) and the equations of heterodiffusion by two ways:

$$\tau = \hat{k}_2 t, \quad \xi = \left(\hat{k}_2/D_1\right)^{1/2}x, \quad \eta = \left(\hat{k}_2/D_1\right)^{1/2}y, \tag{9}$$

where $\hat{k}_2$ is a parameter characterizing the particle transition from slow into quick diffusion.

If the width of area Ω_2 is set closer to infinity $l \to \infty (L \neq 0)$ in the relationships (1)–(8), the Fisher problem [3, 7] is obtained for a layer modeling diffusion of decaying particles in a polycrystal along the grain boundary.

A numerical analysis shows that if a substance decay process is allowed, this can be lead to qualitative changes in the behaviour of concentration functions in layer structural elements.

It should be also remarked that the proposed method for finding an exact solution of contact initial-boundary value problems of decaying substance diffusion does not impose any restrictions on the sizes of contacting areas. Hence, it can be suitable both for bodies with comparable sizes of contacting regions and in cases when one area width is much larger(or smaller) than another.

Finally, it should be noted that taking into account the form of equations (1)–(5), solutions of the mass transfer problem in horizontally periodical structures can be

used for studying heat transfer processes in such bodies considering the conditions of ideal contact as a partial case of the one presented in the work.

Acknowledgements The work is supported by Project No 0107U009406 of DFFD, Ukraine.

References

[1] *Physical Metallurgy* 1965 Edited by R.W.Cahn, North-Holland Publ. Comp., Amsterdam
[2] Nechayev Y. S. 1979 "To the question on interpretation of some heterodiffusion anomalies in metals" *Reports of Academic Institutions*, Iron Ind., **3** 89–92.
[3] Lyubov B. Y. 1981 *Diffusion processes in nonhomogeneous media* Nauka, Moscow
[4] Chaplya Y. Y., Chernukha O. Y. 2002 "Diffusion processes in a body with periodical structure" *Math. methods and physico-mechanical fields* **45** (4) 124–131
[5] Chernukha O. 2005 "Admixture mass transfer in a body with horizontally periodical structure" *Int.J.Heat and Mass Transfer* **48** 2290–2298
[6] Chaplya Y. Y., Chernukha O. Y. 2003 *Physical-mathematical modelling heterodiffusive mass transfer* SPOLOM, L'viv
[7] Fisher J. C. 1951 "Calculation of diffusion penetration curves for surface and grain boundary diffusion" *J. Appl. Phys.* **22** 74–77

On Electromechanical Coupling in Thin Dielectric Films

Ye. Chaplya[1,2], V. Kondrat[1], O. Hrytsyna[1], S. Kondrat[3]

[1] *Center of Mathematical Modeling*
Institute of Applied Mathematics and Mechanics, NAS of Ukraine
Dudajeva 15, 79005 L'viv, Ukraine

[2] *Kazimierz Wielki University*
Institute of Environmental Mechanics and Applied Computer Science
Chodkiewicza 30, 85-064 Bydgoszcz, Poland

[3] *Max Planck Institut fur Metallforschung*
Heisenbergstrasse 3, D-70569 Stuttgart, Germany

The linearized classical theory of piezoelectrics does not take into account the interaction between mechanical and electromagnetic fields in isotropic materials [1, 2]. One of the first attempts to take such an interaction into account has been made in Ref. [3] where the parameters space which describes the state of a dielectric has been extended to contain the tensors of induced charges and electromagnetic stresses in addition to the usual parameters such as temperature, strain tensor and mechanical stresses [3]. In Ref. [4] a gradient model of piezoelectrics has been proposed in which it is assumed that the state of a dielectric depends on the polarization vector gradient. The model modified in this way describes correctly the anomalous dependence of a thin dielectric layer's capacitance on its thickness [5], observed experimentally by Mead [6]. It predicts the electric potential's non-linear distribution and polarization in thin dielectric films [5].

Recently, it has been proposed [7, 8] to take into account the local mass displacement effect in order to describe correctly the electro-magneto-thermo-mechanical processes in polarized solids; the reason for the local mass displacement is the ordering of the molecular structure of a solid. The local mass displacement leads to an extension of the parameters space and to additional bulk ponderomotive forces. Now, two additional pairs of parameters are introduced to describe the local thermodynamic state of a dielectric: (i) the specific density of induced mass ρ_m and the reduced potential, $\mu'_\pi = \mu_\pi - \mu$, where μ_π is the energy measure of the influence of the mass displacement on the internal energy and μ is the chemical potential, and (ii) the vector $\boldsymbol{\pi_m}$ of specific mass displacement and the gradient of the reduced potential $\nabla\mu'_\pi$.

The basic set of equations for a non-ferromagnetic, isotropic, polarized medium, expressed in terms of the displacement vector $\mathbf{u}$, magnetic induction $\mathbf{B}$, electric field $\mathbf{E}$ and the function μ'_π is [7] (we have used the isothermic approximation and neglected the irreversibility of the local mass and charge displacements):

$$\rho_0 \frac{\partial^2 \mathbf{u}}{\partial t^2} = \left(a_1^\sigma + a_2^\sigma - \frac{a_{e\rho}^2}{\rho_0 a_\rho^\mu} \right) \nabla \left(\nabla \cdot \mathbf{u} \right) + a_2^\sigma \Delta \mathbf{u} + \frac{a_{e\rho}}{a_\rho^\mu} \nabla \tilde{\mu}'_\pi + \rho_0 \mathbf{F},$$

$$\nabla\cdot\mathbf{B}=0,\quad \nabla\times\mathbf{E}=-\frac{\partial\mathbf{B}}{\partial t},\quad \nabla\cdot\left[\left(\varepsilon_0-\rho_0 a_E^p\right)\mathbf{E}-\rho_0 a_{E\mu}\nabla\tilde{\mu}'_\pi\right]=\rho_e,$$

$$\nabla\times\mathbf{B}=\mu_0\sigma_e\mathbf{E}+\mu_0\left(\varepsilon_0-\rho_0 a_E^p\right)\frac{\partial\mathbf{E}}{\partial t}-\rho_0\mu_0 a_{E\mu}\frac{\partial\nabla\tilde{\mu}'_\pi}{\partial t},$$

$$\Delta\tilde{\mu}'_\pi+\frac{1}{a_\mu^\pi a_\rho^\mu}\tilde{\mu}'_\pi=\frac{1}{a_\mu^\pi a_\rho^\mu}\frac{a_{e\rho}}{\rho_0}\nabla\cdot\mathbf{u}-\frac{a_{E\mu}}{a_\mu^\pi}\nabla\cdot\mathbf{E}, \tag{1}$$

where ε_0 and μ_0 are the electric permittivity and magnetic permeability of vacuum (electric and magnetic constants), ρ_e is the density of free electric charges and ρ_0 is the mass density in the reference state, t is the time, a_1^σ, a_2^σ, σ_e, a_ρ^μ, a_E^p, a_μ^π, $a_{e\rho}$, and $a_{E\mu}$ are material parameters, $\tilde{\mu}'_\pi=\mu'_\pi-\mu'_{\pi0}$, $\mu'_{\pi0}$ is the reduced potential μ'_π in the reference state, and ∇ is the nabla operator.

It is worth noting that if we exclude the function μ'_π from the set of equations (1), we obtain a set of non-local linearized equations for a polarized isotropic medium which takes into account the interaction between the mechanical and electrical processes.

As an example, we apply the above-mentioned equations to the investigation of coupled electromechanical fields in a thin dielectric film. Let us consider a dielectric layer placed between $x=\pm l$. The electric potential $\varphi=\pm V$ is kept fixed on the corresponding surfaces of the dielectric. From the set of equations (1), and using the appropriate boundary conditions (see Refs. [2, 5]), we obtain for the inverse capacitance C^{-1}, electric potential φ, and polarization p:

$$C^{-1}=\frac{2l}{\varepsilon_0\left(1+\chi\right)}\cdot\frac{1+\chi\left(\lambda_* l\right)^{-1}\operatorname{tgh}\left(\lambda_* l\right)}{1+k\chi\left(\lambda_* l\right)^{-1}\operatorname{tgh}\left(\lambda_* l\right)}, \tag{2}$$

$$\varphi(x)=V\frac{x}{l}+V\left(k-1\right)\frac{1}{1+\chi^{-1}\lambda_* l\coth\left(\lambda_* l\right)}\left[\frac{x}{l}-\frac{\sinh\left(\lambda_* x\right)}{\sinh\left(\lambda_* l\right)}\right], \tag{3}$$

$$p(x)=-\chi\frac{\varepsilon_0}{\rho_0}\frac{V}{l}-\chi\frac{\varepsilon_0}{\rho_0}\frac{V}{l}\left(k-1\right)\frac{1+\chi^{-1}\lambda_* l\cosh\left(\lambda_* x\right)\sinh^{-1}\left(\lambda_* l\right)}{1+\chi^{-1}\lambda_* l\coth\left(\lambda_* l\right)}, \tag{4}$$

where χ is the dielectric susceptibility, k is a phenomenological constant, $0\leqslant k\leqslant 1$ [1, 5], and

$$\lambda_*^2=-\frac{1}{a_\rho^\mu a_\mu^\pi}\left[1+\frac{a_{e\rho}^2}{\rho_0 a_\rho^\mu}\cdot\frac{1}{a_1^\sigma+2a_2^\sigma-a_{e\rho}^2/\left(\rho_0 a_\rho^\mu\right)}\right]\left[1-\frac{\rho_0 a_{E\mu}^2}{a_\mu^\pi\varepsilon_0\left(1+\chi\right)+\rho_0 a_{E\mu}^2}\right]>0$$

We have taken advantage of the fact that $a_E^p=-\chi\varepsilon_0/\rho_0$ and $a_\rho^\mu a_\mu^\pi<0$. The quantity $1/\lambda_*$ has a length dimension and describes characteristic distances of the problem in question.

The results of our calculations are shown in Fig. 1. The solid lines are obtained using Eq. (2) while the dashed lines correspond to the classical theory of piezoelectrics. As can be seen, the linear part of the plot in Fig. 1a is well above the curve obtained from the classical theory which is in agreement with the experimental results [6].

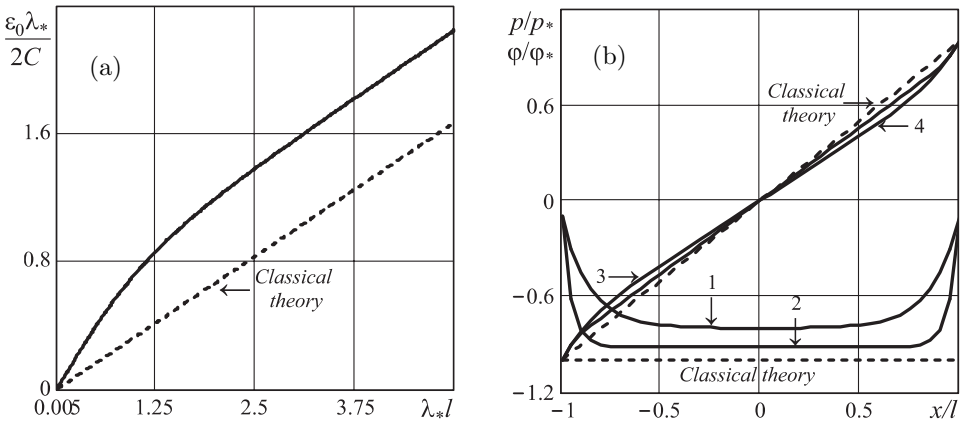

Figure 1: (a) Dependence of capacitance on film thickness; the solid line is obtained using Eq. (2) and the dashed line corresponds to the classical theory; (b) the polarization (curves 1 and 2) and the electric potential (curves 3 and 4) as functions of the distance x/l for $\lambda_* l = 5$ (curves 1 and 3) and $\lambda_* l = 20$ (curves 2 and 4), the line code as in (a)

Figure 1b illustrates the non-linearity of the polarization (curves 1 and 2) and the electric potential (curves 3 and 4) in films of different thicknesses (curves 1, 3 and 2, 4 correspond to $\lambda_* l = 5$ and $\lambda_* l = 20$, respectively). We note that similar results have also been obtained by [4, 5] who have used the gradient model of piezoelectrics.

Using the present approach (described in detail in Refs. [7, 8]), the stress-strained state of a dielectric film, the surface polarization and the charge, the disjoining pressure and their dependence on the film thickness and material characteristics have also been studied. The solutions of the corresponding boundary problems have been used to calculate the lateral force which appears in films of a varying thickness. We note that also the irreversibility of local displacement of mass is taken into account. It has also been shown that the disjoining pressure and lateral forces can highly influence the strength and stability of thin films in which non-uniform surface regions intersect. We have also shown that the formation of a new surface in a dielectric leads to an electromagnetic "signal" which can be used, for instance, for passive (electromagnetic) diagnostics of constructions built from dielectric materials.

References

[1] Landau L. D. and Lifshitz E. M., 1984, *Electrodynamics of Continuous Media*. Pergamon, Oxford
[2] Nowacki W., 1983, *Efekty elektromagnetyczne w stałych ciałach odkształcalnych* Warszawa: Panstwowe Wydawnictwo Naukowe
[3] Burak Ya., 1967, *J. Materials Science* **2** (1), 40–44.
[4] Mindlin R. D., 1968, *Int. J. Solids and Structures* **4**, 637
[5] Mindlin R. D., 1969, *Int. J. Solids and Structures* **5**, 1197–1208
[6] Mead C. A., 1961, *Physical Review Letters*, **6** (10), 545–546
[7] Burak Ya. I., Kondrat V. F., and Hrytsyna O. R., 2007, *Materials Science* **43** (4), 449–463
[8] Burak Ya., Kondrat V., and Hrytsyna O., 2008, *J. of Mechanics of Materials and Structures* (2), 101–110.

Temperature Dependence of FMR Spectra of γ-Fe_2O_3 Magnetic Nanoparticles Forming Different Agglomerates in Glue

N. Guskos[1a, 2], G. Żołnierkiewicz[2], J. Typek[2], M. Orłowski[2], A. Guskos[2], Z. Czech[3], A. Mickiewicz[2]

[1] *Solid State Section, Physics Department, University of Athens Panepistimiopolis, 15 784 Zografou, Athens, Greece*
[a] *ngouskos@phys.uoa.gr*

[2] *Institute of Physics, Szczecin University of Technology Al. Piastów 17, 70-310 Szczecin, Poland*

[3] *Institute of Chemical and Polymer Engineering, Szczecin University of Technology Pułaskiego 10, 70-332 Szczecin, Poland*

Two samples of magnetic nanoparticles γ-Fe_2O_3 (with an average size of about 10 nm) forming two different agglomerates (one about 1.5 mm (sample 2) and the

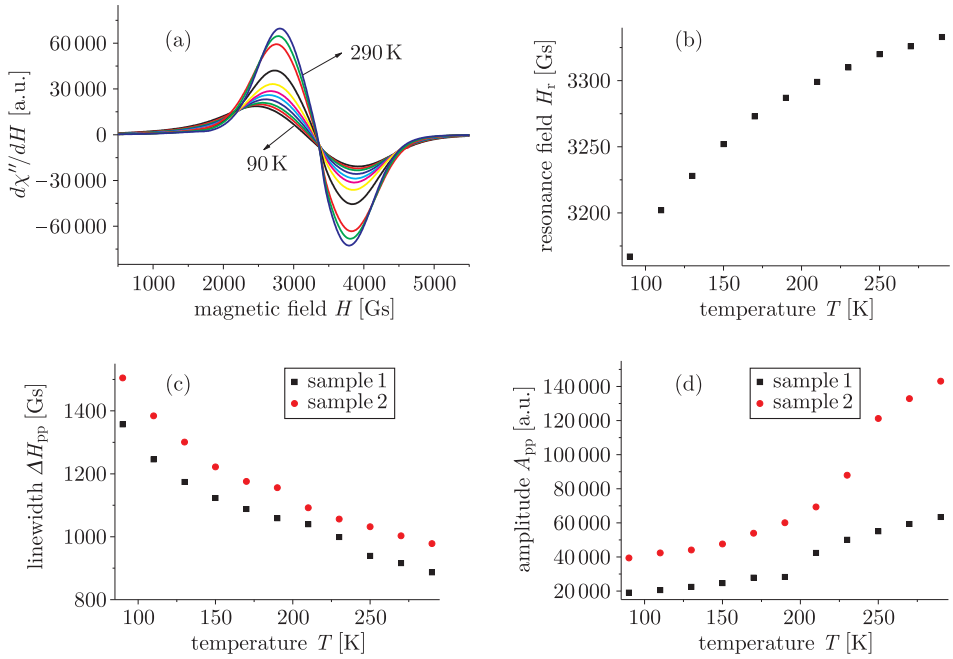

Figure 1: (a) Temperature dependence of FMR spectra; (b) temperature dependence of resonance field $H_r(T)$; (c) temperature dependence of linewidth $\Delta H_{pp}(T)$; (d) temperature dependence of amplitude $A_{pp}(d)$

other 0.5 mm (sample 1)) in glue have been prepared. The the FMR (ferromagnetic resonance) line position at room temperature is centered at about $g_{\text{eff}} \sim 2$ which is essentially different from the FMR line position for small size agglomerates [1, 2]. The temperature dependence of FMR spectra has been investigated (Fig. 1a, sample 2). Very interesting behavior of the FMR parameters has been observed (Fig. 1b, c, d). The resonance field is strongly dependent on temperature in both the investigated samples but the thermal dependence of other FMR parameters is strongly influenced by the agglomerate size.

References

[1] N. Guskos, J. Typek, M. Maryniak, Z. Rosłaniec, D. Petridis, and M. Kwiatkowska (2005) *Materials Science – Poland* **23** 972

[2] N. Guskos, G. Żołnierkiewicz, J. Typek, A. Guskos, and Z. Czech (2007) *Rev. Adv. Mat. Sci.* **14** 57

The Dynamics of Endohedral Fullerene $K^+@C_{60}$ Inside Single-walled Carbon Nanotube: MD Simulation

A. Dawid

University of Silesia, Institute of Physics
Uniwersytecka 4, Katowice 40-007, Poland
dawid@us.edu.pl

The composite of *endo*-fullerenes and a carbon nanotube has many interesting electrical and mechanical properties that make it a candidate for a nanoelectronics switching device [1]. $K^+@C_{60}$ endohedral fullerenes have been simulated inside armchair and zigzag nanotubes. The Brenner-Tersoff potential has been used to simulate bonds in carbon structures, the Lennard- Jones potential for the carbon-carbon interaction in different carbon structures and the Coulomb interaction for K^+-K^+ ions. No extra conditions have been imposed on my system. The potassium ions velocity autocorrelation function and its Fourier transform, the angular velocity correlation function of C_{60} molecules, the radial distribution function of K^+ ions and the velocity autocorrelation function of a nanotube surface have been calculated as the dynamical properties.

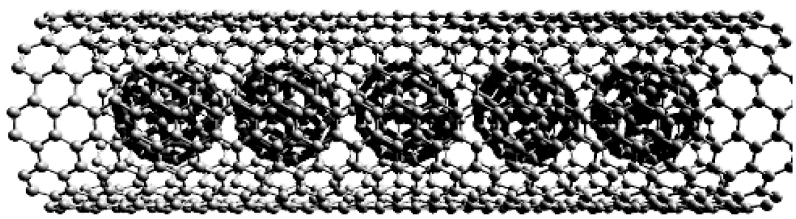

Figure 1: Endohedral fullerene molecules trapped inside carbon nanotube cage

References

[1] J. W. Kang and H. J. Hwang, *J. Phys. Soc. Jap.* **73** 1077 (2004)

The Dynamics of 5CB Mesogene Molecules Between Graphite Walls – MD Study

A. Dawid[a], W. Gwizdała

University of Silesia, Institute of Physics
Uniwersytecka 4, Katowice 40-007, Poland
[a] *dawid@us.edu.pl*

Classical molecular dynamics simulations have been performed for a thin layer of 5CB (4-n-pentyl-4'-cyanobiphenyl) molecules confined between two parallel graphite walls. The molecules have been treated as rigid bodies interacting via the van der Waals interaction with 2-dimensional periodic boundary conditions. The distance between the graphite walls has been changing between 2.2–3.0 nm. The dynamics of a thin layer of 5CB mezogenes has been investigated at room temperatures by calculating the translational and angular velocity autocorrelation functions of the mesogene molecule, its mean square displacement and diffusion coefficient. Several liquid crystal properties of a thin film have been studied. We have found a strong correlation between the dynamics of mesogene molecules and the separation distance between graphite planes.

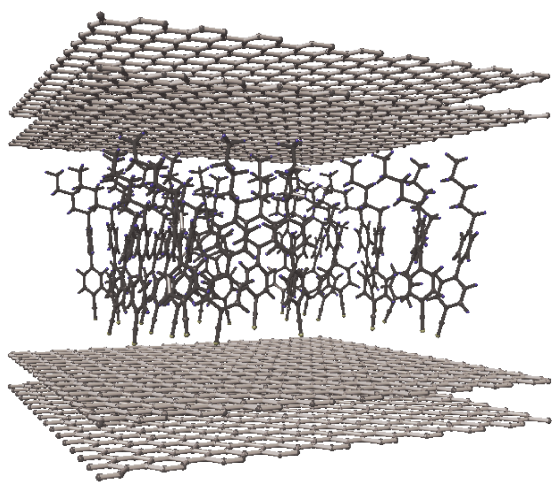

Figure 1: A snapshot of instantaneous configuration of 5CB molecules between graphite walls

References

[1] A. Dawid and Z. Gburski *J. Non-Cryst. Solid.* **353** (2007) 4339

Properties of Glycerol Molecular Cluster Confined in Carbon Nanotube

Z. Dendzik[1], K. Górny[1], M. Kośmider[2], S. Żurek[2]

[1] *Institute of Physics, University of Silesia*
Uniwersytecka 4, 40-007 Katowice, Poland

[2] *Institute of Physics, University of Zielona Góra*
Prof. Szafrana 4a, 64-516 Zielona Góra, Poland

Studying the properties of molecules in nanoscale confinement reveals effects not observed in bulk systems [1–2] and is of great importance to biology, geology and materials science. Glycerol belongs to the most extensively studied hydrogen-bonded systems. The presence of three hydroxy groups in a glycerol molecule gives rise to its complex structural properties and dynamical behaviour. We have performed a molecular dynamics simulation of a glycerol molecular cluster confined inside a single walled carbon nanotube and we have studied the effect of confinement on the cluster's structure and dynamics.

References

[1] Zhao J C, Buldum A, Han J and Lu JP 2002 *Nanotechnology* **13** 195
[2] Kolesnikov I A, Zanotti J M, Loong C K, Thiyagarajan, Moravsky A P, Loutfy R O and Burnham C J 2004 *Phys. Rev. Lett.* **93** 035503

Simultaneous Coupling of Three HFS Components in a Cascade Scheme of EIT in Cold ^{85}Rb Atoms

K. Kowalski[1a], V. Cao Long[2b], H. Nguyen Viet[3], K. Dinh Xuan[4], S. Gateva[5], M. Głódź[1], J. Szonert[1]

[1] *Institute of Physics, PAS*
Al. Lotników 32/46, 02-668 Warsaw, Poland
[a] *krkowal@ifpan.edu.pl*

[2] *Institute of Physics, University of Zielona Góra*
Podgórna 50, 65-246 Zielona Góra, Poland
[b] *V.CaoLong.@if.uz.zgora.pl*

[3] *The Andrzej Soltan Institute for Nuclear Studies*
Hoża 69, 00-681 Warsaw, Poland

[4] *Vinh University, Nghe An, Vietnam*

[5] *Institute of Electronics, BAS*
72 Tzarigradsko Chaussee, 1784 Sofia, Bulgaria

Schemes in electromagnetically induced transparency (EIT) which would support multiple-transparency windows are of interest, e.g., for slowing light pulses, simultaneously at close-lying wavelengths. For this purpose a dense hfs structure of the ^{85}Rb($5D_{5/2}$) state can be utilized in a stepwise $5S_{1/2}(F=3) \rightarrow 5P_{3/2}(F'=3) \leftrightarrow 5D_{5/2}(F''=4, 3, 2)$ process [1].

The experiment was performed with cold ^{85}Rb atoms in a magneto-optical trap (MOT) [2]. The coupling laser was set in the region of $5P_{3/2}(F'=3) \leftrightarrow 5D_{5/2}(F''=4, 3, 2)$ triple resonance. The probing laser was tuned across the transition $5S_{1/2}(F=3) \rightarrow 5P_{3/2}(F'=3)$ and its transmission was registered.

In the presence of a coupling laser, the absorption line is engraved with the transparency windows. These windows are due to the hfs structure of the $5D_{5/2}$ state. The shape of transmission spectra depends on the intensity and detuning of the coupling laser. In order to reproduce and interpret our experimental results, a five-level model of the hfs structure of an Rb atom (similar to the one used in [1]) was applied. All the experimental results agree well with the theoretical results.

References

[1] J. Wang et al. (2004) *Phys. Lett.* **A328** 437
[2] K. Kowalski et al. (2006) *Optica Applicata* **36** 559

Synthesis and Transport Properties of Porous Superconducting Ceramics of $YBa_2Cu_3O_{7-\delta}$

P. Fiertek[1a], B. Andrzejewski[2], W. Sadowski[1]

[1] *Faculty of Applied Physics and Mathematics*
Gdansk University of Technology
Narutowicza 11/12, 80-952 Gdansk, Poland
[a] *pafiertek@wp.pl*

[2] *Instytut Fizyki Molekularnej PAN*
M. Smoluchowskiego 17, 60-179 Poznan, Poland

This work presents a method of producing an open porous structure based on a ceramic high T_c $YBa_2Cu_3O_{7-\delta}$ (YBCO) superconductor "filled with a sugar supplement". The basic characteristic $R(T)$ curves for various external magnetic fields are also presented. The obtained results reveal a significant influence of the pore presence in the samples on the electrical resistance values, especially in the range of T_c (off set).

Molecular Dynamics Simulation Study of Titanium-decorated Fullerene Cluster

A. Piątek, Z. Gburski[a]

University of Silesia, Institute of Physics
Uniwersytecka 4, Katowice 40-007, Poland
[a] *zgburski@us.edu.pl*

Titanium decorated carbon nanotubes or fullerenes are considered to be a potential hydrogen-storage media. We have studied (MD method) a small titanium-decorated fullerene cluster $(C_{60}[TiH_2]_6)_7$ over a wide range of energy, from the solid state to the vaporization of the nanosystem. A low energy, solid state structure of the cluster has been obtained (pentagonal bipyramid). Several physical characteristics: the radial distribution function, the mean square displacement, the translational velocity autocorrelation function and its Fourier transform, the Lindemann index, the specific heat, etc. have been calculated for a wide range of energy of the studied system.

Dielectric Relaxation of Homocysteine Layer Between Graphite Walls – Computer Simulation

Z. Gburski[a], P. Raczyński

University of Silesia, Institute of Physics
Uniwersytecka 4, Katowice 40-007, Poland
[a] *zgburski@us.edu.pl*

Molecular dynamics (MD) studies for a homocysteine ($C_4H_9NO_2S$) layer located between parallel graphite walls are presented. We have calculated several dynamical observables of a homocysteine at the physiological temperature of $T = 309$ K. Several physical characteristics: the radial distribution function, the mean square displacement, the translational velocity autocorrelation function and its Fourier transform, the second rank order parameter have been calculated. The attention has been focused on the total dipole moment autocorrelation function, the dielectric loss spectrum $\varepsilon''(\nu)$ and the absorption coefficient $\alpha(\nu)$. A comparison with the dielectric relaxation of a pure homocysteine sample (without a graphite wall) is also presented and discussed.

Spin Reorientation Processes in (TiC_xN_{1-x}−Si−(C−N)/C System

N. Guskos[1,2], E. A. Anagnostakis[3], G. Żołnierkiewicz[2], J. Typek[2], A. Biedunkiewicz[4], P. Figiel[4], A. Guskos[2], K. A. Karkas[1]

[1] *Solid State Section, Department of Physics*
University of Athens
Panepistimiopolis, 15 784 Zografos, Athens, Greece

[2] *Institute of Physics*
Szczecin University of Technology
Al. Piastów 17, 70-310 Szczecin, Poland

[3] *Department of Computer and Communication Engineering*
University of Thessaly
Pedion Areos, 38 334 Volos, Greece

[4] *Institute of Materials Science and Engineering*
Szczecin University of Technology
Al. Piastów 17, 70-310 Szczecin, Poland

Samples of a (TiC_xN_{1-x}−Si−(C−N))/C system encapsulated in carbon cages have been prepared by a sol-gel method, both before and after a thermal annealing process. In both kinds of samples a very narrow ESR line arising from electron magnetic localized centers can be observed. At low temperatures in particular, a spin reorientation process, plausibly influencing the magnetic interaction character is registered. On the other hand, the thermal annealing process in an NH-atmosphere is recognizable as a critical factor of the critical points of a magnetic transition within a nanocomposite as well as the prevailing interaction mechanism for each major temperature regime.

Spinodal Decomposition Phenomenon in the Ising Model within the Dynamic Lattice Liquid (DLL) Model

K. Hałagan, P. Polanowski[a]

Department of Molecular Physics, Technical University of Lodz
Żeromskiego 116, 90-925 Lodz, Poland
[a]*ppolanow@p.lodz.pl*

The phase separation process during phase transition has been investigated for many years. This phenomenon is of great importance for materials engineering. When a single phase binary system, being initially in a homogeneous (disordered) phase, is rapidly quenched into a two-phase inhomogeneous (ordered) region, small inhomogeneities evolve into a macroscopic network of domains of equilibrium phases. A unique pattern occurs. The length scale of the ordered regions increases with time to achieve the equilibrium state. This phenomenon is known as a spinodal decomposition. There are several approaches to a numerical simulation of this process: the Cahn-Hilliard (CH) equation and its modifications [1], molecular dynamics and Monte Carlo (MC) methods. The last group of methods allows us to investigate relatively big systems and long times. A typical model used in MC simulations is the Ising model which represents a mixture consisting of two types of particles on a lattice with the nearest neighbor interaction. Two sorts of movement mechanism have been used in most common investigations: Kawasaki (direct exchange of two particles) [2] and vacancy dynamics (empty sides are present on the lattice) [2, 3]. Nevertheless, those methods have weak representation in real systems. A high vacancy concentration leads to unrealistic results. On the other hand, a single vacancy (which corresponds to vacancy concentration $\approx 10^{-6}$ for typical system size) does not change the phase diagram considerably [2] but the following questions may be asked: Why not to use two or more vacancies? How big should the system be to ensure proper dynamics of phase separation in that case?

In our approach we have used the Dynamic Lattice Liquid algorithm (DLL) [4]. It permits simulation of dense systems with all the lattice sites occupied (it is not accessible by other known lattice simulation methods) and parallel treatment of all particles. A simple model of a liquid, within the DLL frame, is considered as an assembly of structureless beads occupying lattice sites, as illustrated in Fig. 1. Beads oscillate around lattice nodes with a frequency of attempts to move to the neighboring lattice sites. Those attempts can be successful only when the sum of vectors, representing simultaneously attempted displacements of a group of elements is close to zero (a dense system under the excluded volume condition and local continuity preservation). In the other case, the attempts fail and the beads remain in the presently occupied lattice sites.

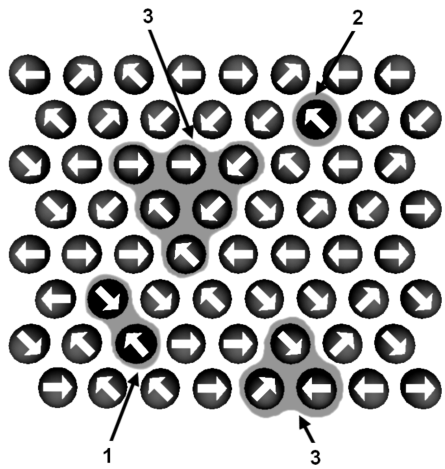

Figure 1: Figure 1: Schematic system representation in the DLL algorithm, the vector field represents displacement attempts to the neighboring lattice sites. The marked areas illustrate various local situations: 1 – elements are trying to move in the opposite direction (unsuccessful attempt), 2 – an attempt of motion starts from an element which will not be replaced by any of its neighbors (unsuccessful attempt), 3 – each element replaces one of its neighbors (successful attempt)

Practical application of the DLL algorithm of a simple liquid consists of three main steps.

(1) Random generation of the vector field representing motion attempts (one vector is assigned to each bead in the athermal case).

(2) Selection of attempts satisfying the continuity condition – closed loops, indicating paths of possible successful rearrangements.

(3) Displacement of beads along these closed paths to the neighboring sites (each bead replaces its neighbor).

Every bead attempts to move simultaneously (in parallel) towards one of the nearest-neighboring sites, within every time step. An element attempts to move only in one direction within a single time step (it is impossible to cross the motion paths). The DLL algorithm is ergodic and has been successfully used in a diffusion limited aggregation simulation [5], polymer dynamics and reaction front evolution investigation [6]. Our results have been obtained on a two dimensional triangular lattice (128×128) with periodic boundary conditions. The number of particles has been constant with the particle exchange probability following the Metropolis rule. We have focused on a scaling regime that develops at different times after the quench (the size of domains follows the Lifshitz scaling law), local concentration field and system morphology (Figure 2).

We have noticed that the domain structure is similar to those obtained with the vacancy models [2] and starts to develop after about 1000 MCs. This value is in disagreement with previous studies because the introduction of vacancy into the system

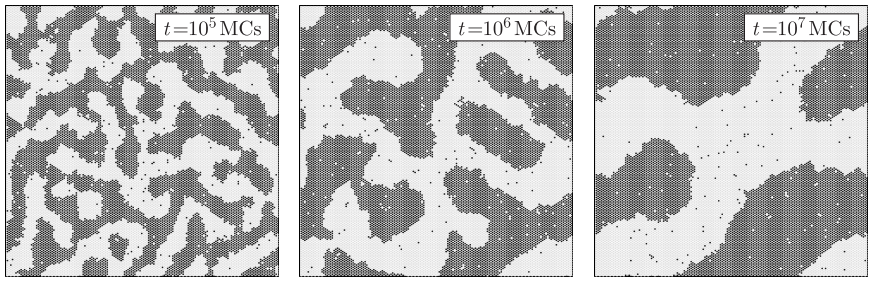

Figure 2: Snapshot pictures of the system ($2J/kT = 0.70$) for different time moments (Monte Carlo steps)

accelerates the phase separation kinetics. We believe that vacancy dynamics is too fast despite a local effect on the domain interfaces because it does not involve cooperative displacements of particles. We have also investigated the threshold value of the interaction parameter J for order-disorder transition (Figure 3).

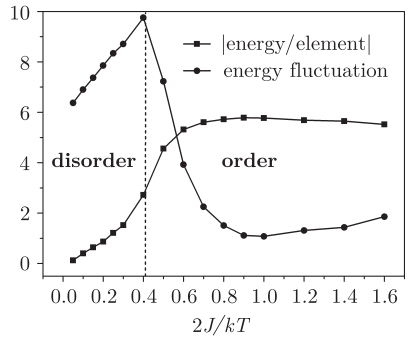

Figure 3: Energy per particle and energy fluctuation versus the interaction parameter for a given time moment; order-disorder transition is evident

The critical value of $2J/kT$ is about 0.4 and it is in perfect agreement with the theoretical value close to 0.405 from the effective Hamiltonian approximation method by T. Oguchi for a triangular lattice. The critical $2J/kT$ for vacancy dynamics is about 0.45.

Acknowledgements
This work was partially supported by MNiSW grant projects No. 3 T08E 104 29 (Poland).

References

[1] A. J. Bray (2003) *Phil. Trans. R. Soc. Lond.* **A 361**, 781
[2] P. Fratzl, O. Penrose (1994) *Phys. Rev.* **B 50**, 3477
[3] R. Weinkamer, P. Fratzl, B. Sepiol, and G. Vogl (1998) *Phys. Rev.* **B 58**, 3082
[4] P. Polanowski, T. Pakula (2002) *J. Chem. Phys.* **117**, 4022
[5] P. Polanowski (2007) *J. Non-Cryst. Solids* **353**, 4575
[6] P. Polanowski, Z. Koza (2006) *Phys. Rev.* **E 74**, 036103

EPR Properties of $Cr_2P_4O_{13}$, β-$CrPO_4$, $Cr_4(P_2O_7)_3$ and $Cr(PO_3)_3$

H. Fuks[1], S. M. Kaczmarek[1a], M. Bosacka[2]

[1] *Institute of Physics, Szczecin University of Technology*
Al. Piastów 48, 70-310 Szczecin, Poland
[a] *skaczmarek@ps.pl*

[2] *Department of Inorganic and Analytical Chemistry*
Szczecin University of Technology
Al. Piastów 42, 71-065 Szczecin, Poland

A group of four chromium phosphate powder samples: $Cr_2P_4O_{13}$, β-$CrPO_4$, $Cr_4(P_2O_7)_3$ and $Cr(PO_3)_3$ has been investigated using the X-band electron paramagnetic resonance (EPR) technique. The crystal structure of all the compounds is known and has been confirmed by the XRD powder diffraction method. The appearance of CrO_6 octahedra, edge shared with a group of PO_4 tetrahedra, is a characteristic feature of the analyzed structures determining also the magnetic properties of chromium phosphates.

An analysis of the EPR signal has been performed in the temperature range of 68–300 K. A strong EPR signal from chromium isolated ions has appeared for the whole samples. The signal has consisted of two Lorentzian lines, split to a larger or smaller extent, at a constant resonance position, described by the spectroscopic parameter $g_{\text{eff}} \approx 1.972$, being a typical value for Cr^{3+} ions. The EPR signal integral intensity as a function of a temperature has indeed revealed some deviation from the Curie-Weiss behavior, suggesting that for the resonance signal not only isolated Cr^{3+} paramagnetic ions are responsible but complex chromium magnetic systems, i. e. pairs or clusters, as well.

An analysis of the EPR linewidth and integral intensity has allowed us to estimate the relative concentration of the isolated chromium paramagnetic sites in relation to the concentration of the complex magnetic centers. A concentration of the isolated Cr^{3+} paramagnetic sites is relatively highest in the $Cr_2P_4O_{13}$ compound and lowest in the $Cr(PO_3)_3$ ones. In this latter case the EPR signal arises mainly from complex chromium magnetic centers. The linewidth increases with the increasing temperature in this case, contrary to the other analyzed compounds.

Strong antiferromagnetic interactions between Cr^{3+} paramagnetic centers have been found for all investigated phosphates with the Curie-Weiss temperature parameter of $\theta \approx -140$ K. The Cr^{3+} centers appear to be substituted at the octahedral sites and the exchange antiferromagnetic interactions are transferred by phosphorus tetrahedra permitting collective behavior of Cr ions and creation of complex chromium magnetic centers.

EPR and IR Study of a Dy(III) Macroacyclic Schiff Base Complex

G. Leniec, S. M. Kaczmarek[a], J. Typek

Institute of Physics, Szczecin University of Technology
Al. Piastów 48, 70-310 Szczecin
[a]*skaczmarek@ps.pl*

Application of lanthanide(III) ions in molecular chemistry has been a very active field of research recently. These ions can be used in the design of novel probes of biomedical interest [1] and in the preparation of new kinds of catalysts and enzymes [2–4]. Their high magnetic moments together with their magnetic anisotropy are of particular interest in the field of molecular magnetism. The magnetic studies have been mostly limited to the case where the lanthanide(III) ion is Gd(III). In one of our previous papers we have presented the EPR properties of a gadolinium Schiff base macroacyclic complex (LnL = (Ln = Gd, L = tripodal heptadentate N_4O_3 tris [2-(salicylideneamino)ethyl]amine: $C_{27}H_{27}N_4O_3Cl_3Gd$, marked also as 33TGd) [5]. In this paper, IR spectroscopic and magnetic properties of the dysprosium(III) macroacyclic tripodal Schiff base (tris[5-(chlorosalicylideneamino)ethyl]amine) complex are reported (33TDy). The positions of ν(C = N) and ν(OH) stretching bonds indicate that the azomethine group nitrogen and the phenolic OH group oxygen are coordinated to a rare earth ion. In the EPR spectra, two main spectral components at a low magnetic field region (< 300 mT) are observed independently from the temperature. The components in questions are attributed to Dy^{3+} ions with the effective spin $S = 1/2$. The magnetic anisotropy between 3 and 23 K is practically constant as evidenced by only a marginal change of the spread of g-factors. Above 23 K the g_y-factor increases strongly with the temperature increase giving rise to a very high magnetic anisotropy of the complex. Such behaviour of the magnetic anisotropy at higher temperatures could be an effect of the dynamical changes caused by an increase in the spin-lattice rate. A very small value of the Curie-Weiss constant and the lack of any meaningful thermal changes of the linewidths indicate the absence of any significant interactions between the Dy(III) complexes below 20 K. The temperature dependence of the total integrated intensity above 20 K indicates the existence of a small number of antiferromagnetically coupled pairs with the excited, non-magnetic state, lying about 33(1) K above the ground state.

References

[1] Bunzli J.-C., Choppin G. R. *Lanthanide probes in life, chemical and earth sciences. Theory and practice* Elsevier Science Publishers, 1989
[2] Roigk A., Hettich R., Schneider H. *Inorg. Chem.* **37** (1998) 751; Kobayashi S., Kawamura M., *J. Am. Soc. Chem.* **120** (1998) 5840
[3] Guerriero P., Tamburini S., Vigato P. A. *Coord. Chem. Rev.* **139** (1995) 17

[4] Guerriero P., Vigato P. A., Fenton D. E., Hallier P. C. *Acta Chem. Scand.* **46** (1992) 1025
[5] Leniec G., Kaczmarek S. M., Typek J., Kołodziej B., Grech E., Schilf W. *Solid State Sciences* **9**, (2007) 267–273

Magnetic Properties of Compounds Formed from $CuWO_4$, $CdWO_4$, $CoWO_4$ and Gd_2WO_6, Er_2WO_6 Due to Solid State Reaction

E. Tomaszewicz[1], S. M. Kaczmarek[2a]

[1] *Department of Inorganic and Analytical Chemistry*
Szczecin University of Technology
Al. Piastów 42, 71-065 Szczecin, Poland

[2] *Institute of Physics, Szczecin University of Technology*
Al. Piastów 17, 70-310 Szczecin, Poland
[a] *skaczmarek@ps.pl*

Some new cobalt, copper, cadmium and rare-earth metal tungstates (RE = Gd and Er) prepared by the conventional solid-state reaction are presented in this paper. The obtained phases have been studied by the X-ray powder diffraction (XRD), DTA-TG, IR and EPR methods to provide some information concerning their physical and chemical properties. A particular emphasis has been placed on determining the basic properties of the new obtained compounds $CoRE_4W_3O_{16}$, $Co_2RE_2W_3O_{14}$, $Cu_3RE_2W_4O_{18}$, $CoRE_2W_2O_{10}$, $CuRE_2W_2O_{10}$ and $CdRE_2W_2O_{10}$. The authors suggest that the anion lattice of $Cu_3RE_2W_4O_{18}$ compounds has been built by isolated groups of octahedra $(W_4O_{18})^{8-}$, while the anion lattice of the $CuRE_2W_2O_{10}$ phases has been built by joint WO_6 octahedra forming structural elements $[(W_2O_9)^{6-}]_\infty$.

The observed EPR spectra of the $Cu_3RE_2W_4O_{18}$ compounds consist of a broad, intense line from rare-earth ions and a narrow line ($g \approx 2.0$) from isolated Cu^{2+} ions. A similar pattern has been observed in case of the $CdRE_2W_2O_{10}$ compound excluding the Cd signal forming fine and hyperfine structures. The EPR spectrum of the $CoGd_4W_3O_{16}$ compound reveals the presence of a single, asymmetric, featureless, wide, dysonian like a signal originating from exchange interactions of Gd^{3+} ions. The EPR spectrum of $Co_2Gd_2W_3O_{14}$ is very similar. Such a signal is characteristic for condensed conducting magnetic materials. The intensity versus temperature reveals a Curie-Weiss dependence, giving $T_c = -11.7$ for $CoGd_4W_3O_{16}$ and $T_c = -12$ K for $Co_2Gd_2W_3O_{14}$, indicating an antiferromagnetic interaction. In most cases of $CuWO_4 + RE_2WO_6$ compounds the dominating interaction in the rare earths spin system is ferromagnetic (T_{CW}=1, 5–3, 5 K). In case of the $CdGd_2W_2O_{10}$ compound, the dominating interaction is antiferromagnetic ($T_{CW} \approx -20$ K).

Ferroelectric Properties of Relaxor Type SBN Single Crystals Doped with Co, Cr, Ni and Ce

S. M. Kaczmarek[1a], M. Orłowski[1], D. Piwowarska[1], K. Matyjasek[1], L. I. Ivleva[2]

[1] *Institute of Physics, Szczecin University of Technology*
Al. Piastów 17, 70-310 Szczecin, Poland
[a] *phone: +48 091 449 40 32, fax: +48 091 434 21 13, skaczmarek@ps.pl*

[2] *A. M. Prokhorov General Physics Institute*
Russian Academy of Sciences
119991 Moscow, 38 Vavilov Street, Russia

SBN61 pure, SBN61:Cr (0.01 wt. %), SBN61:Co (0.01 wt. %), SBN61:Ni (0.01 wt. %, 0.5 wt. %) and SBN61:Ce (0.01 wt. %) single crystals were grown using the modified Stepanov technique in the A. M. Prokhorov General Physics Institute, Russian Academy of Sciences. Absorption measurements of the crystals were taken using a Perkin-Elmer spectrophotometer and compared to the SBN58 single crystals obtained by the Czochralski method, and analyzed elsewhere [1].

The following parameters were analyzed in the frame of dielectrical measurements: electric permittivity ε', the compound's conductivity and loss tangent, both as a function of temperature (290–400 K) at 10 kHz and frequency (1 Hz–100 kHz). Conductivity activation energies and ferroelectric temperatures of relaxor type phase transitions of pure and SBN61 crystals doped with Co, Cr, Ni and Ce were established and compared with SBN58 crystals [2, 3]. The measurement set consisted of a Hewlett Packard bridge HP4192A, a wide temperature range measurement chamber, a temperature control unit (SHIMADEN TSR25/Pt100), and a computer. Direct observations of the domain structure's evolution during the polarization reversal were made for pure SBN61 by the nematic liquid crystal decoration technique and compared with the previous results for SBN58:Cr crystal.

References

[1] S. M. Kaczmarek, M. Berkowski, K. Repow, M. Orłowski, A. Worsztynowicz, M. Włodarski (2007) *Rev. Adv. Mat. Sci.* **14** 49
[2] K. Matyjasek, K. Repow, S. M. Kaczmarek, M. Berkowski (2007) *J. Phys.:Cond. Mat.* **19** 466207 (10pp)
[3] K. Matyjasek, K. Wolska, S. M. Kaczmarek (2008) *J. Phys.: Cond. Mat.* (submitted)

Bound States Induced by Interaction Potential Deformation

S. Kondej, M. R. Dudek

Institute of Physics, University of Zielona Góra
ul. Szafrana 4a, 65-069 Zielona Góra, Poland

It is an open question how the energy spectrum of a quantum system is related to the interaction potential geometry. A simplified diatomic model in which interaction is represented by the Morse potential is studies. In particular, the question whether a new bound state appears due to the interaction potential deformation is investigated. The problem of possible new bound states is important for the nanotube technology.

References

[1] P. Exner, S. Kondej, "Bound states due to a strong δ interaction suported by a curved surface" *Journal of Physics A: Mathematical and General* **36**, (2003) 443–457
[2] S. Kondej, I. Veselić, "Lower bounds on the lowest spectral gap of singular potential Hamiltonians" *Annales Henri Poincaré* **8** 1 (2007) 109–134
[3] M. M. Nieto and L. M. Simmons, Jr, "Eigenstates, coherent states, and uncertainty products for the Morse oscillator" *Phys. Rev.* **A 19** (1979) 438–444

Interaction of Components and Anomalous High Conductivity in Polyaniline-Polymethylmethacrylate Nanocomposites

O. Aksimentyeva[1], O. Konopelnyk[1], B. Tsizh[2], I. Opainych[1], J. Ulanski[3], G. Martyniuk[1]

[1] *L'viv Ivan Franko National University*
6 Kyrylo and Mephodii str., 79005 L'viv, Ukraine

[2] *Kazimierz Wielki University in Bydgoszcz*
Chodkiewicza 30, Bydgoszcz, 85-064, Poland

[3] *Technical University of Lodz*
Żeromskiego 116, 90-924 Lodz, Poland

Conducting polymers such as polyaniline (PANI) have received great attention due to their simple synthesis, good environmental stability and electrical conductivity. However, major problems relating to successful utilization of PANI such as poor mechanical properties and solubility remain an unsolved problem [1]. To improve the mechanical properties and processability of PANI, blending with other polymers such as polymethylmethacrylate (PMMA) is employed. PANI may be considered as a mesoscopic metal (a "nanometal") with the primary particle diameters in the range between 10 and 20 nm [2]. A nanosize of polymer particles is preserved in the polymer composites obtained by nanotechnology methods (polymer blending in cosolvent, template and matrix synthesis, etc.). The mechanism of electron transport in such nanosystems is a topic of great interest. One of the reasons for the anomalous behavior of conductivity in polymer blends may be the interaction of components. To disclose this problem the structure and electrical properties of the nanocomposites obtained by disperse PANI blending in a PMMA dielectric matrix [3] have been studied.

It is found that electrical conductivity of polymer composites can be controlled in a wide range (more than 12 orders of magnitude) by a small amount of PANI. The conductivity dependence on the PANI concentration can be explained by a percolation model with an extremely low „percolation threshold" in the range of 0.8–2.6 vol. % of PANI. The temperature dependence of the specific conductivity for PMMA-PANI composites is characteristics for organic semiconductors. The effective activation energy for charge transport depends on the PANI content in the composite. An anomalously high specific conductivity in PMMA-PANI composites is observed at the PANI concentration exceeding the percolation threshold, in the interval of 5–10 vol. %. Its value exceeds the value of specific conductivity for acid doped PANI. To explain this phenomenon, the methods of IR Raman spectroscopy, electron spin resonance (ESR) and UV-vis. absorption spectroscopy have been employed.

Raman spectra (Figure 1) show that significant changes occur in the bands corresponding to the nitrogen atom in the PANI macrochain (2500–3500 cm^{-1}) and ester oxygen attributed to PMMA (1270–1200 cm^{-1} and 2180 cm^{-1}) as the PANI content of composites increases.

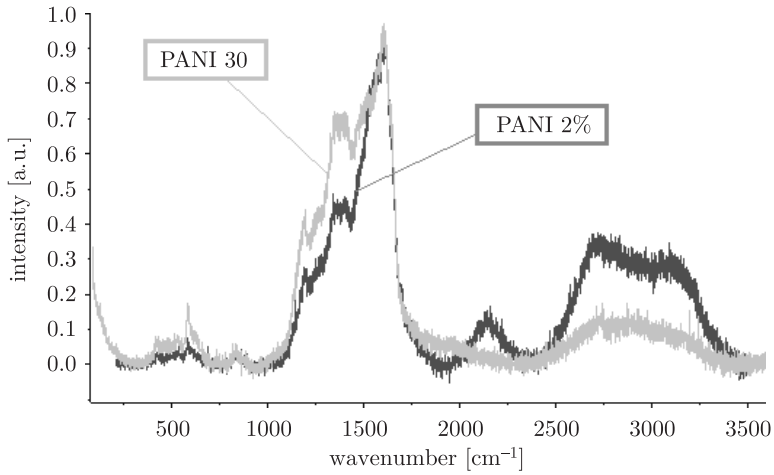

Figure 1: Raman spectra of PMMA-PANI composites

An ESR study of the spin dynamic in PANI-PMMA composites has been carried out in the temperature interval of 4.2–300 K. For polymer composites the line width, ΔHpp, broadens from 3.5 Oe (PANI) to 8.3 Oe (PMMA-10%PANI), which is evidence of delocalization of the charge carriers in PANI affected by the PMMA dielectric polymer matrix [4]. The existence of a weak intermolecular interaction in the PMMA and PANI solutions at different ratios of polymers has been confirmed by the electron spectroscopy. The obtained results give a possibility to suggest that the anomalous high conductivity of the PMMA-PANI composites may be caused by "secondary doping" of PANI with a PMMA macrochain. Such additional doping leads to higher electrical conductivity in a composite as compared with unblended PANI.

References

[1] Namazi H., Kabiri R., Entezami A. 2002 *Eur. Polym. J.* **38** 771–778
[2] Srinivasan D., Natarajan T. S., Rangarajan G., Bhat S. V., Wessing B. 1999 *Solid State Comm.* **110** 503–508
[3] Aksimentyeva O. I., Konopelnyk O. I., Yurkiv V. V., Martiniuk G. V., Shapovalov V. A. 2007 *Molec. Cryst. & Liq. Cryst.* **468** 309–316
[4] Aksimentyeva O. I., Tsizh B. R., Konopelnyk O. I., Ukrainets A. M., Shapovalov V. A. 2007 *Nanosystems and Nanotechnology* **5** (1) 273–278

Thermo- and Photostimulated Processes in $Gd_3Ga_5O_{12}$ ceramics

L. Kostyk[a], A. Luchechko, Ya. Zakharko, O. Tsvetkov

Ivan Franko National University of L'viv, Faculty of Electronics
79017 Tarnavs'kogo 107, L'viv, Ukraine
[a]*kostyk@electronics.wups.lviv.ua*

It is known that gadolinium-gallium garnet ($Gd_3Ga_5O_{12}$) is widely used in different areas of science and technology. The luminescence output and threshold generation energy of lasers are to a great extent determined by the presence of trap levels and recombination centers which show up in the thermostimulated luminescence (TSL).

The thermostimulated luminescence, luminescence excitation spectra, emission spectra under photo- and X-ray excitation, luminescence decay kinetics of $Gd_3Ga_5O_{12}$ (GGG) garnet ceramics have been investigated in this paper.

GGG ceramic samples have been prepared by standard ceramic technology such as a high temperature solid-state synthesis. The Cr impurity content varies from 0.01 to 0.1 mol. %.

An X-ray diffraction has been carried out on a DRON-4,0 diffractometer by the powder method using FeK_α-radiation. The formation of a $Cd_3Ga_5O_{12}$ garnet phase has been established from an analysis of the received diffractograms.

There is a wide band in the spectral region 650–800 nm with a maximum at $\lambda_m = 716$ nm in the luminescence spectra of samples with 0.01 and 0.1 mol.% Cr at optical excitation ($\lambda_{exn} = 470$ nm) at a RT which can be attributed to emission transitions ($^4T_2 \rightarrow {}^4A_2$) in the Cr^{3+} activator ions. A redistribution of luminescence bands intensity is observed with the temperature lowering to 85 K. The luminescence spectra of Cr^{3+} ions in GGG at X-ray excitation correlate with the PL spectra.

The decay kinetics of activator ions emission in GGG ceramics has been investigated. The two components of Cr activator luminescence decay are most probably related to the emission transitions in different types of Cr^{3+} ions centers.

Two basic peaks are detected with the maxima at ≈ 360 and 490 K on the thermoluminescence (TL) glow curves of unactivated samples. Besides, a high temperature maximum at 490 K and an additional peak at 384 K appear on the TL glow curve in the activated samples with the chromium impurity concentration of 0.01 mol.%. TSL peaks of GGG: Cr samples are complicated and can occur as a superposition of several elementary peaks. The decomposition of TL glow curves has been realized.

The illumination of preliminary X-ray irradiated GGG: 0.1 mol.% Cr samples leads to a change in the relative intensity of some peaks. Illumination by light through a KS-15 filter does not influence the intensity of the high temperature peaks at 490–510 K and bleaches approximately with the 30% TL glow intensity in the 330–420 K region. Illumination through a OS-12 filter leads to a decrease in the intensity all TSL peaks.

The activation energies of traps which are responsible for the appearance of TSL in the 295–600 K region have been estimated. It is shown that delocalization of electrons from $Cr^{3+}e$ traps leads to the appearance of a TL glow peak at 390 K. The nature of other TSL peaks is discussed. The mechanisms of TSL and OSL processes are suggested.

Structure and Electrical Properties of Nitrided NbN−TiN Sol-gel-derived Films

B. Kościelska[1], A. Winiarski[2], B. Kusz[1]

[1] *Faculty of Applied Physics and Mathematics*
Gdansk University of Technology
Narutowicza 11/12, 80-952 Gdansk, Poland

[2] *A. Chełkowski Institute of Physics*
University of Silesia
Uniwersytecka 4, 40-007 Katowice, Poland

In recent years much attention has been paid to the nitride and oxynitride thin films. In particular, NbN is a hard coating material with many commercial applications. The relatively high superconducting critical temperature (up to 16 K) allows NbN to be used in Josephson junctions and in several superconducting microelectronics applications.

This work presents the results of investigations of the electrical conductivity and structure of NbN−TiN thin films. The nitride films were prepared with the method of thermal nitridation of sol-gel-derived oxide films with ammonia (ammonolysis). Sol-gel-derived $x\mathrm{Nb_2O_5}-(100-x)\mathrm{SiO_2}$ (where $x = 90$, 80, 70, 60, 50, 40, 0 mol%) coatings were nitrided at 1200EC to obtain NbN−TiN films. The structural transformations occurring in the films as a result of ammonolysis were studied using X–ray Diffraction (XRD), Atomic Force Microscopy (AFM) and *X*-ray Photoelectron Spectroscopy (XPS). The electrical conductivity was measured with the conventional four-terminal method in the temperature range from 5 to 280 K. NbN−TiN samples exhibit a negative temperature coefficient of resistivity. The positive temperature coefficient of resistivity was observed only for a TiN sample. The results of conductivity versus temperature may be described on the grounds of a model proposed for a weakly disordered system. The superconducting transition was seen for the sample containing $x = 60\%$ of $\mathrm{Nb_2O_5}$ initially.

Properties of Exohedral Complexes Composed of van der Waals Thin Film and Single Wall Carbon Nanotubes: an MD Study

M. Kośmider[1], Z. Dendzik[2], S. Żurek[1], K. Górny[2]

[1] *Institute of Physics, University of Zielona Góra*
Prof. Szafrana 4a, 65-516 Zielona Góra, Poland

[2] *Institute of Physics, University of Silesia*
Uniwersytecka 4, 40-007 Katowice, Poland

The properties of exohedral and endohedral nano-complexes based on a single walled carbon nanotube are the subject of many theoretical and experimental studies due to their specific properties and potential applications [1–4]. The structure and the dynamics of van der Waals thin film coating of single walled carbon nanotube have been studied in a series of molecular dynamics simulations. The examined systems have been composed of carbon nanotube and the van der Waals mono and multilayer thin film surrounding SWNT. In order to investigate the influence of the substratum to the properties of the thin film, the nanotubes of different chirality and diameter have been used.

References

[1] Dilon A. C., Heben M. J. 2001 *Appl. Phys. A: Mater. Sci. Process* **72** 133
[2] Cvitas M. T., Siber A. 2003 *Phys. Rev. B* **67** 193401
[3] Zhang Y., Dai H. 2000 *App. Phys. Lett.* **77** 3015
[4] Bagci V. M. K., Gülseren O., Yildirimi T., Gedik Z., Ciraci S. 2002 *Phys. Rev. B* **66** 045409-1

Photoacoustic Spectrum of Er(III) in Er_2O_3

N. Guskos[1,2], J. Majszczyk[2], J. Typek[2],
G. Żołnierkiewicz[2], E. Tomaszewicz[3]

[1] *Solid State Section, Department of Physics, University of Athens Panepistimiopolis, 15 784 Zografos, Athens, Greece*

[2] *Institute of Physics, Technical University of Szczecin Al. Piastów 17, 70-310 Szczecin, Poland*

[3] *Department of Inorganic and Analytical Chemistry, Szczecin University of Technology Al. Piastów 42, 71-065 Szczecin, Poland*

Photoacoustic (PA) spectra of f-f transitions in Er_2O_3 have been recorded at room temperature (Figure 1). The PA spectra consist of many absorption lines in the visible region of electromagnetic radiation. The registered spectra have been compared with the PA spectra of Er-hydrazone and Er-hydrazine complexes [1, 2]. A more intense PA line is observed at 523 nm for erbium organometallic complexes in comparison with an erbium oxide sample, while a line at 667 nm has been twice as strong. The oxide erbium has shown more f-f transitions than erbium(III) embedded in an organic matrix (Figure 1) [1, 2].

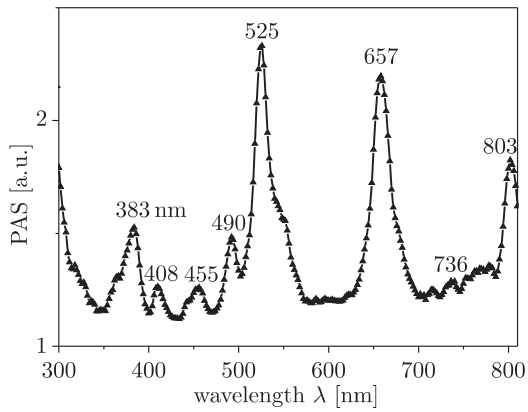

Figure 1: Photoacoustic spectrum of Er(III) in Er_2O_3 oxide

References

[1] N. Guskos, G. Papadopoulos, J. Majszczyk, J. Typek, M. Wabia, V. Likodimos, D. G. Paschalidis, I. A. Tossidis and K. Aidinis (2003) *Acta Phys. Pol.* **A 103** 301

[2] N. Guskos, J. Typek, J. Majszczyk, M. Maryniak, and D. Paschalidis (2006) *Rev. Adv. Mater. Sci.* **11** 59

Influence of Size Distributions of Charged Nanoparticles on Their Self-assembly Process: Computer Simulations

R. Orlik[1], A. C. Mituś[1], A. Z. Patashinski[2], B. A. Grzybowski[2]

[1] *Institute of Physics, Wroclaw University of Technology, Poland*

[2] *Departament of Chemistry, Northwestern University, Evanston, Illinois, USA*

The aggregates of oppositely charged NP are used in the fields of, e.g., optoelectronics, high-density data storage, catalysis or biological sensing [1, 2]. The quality of the aggregates depends strongly on the process of their self-assembly (crystallization). In particular, the size distributions of the NP play the crucial role [3]. However, a deep understanding of the underlying physical phenomena is still missing. We address this topic using Molecular Dynamics technique (Nose-Hoover algorithm) combined with standard Metropolis Monte Carlo method. We study a system of a few thousands of NP, interacting via soft sphere repulsive forces and screened coulombic attraction/repulsion:

$$U(r_{ij}) = 4\epsilon_{LJ}\left(\frac{\sigma}{r_{ij}}\right)^{12} + \frac{q_i q_j}{4\pi\epsilon_0\epsilon_R}\frac{1}{r_{ij}}\,e^{-k\,r_{ij}},$$

where σ denotes the NP diameter, q_i, q_j – the charges, ϵ_0 – dielectric constant of vacuum, ϵ_R – relative dielectric constant of solvent, $k \equiv 1/r_D$ – reciprocal screening length.

We analyze the cases when the size distributions of positively and negatively charged NP are (i) identical δ-like distributions; (ii) non–identical δ-like distributions; (iii) fully overlapping broad identical distributions; and (iv) non-overlapping broad distributions. In each of those cases the distributions of the sizes of the clusters are monitored. The results are in a semi-quantitative agreement with experimental observations.

References

[1] A. M. Kalsin, M. Fijalkowski, M. Paszewski, S. K. Smoukov, K. J. M. Bishop, B. A. Grzybowski (2006) "Electrostatic Self-Assembly of Binary Nanoparticles Crystal with a Diamond-Like Lattice", *Science* 21, **312** 420

[2] K. J. Bishop, B. A. Grzybowski (2007) "'Nanoions': Fundamental Properites and Analytical Applications of Charged Nanoparticles", *Chem. Phys. Chem.* **8** 2171

[3] B. A. Grzybowski at al. (*in preparation*)

Isothermal Crystallization Kinetics in $Fe_{73.1}Si_{15.5}B_{7.4}Nb_{3.0}Cu_{1.0}$ Amorphous Alloy

S. Mudry[1a], Yu. Kulyk[1], B. Tsizh[2]

[1] *Ivan Franko L'viv National University,*
8 Kyrylo and Mephodii str., 79005 L'viv, Ukraine
[a] *mudry@physics.wups.lviv.ua, sihor@ukr.net*

[2] *Kazimierz Wielki University in Bydgoszcz*
Chodkiewicza 30, Bydgoszcz, Poland
(+4852) 3419264, tsizhb@ukw.edu.pl

The nanocrystalline structure formation during a crystallization process in "Finemet" alloys is the reason for the increasing interest in studying crystallization process kinetics at various thermal treatment regimes. In this work the isothermal crystallization kinetics occurring in an $Fe_{73.1}Si_{15.5}B_{7.4}Nb_{3.0}Cu_{1.0}$ alloy at temperatures 683, 695 and 708 K has been studied by means of the X-ray high temperature diffractometry. In order to determine the volume fraction of crystalline phase ($X(t)$) the diffraction curves have been considered as a total of partial curves related to amorphous and crystalline phases, comparing their integral intensities. The phase transformation mechanism at isothermal annealing process has been studied analyzing the time dependence of the crystalline phase volume fraction. The slope of $X(t)$ plotted in a double logarithmic scale has been used to calculate both the kinetics coefficient and the crystallization activation energy of 0.5 and 207 kJ/mol, respectively. This kinetic coefficient value suggests the governing role of the diffusive-controlled growth factor in the formation of a nanocrystalline structure during initial crystallization of an $Fe_{73.1}Si_{15.5}B_{7.4}Nb_{3.0}Cu_{1.0}$ amorphous alloy.

This conclusion is confirmed by the fact that the Fe_3Si nanocrystalls density equals to 10^{23} m^{-3} and is in fact unchangeable in the annealing duration. Besides, the diffusive-controlled mechanism of nanocrystalls growth is confirmed by an analysis of Fe_3Si mean nanocrystalls size dependence on time. It has been found that the effective diffusion coefficient value at 683 K equals to 10^{-22} m^2/s which is evidence of the damping of the Fe_3Si nanocrystalls growth process. The most probable reason for this damping is a collision of diffusion regions enriched with Nb and B.

Structure of Liquid Copper from Tight-binding Driven Molecular-dynamics

J. Dziedzic[1a], V. Mykhaylyuk[2b], J. Rybicki[1,2,3c]

[1] *Faculty of Technical Physics and Applied Mathematics*
Gdansk University of Technology
Narutowicza 11/12, 80-952 Gdansk, Poland
[a] *jaca@kdm.task.gda.pl*

[2] *Institute of Mechatronics, Nanotechnology and Vacuum Techniques*
Koszalin University of Technology
Racławicka 15–17 F, 75-620 Koszalin, Poland
[b] *mvova@kdm.task.gda.pl*

[3] *TASK Computer Centre, Gdansk University of Technology*
Narutowicza 11/12, 80-952 Gdansk, Poland
[c] *ryba@task.gda.pl*

A tight-binding (TB) driven molecular-dynamics (MD) simulation of liquid copper in a periodic supercell was performed using our own computer code. The structure of the obtained liquid is discussed and compared with the available empirical data and results of other simulations, in terms of pair correlation functions, angular distribution functions and electronic density of states.

Thermodynamical Model of Thermo-Mechanical Fields in Thin-Film Systems

T. Nagirny[1], K. Tchervinka[2]

[1] *Centre of mathematical modelling IAPMM NAS of Ukraine*
15, Dudaev's str., L'viv, 290005, Ukraine
tnagirny@yahoo.com, phone (0322) 74 11 68

[2] *Mechanical and mathematical Department*
Ivan Franko National University of L'viv
1, Universytetska str., L'viv, 290000, Ukraine
k.tchervinka@gmail.com, phone (032) 239 41 45

The methods of non-equilibrium thermodynamics and solid mechanics make it possible to formulate a set of equations for describing physic-mechanical processes in solids. The basic model constructing concepts and model parameters being considered yield a different circle of effects that the obtained theory is capable of describing. A variety of size effects characteristic for thin films and fibres is well-known to be described with an approach of nonlocal theories [1]. It is known that the account of a gradient of chemical potential for the local gradient approach theory in thermomechanics makes it possible to describe interface phenomena as well as a possibility of investigating the size effect of strength and the plasticity point [2]. We shall not attempt to compare the approach considered in this paper to different approaches in nonlocal theories of solids which have been developed over the last decades to study interface phenomena. We shall formulate constitutive equations for the geometrical linearized approach using the values per unit volume.

Let us consider a deformable thermoelastic solid. Neglecting the convective time derivative component, the balance equations for total energy E, mechanical motion momentum $\vec{k}$, entropy S and density of mass ρ are the following:

$$\frac{\partial E}{\partial \tau} = \vec{\nabla}\left(\hat{\sigma}\cdot\vec{v} - T\vec{J}_s - H\vec{J}_m\right), \qquad \frac{\partial \vec{k}}{\partial \tau} = \vec{\nabla}\cdot\hat{\sigma},$$
$$\frac{\partial S}{\partial \tau} = -\vec{\nabla}\cdot\vec{J}_s + \sigma_s, \qquad \frac{\partial \rho}{\partial \tau} = -\vec{\nabla}\cdot\vec{J}_m. \tag{1}$$

where $\vec{v}$ represents the velosity vector; T and H are the temperature and chemical potential; $\vec{J}_s, \vec{J}_m$ are the vectors of entropy and mass fluxes.

For a classical thermoelastic body model $\vec{J}_m = 0$ resulting in the relation $\rho = \rho_* = const$, whereas for a local gradient thermoelastic body model for one component solids we suppose [2]

$$\vec{J}_m = -\frac{\partial \vec{\Pi}_m}{\partial \tau} \qquad \Longrightarrow \qquad \frac{\partial}{\partial \tau}\left(\rho - \vec{\nabla}\cdot\vec{\Pi}_m\right) = 0. \tag{2}$$

For entropy flux $\vec{J}_s$ in common case we can write its dependence on the corresponding thermodymamical force for a given state:

$$\vec{J}_s = \vec{J}_s\left(-\frac{\vec{\nabla}T}{T}; U\right), \qquad \vec{J}_s(0;U) = 0. \tag{3}$$

The generalisation of Gibbs' relation for local gradient approach takes the form

$$dU = TdS + Hd\rho + \vec{\nabla}H \cdot d\vec{\Pi}_m + \hat{\sigma} : d\hat{e}, \tag{4}$$

where U is the internal energy, $\hat{e}$ is the strain tensor.

On the basis of the relation (4) it can be said that the basic state parameters $S, \rho, \vec{\Pi}_m, \hat{e}$ determine the conjugate parameters $T, H, \vec{\nabla}H, \hat{\sigma}$ by such state equations

$$T = \frac{\partial U}{\partial S}, \qquad H = \frac{\partial U}{\partial \rho}, \qquad \vec{\nabla}H = \frac{\partial U}{\partial \vec{\pi}_m}, \qquad \hat{\sigma} = \frac{\partial U}{\partial \hat{e}}. \tag{5}$$

We shall consider linear constitutive equations (3),(5) for isotropic materials. Using the balance equations (1),(2) and the strain compatibility conditions a full set of linearized equations for isotropic thermoelastic body model in a steady state at a local gradient approach choosing stresses $\hat{\sigma}$, temperature $\theta = T - T_*$ and chemical potential $\eta = H - H_*$ perturbations for key functions have the form:

$$\vec{\nabla} \times \left\{\hat{\sigma} - \left[\frac{\lambda}{3\lambda + 2\mu}\sigma - 2\mu(\alpha_t\theta - \alpha_m\eta)\right]\hat{I}\right\} \times \vec{\nabla} = 0,$$

$$\vec{\nabla} \cdot \hat{\sigma} = 0, \qquad \nabla^2\eta - \kappa^2\eta - \kappa_t^2\theta - \kappa_s^2\sigma = 0, \qquad \nabla^2\theta = 0. \tag{6}$$

Here $\hat{I}$ is the identity tensor; $\sigma = \hat{\sigma} : \hat{I}$; "$\times$" denotes tensor product; λ, μ, α_t, α_m, κ^2, κ_t^2, κ_s^2 are constants.

Let us consider an equilibrium state of the isotropic thermoelastic layer (domain $|x| \le l$ in the Cartesian coordinates (x, y, z)). Assuming that the boundary conditions permit a one-dimensional solution the set (6) can be written in the form:

$$\frac{d^2\sigma_y}{dx^2} = \frac{d^2\sigma_z}{dx^2} = \frac{b_m}{2}\frac{d^2\eta}{dx^2}, \quad \frac{d\sigma_x}{dx} = 0, \quad \frac{d^2\eta}{dx^2} - \kappa^2\eta - \kappa_t^2\theta - \kappa_s^2\sigma = 0, \quad \frac{d^2\theta}{dx^2} = 0, \tag{7}$$

where $b_m = 4\mu(3\lambda + 2\mu)\alpha_m/(\lambda + 2\mu)$.

We accept the following boundary conditions:

$$\sigma_x(\pm l) = 0, \qquad \eta(\pm l) = \eta_a, \qquad \theta(\pm l) = \theta_a,$$

$$\int_{-l}^{l}\sigma_y dx = 2lp, \quad \int_{-l}^{l}\sigma_z dx = 0, \quad \int_{-l}^{l}x\sigma_y dx = 0, \quad \int_{-l}^{l}x\sigma_z dx = 0. \tag{8}$$

We get a solution of the problem (7),(8)in the following form:

$$\eta(x) = \eta_a + \frac{\kappa^2\eta_a + \kappa_s^2 p + \kappa_t^2\theta_a}{\xi^2\chi(\xi l)}\left(\frac{\cosh(\xi x)}{\cosh(\xi l)} - 1\right),$$

$$\sigma_z(x) = \frac{b_m}{2}\frac{\kappa^2\eta_a + \kappa_s^2 p + \kappa_t^2\theta_a}{\xi^2\chi(\xi l)}\left(\frac{\cosh(\xi x)}{\cosh(\xi l)} - \frac{\mathrm{tgh}(\xi l)}{\xi l}\right),$$

$$\sigma_y(x) = p + \sigma_z(x), \qquad \theta(x) = \theta_a. \tag{9}$$

Here $\xi^2 = \kappa^2 + b_m\kappa_s^2$, $\chi(\xi l) = 1 - D(1 - \mathrm{tgh}(\xi l)/(\xi l))$, $D = b_m\kappa_s^2/\xi^2$.

Now, it is clear from (9) that the chemical potential η/η_a equals 1 at the body boundary and decreases at $|x| \to 0$. It approaches 0 in the middle of thick layers, therefore, in this case, the chemical potential approximately equals one for media ($H \approx H_*$). In a natural body state ($p = 0, \theta_a = 0$) stresses $\sigma_y(x), \sigma_z(x)$ in the middle of the layer are negative while they are positive near the surface and reach an extreme value at surfaces $x = \pm l$. Surface stresses in a layer depend on the thickness. The value of $\sigma_y(\pm l)$ increases at $l \to \infty$ to the surface stress quantity for the semispace.

The extremal values of stresses are important for strength investigations. The maximum extending stress in the layer is $\sigma_y(\pm l)$ that is equal to

$$\sigma_y(\pm l) = p + \frac{1}{2}\frac{\kappa^2\eta_a + \kappa_s^2 p + \kappa_t^2\theta_a}{\kappa_s^2}\frac{1 - \chi(\xi l)}{\chi(\xi l)}. \tag{10}$$

We suppose that the theoretical breaking stress (the first classical theory in fracture mechanics) is σ^p. Assuming that the body will collapse if fracture condition holds at a point of the body, we obtain $\sigma_y(\pm l) = \sigma^p$ as a fracture criterion for the stretched layer. From (10) we find the breaking load of the layer:

$$p^k = \frac{2\chi(\xi l)}{1 + \chi(\xi l)}\sigma^p - \frac{\kappa^2\eta_a + \kappa_t^2\theta_a}{\kappa_s^2}\frac{1 - \chi(\xi l)}{1 + \chi(\xi l)}. \tag{11}$$

For thick layers $\chi(\xi l) \approx 1 - D$ and by

$$\sigma_+ = \frac{2(1 - D)}{2 - D}\sigma^p - \frac{\kappa^2\eta_a}{\kappa_s^2}\frac{D}{2 - D} \tag{12}$$

the quantity that can be interpreted as a strength point for the load of thick layers at the initial temperature on the basis of (11)and (12) we obtain the relation:

$$p^k = \frac{2 - D}{1 - D}\frac{\chi(\xi l)}{1 + \chi(\xi l)}\sigma_+ + \left(\frac{\chi(\xi l)}{1 + \chi(\xi l)}\frac{D}{1 - D} - \frac{1 - \chi(\xi l)}{1 + \chi(\xi l)}\right)\frac{\kappa^2\eta_a}{\kappa_s^2} - \frac{1 - \chi(\xi l)}{1 + \chi(\xi l)}\frac{\kappa_3^2\theta_a}{\kappa_s^2}. \tag{13}$$

The relation (13) describes both the temperature and size effects of strength. For thick layers ($\xi l >> 1$) we obtain a linear decrease in strength with temperature

$$p^k = \sigma_+ - \frac{D}{2 - D}\frac{\kappa_3^2}{\kappa_s^2}\theta_a, \tag{14}$$

that corresponds to the known experimental data. As follows from (12) and (11) magnitude of p^k changes between the σ^p and σ_+, i.e.

$$\sigma^p > p^k \geqslant \sigma_+.$$

Now, we will consider the deformation criterion of a fracture. The constitutive equation for strain can be written in the form:

$$\hat{e} = \frac{1}{2\mu}\hat{\sigma} + \left(\alpha_t\theta - \alpha_m\eta - \frac{\lambda}{2\mu(3\lambda + 2\mu)}\sigma\right)\hat{I}. \tag{15}$$

Taking into account the fact that $\sigma_x = 0$, $\sigma_y = p + \sigma_z$ from (15) we have

$$e_y = \frac{\lambda + \mu}{\mu(3\lambda + 2\mu)} p + \frac{\lambda + 2\mu}{2\mu(3\lambda + 2\mu)} \sigma_z + \alpha_t \theta - \alpha_m \eta.$$

If mechanical and thermal load is absent ($p = 0$, $\theta_a = 0$) then

$$e_y = e_y^* = \frac{\lambda + 2\mu}{2\mu(3\lambda + 2\mu)} \sigma_z - \alpha_m \eta.$$

The layer loading changes the deformation for the value

$$e_y - e_y^* = \frac{\lambda + \mu}{\mu(3\lambda + 2\mu)} p + \alpha_t \theta.$$

As a result, if there is an accepted strain criterion of the fracture, the size effects are absent. This result corresponds to the experimental investigations of the fracture size effects [3].

References

[1] Eringen A C and Edelen D G 1972 *On Nonlocal Elasticity, Int. J. Eng. Sci* **10** 233–248
[2] Nagirny T and Burak Y 1998 *Thermodynamical models of continual description of the coupled processes in thin-film systems, in Proc. Int. Conf. TRECOP'98*, World Scientific, 263–276
[3] Jono M, Sigeta A, Kimura T and Konzaki S 1992 *J. Soc. Mater. Sci. Jap* **41** 470

Elastic Properties of 3D Soft Dimers System at Zero Temperature

J. W. Narojczyk[a], K. W. Wojciechowski[b]

Institute of Molecular Physics, Polish Academy of Sciences,
M. Smoluchowskiego 17, 60-179 Poznan, Poland
[a] *narojczyk@ifmpan.poznan.pl*
[b] *kww@ifmpan.poznan.pl*

Elastic properties are among the fundamental characteristics of a material in terms of practical application. One of the quantities describing the elastic properties of solids is the Poisson's ratio [1]. In recent years a growing interest in materials exhibiting anomalous elastic properties, such as the negative Poisson ratio [2] has been observed. These materials, commonly known as *auxetics* [3], behave contrary to what we see every day, i.e. they increase (decrease) their transverse dimensions as a result of the applied longitudinal stretching (compressing). To manufacture a material with such extraordinary elastic property which is very useful from the point of view of the practical applications [2, 4–6], broad knowledge and deep understanding of the processes and phenomena governing the material's elastic properties is required. One way to acquire such knowledge is to study simple, well defined models where the influence of various structural level factors on macroscopic, elastic properties of the material can be shown explicitly.

Our research is focused on examining the influence of various types of structural aperiodicity on macroscopic elastic properties of the studied models. In this work a three-dimensional model system of diatomic, rigid molecules (*dimers*), interacting via soft, pair potential (n-inverse-power) is studied. Dimers form both, periodic and aperiodic (DC) phases. A comparison of elastic properties of periodic and aperiodic systems, and thus the influence of a structural disorder, is presented. This research is meant to extend the knowledge about possible microscopic mechanisms, both in two- [7] and three- dimensions [8, 9] which may lead to anomalous elastic properties of materials [10, 11]

Acknowledgements
This work was supported in part by the Ministry of Science and Higher Education grants Nos. N202 07032/1512 and NN 202 1353 33. Some simulations were performed at the Poznań Supercomputing and Networking Center (PCSS).

References

[1] L. D. Landau and E. M. Lifshitz 1986 *Theory of Elasticity* Pergamon Press, London
[2] R. S. Lakes 1987 "Negative Poisson's Ratio Materials" *Science* **238** 551
[3] K. E. Evans, M. A. Nkansah, I. J. Hutchinson, and S. C. Rogers 1991 "Molecular Network Design" *Nature* **353** 124

[4] K. E. Evans and K. L. Alderson 2000 "Auxetic Materials: the Positive Side of Being Negative" *Engineering Science and Education Journal* **9** (4) 148–54
[5] R. H. Baughman 2003 "Avoiding the Shrink" *Nature* **425** 667
[6] Ch. W. Smith and K. W. Wojciechowski 2008 Preface *Physica Status Solidi (b)* **245** 486–488 (see also other papers and references there)
[7] J. W. Narojczyk and K. W. Wojciechowski 2006 "Elastic Properties of Two-Dimensional Soft Discs of Various Diameters at Zero Temperature" *Journal of Non-Crystalline Solids* **352** (40–41) 4292–4298
[8] M. Kowalik and K. W. Wojciechowski 2005 "Poisson's Ratio of Degenerate Crystalline Phases of Three-Dimensional Hard Dimers and Hard Cyclic Trimers" *Physica Status Solidi (b)* **242** 626–631
[9] M. Kowalik and K. W. Wojciechowski 2006 "Poisson's ratio Of Orientationally Disordered Hard Dumbbell Crystal in Three Dimensions" *Journal of Non-Crystalline Solids 352* 4269–4278
[10] J. W. Narojczyk and K. W. Wojciechowski 2007 "Elastic Properties of Two-dimensional Soft Polydisperse Trimers at Zero Temperature" *Physica Status Solidi (b)* **244** (3) 943–954
[11] J. W. Narojczyk, A. Alderson, A.R. Imre, F. Scarpa, and K. W. Wojciechowski 2008 "Negative Poisson's Ratio Behavior in the Planar Model of Asymmetric Trimers at Zero Temperature" *Journal of Non-Crystalline Solids* (in print)

Polymer Assisted Fabrication and Properties of Nanocomposites with Non-Aggregated Magnetic Particles

I. Opainych[1], O. Aksimentyeva[1], H. Szymczak[2], V. Dyakonov[2], M. Melnik[1]

[1] *Ivan Franko National University of L'viv*
6 Kyrylo and Mephodii str., 79005 L'viv, Ukraine

[2] *Institute of Physics, Polish Academy of Science*
Al. Lotników 32/46, 02-668, Warsaw, Poland

Nanoscale magnetic composites have unique properties for application in biology, medicine, digital technology and theoretical investigations [1–4]. Creation of polymer composites with metal oxide compounds requires an understanding of the component interaction nature and studying the size effect in composites which may provide control over the parameters in the obtained materials. In our report the investigation of the synthesis and characterization of polymer nanocomposites with non-aggregated magnetic particles, synthesized on the basis of a high dispersion magnet suspension is presented. One of the most important features of finely divided materials determining their physico-chemical and processing properties is their granulometric composition. The quality of the produced composites depends to a considerable extent on the dispersion ability of a magnetic slurry. In most cases magnetic dispersion is obtained by mechanical dispersion. However, it does not give a possibility of obtaining a magnetite with a high scale of dispersion ability. It is expedient to obtain a highly dispersive magnetite by a condensation method. Besides inflecting the conditions of synthesizing, a possibility is afforded to influence the degree of dispersion.

We have studied the aggregate stability of magnetite samples obtained by the condensation method [5]. A sedimentation analysis is frequently applied to control the dispersivity of powders in both industry and science.

A sedimentation analysis of aqueous dispersions of magnetite models has been carried out by the weight method, applying torsion-balance techniques. The sedimentation curves have been processed by the piece-wise smooth-approximation method, and a set of dispersivity parameters has been determined. This method makes it possible to describe the kinetics of subsidence of a slurry by a finite number of rectilinear parts and to gain accounts characteristic for an analytical method, of the average quantitative characteristics of the dispersion ability.

The curves of sedimentation of a powdered magnetite included in miscellaneous amounts in the investigated disperse systems are presented in Figure 1.

The histograms characterizing a fractional composition of the obtained slurries represent a synthesized magnetite in an acidic environment and much highly dispersive magnetite particles are formed which is testified by the histograms in Figure 2.

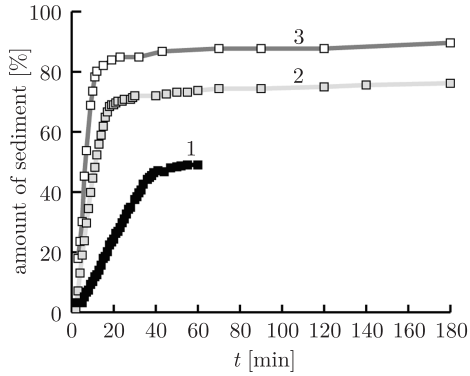

Figure 1: Curves of powdered magnetite sedimentation; magnetite synthesized in acidic environment. The concentration of the disperse phase: 1 – 0.50%, 2 – 0.25%, 3 – 0.13%

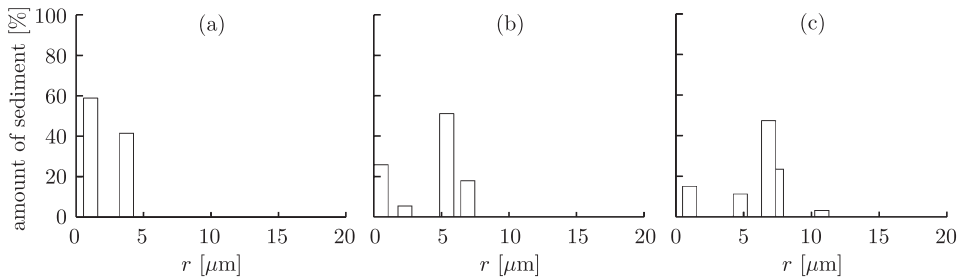

Figure 2: Histograms distribution of magnetite particles by radius. Magnetite synthesized in acidic environment; the concentration of the disperse phase: (a) 0.50%, (b) 0.25%, (c) 0.13%; probable radii of magnetite particles: (a) 1.84 μm, (b) 3.61 μm, (c) 5.32 μm

The influence of the quantitative substance on the aggregate stability of aqueous dispersions of a magnetite has been studied in a dispersing medium by the sedimentation analysis method. It has been shown that a reduction of the dispersed phase amount leads to magnification of the aggregate stability of a magnetite in an aqueous dispersing medium and reduction. The presence of an acidic environment results in the formation of a more highly dispersive slurry [5].

Table 1: Physical-chemical properties of magnetite-polymer composites

Sample No.	Fe_3O_4 concentration [%]	Radius of particles Fe_3O_4 [μm]	Magnetic susceptibility $\chi \cdot 10^{-6}$ [cm^3/g]	Granule radius for composite [μm]	Temperature of polymerization t [°C]	Fe atom content in composite [at. %]	Period of elementary cell [Å]
1	5.83	4.29	1797	1.5–2.0	65	4.2167	8.36(2)
2	5.97	4.29	1969.2	1.5–2.0	65	4.3119	8.357(9)
3	7.40	2.53	2822	2.0–2.5	80	5.3555	8.333(9)
4	7.71	2.53	2589	2.0–2.5	80	5.5788	8.35(2)
5	8.53	2.53	2123	2.5–3.0	80	6.1722	8.36(2)
6	11.03	4.29	2676	1.5–2.0	65	7.9793	8.338(2)

Based on the obtained magnetite dispersion, the polymer assisted fabrication of nanocomposites with non-aggregated magnetic particles by suspension polymerization of vinyl monomers (styrene and butyl acrylate) has been carried out. The properties of synthesized magnetic composites have been studied by investigation of the magnetic susceptibility and an X-ray analysis [6]. The obtained results are presented in Table 1.

An analysis of the obtained results shows that the properties of magnet contained composites depend both on the size of magnetite particles and the size of granules for the dispersion of the investigated composites.

References

[1] Sawada H, Yoshioka H, Kawase T, et al 2005 *Journal of Fluorine Chemistry* **126** 914.
[2] Xiao J, Otaigbe J U and Jiles D C 2000 *Journal of Magnetism and Magnetic Materials* **218** 60
[3] Vasyukov V N, Dyakonov V P, Shapovalov V A, Aksimentyeva E I, Szymczak H and Piehota S 2000 *Low Temperature Phys3cs* **26** (4) 265
[4] Opaynych I, Maleytv I and Tsvetkov M 2002 *Book of Abstracts of NIP18 International Conference on Digital Printing Technologies. San Diego, California, USA.* 148
[5] Opaynych I and Maleev I 2003 *Patent No. 62416A. (UA)*
[6] Opaynych I, Aksimentyeva O, Belan B, Mańcako M, Stadnyk Yu and Nierpewski K 2005 *Book of Abstracts of 2O International Conference on.Crystal Chemistry of Intermetalic Compounds, Lviv. Ukraine, 20-24 September* 132

FMR Study of Nickel Nanoparticles in Concrete

N. Guskos[1,2], G. Żołnierkiewicz[2a], M. Orłowski[2], J. Typek[2], J. Błyszko[3], W. Kiernożycki[3], U. Narkiewicz[4], M. Podsiadły[4]

[1] *Solid State Section, Department of Physics, University of Athens Panepistimiopolis, 15 784 Zografou, Athens, Greece*

[2] *Institute of Physics, Szczecin University of Technology Al. Piastów 17, 70-310 Szczecin, Poland*
[a] *grzegorz.zolnierkiewicz@ps.pl, phone +48914494181*

[3] *Faculty of Civil Engineering and Architecture Szczecin University of Technology Al. Piastów 50, 70-311 Szczecin, Poland*

[4] *Institute of Chemical and Environment Engineering Szczecin University of Technology Pułaskiego 10, 70-332 Szczecin, Poland*

Three types of samples containing concrete with and without a low concentration of magnetic nanoparticles of nickel enclosed in carbon have been prepared. The samples have been investigated by the ferromagnetic resonance (FMR) and compression strength methods.

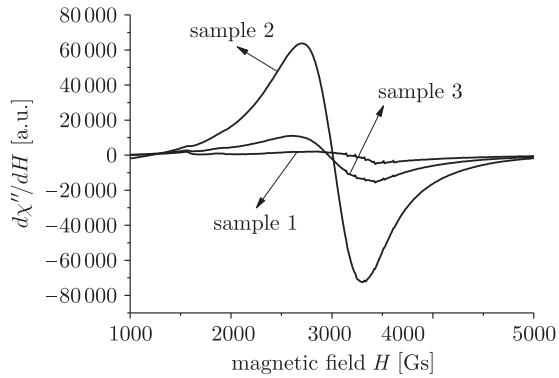

Figure 1: Room temperature EPR spectra of concrete with and without magnetic – nanoparticles

Figure 1 presents the FMR spectra of the following samples: concrete in powder form (sample 1), concrete powder/nanoparticles (sample 2), and powder/nanoparticles/water (sample 3). No difference is observed in the FMR spectra for the two former

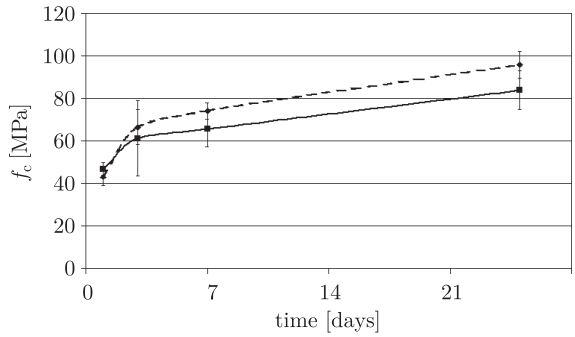

Figure 2: Room temperature compression strength (f_c) of concrete with and without magnetic nanoparticles (dashed and solid lines, respectively)

cases. Samples containing magnetic nanoparticles have shown a wide and intense, almost symmetrical, FMR line (Fig. 1), while a sample with additional water molecules have displayed an essentially lower intensity spectrum. These differences arise from water molecules with a high dielectric constant value. A compression strength study of samples with and without nickel nanoparticles has shown an over 15% difference in both types of samples (Fig. 2). Interaction of magnetic nanoparticles in non-magnetic materials could essentially change their physical properties.

Optical Spectroscopy and Up-Conversion Luminescence of Ho^{3+} Centres in Glass with $3CaO-Ga_2O_3-3GeO_2$ Composition

B. V. Padlyak[1a], Cz. Koepke[2], D. Piątkowski[2], K. Wiśniewski[2,3], B. Kukliński[3]

[1] *Institute of Physical Optics of the Ministry of Education and Science of Ukraine*
23 Dragomanov Str., 79-005, L'viv, Ukraine
[a] *bohdan@mail.lviv.ua*

[2] *Institute of Physics, Nicolaus Copernicus University*
Grudziądzka 5, 87-100 Torun, Poland

[3] *Institute of Experimental Physics, University of Gdansk*
Wita Stwosza 57, 80-952 Gdansk, Poland

Crystals and glasses activated by Ho^{3+} are promising materials for active elements of solid-state lasers, including diode pumped up-converted lasers. For these reasons optical and spectroscopic properties of such materials have been extensively investigated during last years [1]. This also concerns disordered crystals and glasses of $CaO-Ga_2O_3-GeO_2$ (CGG) and similar systems activated by Ho^{3+} that seem to be promising materials for solid state lasers. At the present time, high quality Ho-doped glasses with $Ca_3Ga_2Ge_3O_{12}$ (or $3CaO-Ga_2O_3-3GeO_2$) garnet composition have been obtained in corundum crucibles by a high-temperature synthesis technique according to [2].

In the presented work the results of investigations of the ground state absorption (GSA), excited state absorption (ESA), Stokes and anti-Stokes (up-converted) emission spectra as well as luminescence kinetics and the local structure of Ho^{3+} centres in a holmium doped glass (content of Ho_2O_3 is 0.7 wt. %) are summarised and discussed.

Using electron paramagnetic resonance (EPR) and optical spectroscopy techniques it has been shown that the Ho impurity is build in into the $3CaO-Ga_2O_3-3GeO_2$ glass network exclusively as Ho^{3+} ions [3, 4] (electron configuration – $4f^{10}$, ground state – $^5I_8$). All transitions typical for Ho^{3+}, in the UV and visible (absorption and luminescence spectra) have been identified [3, 4]. The GSA absorption and luminescence excitation spectra, measured in the 270–700 nm spectral range at temperatures 300 and 85 K consist of several absorption bands with a weakly resolved structure, which correspond to the following f-f transitions: (^{3}H, ^{5}D, ^{1}G)$_4$, (^{5}G, ^{5}D, ^{3}G)$_4$, (^{5}F, ^{3}F, ^{5}G)$_2$, ($^3H_6$+$^3H_5$), ($^3K_7$+$^5G_4$), (^{5}G, ^{3}G)$_5$, ($^5F_1$+$^5G_6$+$^3K_8$), ($^5F_2$+$^5F_3$), ($^5F_4$+$^5S_2$), and $^5F_5$.

The emission spectra measured at room and liquid nitrogen temperatures, under excitation at $\lambda_{exc} = 455$ nm, consist of an intense band with a maximum near 545 nm ($^5F_4$, $^5S_2 \rightarrow {}^5I_8$ transitions) and several weak bands corresponding to $^5F_3 \rightarrow {}^5I_8$, $^5F_5 \rightarrow {}^5I_8$, and $^5S_2 \rightarrow {}^5I_7$ transitions in the 480–800 nm spectral range [3].

The GSA and luminescence (emission and excitation) spectra of the Ho^{3+} centres in glasses of a CGG system are almost independent on the basic glass composition and temperature in the 85–300 K range and are characterised by significant inhomogeneous broadening related to a disorder in the glass structure. The inhomogeneous broadening in the optical spectra reflects a broad distribution of interatomic distances in the first coordination sphere around the Ho^{3+} centres and is connected with compositional disordering of the second coordination sphere.

The Ho^{3+} optical spectra have been analysed using the Judd-Ofelt theory. As a result, the oscillator strengths, intensity parameters Ω_2, Ω_4, and Ω_6, radiative emission rates, branching ratios and radiative lifetime for Ho^{3+} centres in the glass of $Ca_3Ga_2Ge_3O_{12}$ composition have been calculated and analysed in comparison with the corresponding parameters of oxide crystal and glasses of different compositions.

The luminescence decay curve for $^5S_2 \rightarrow {}^5I_8$ transition ($\lambda_{max} = 545$ nm) of the Ho^{3+} centres under excitation with $\lambda_{exc} = 455$ nm has been satisfactorily described in the framework of two-exponential approximations with lifetimes: $\tau_1 = 7.5$ μs, $\tau_2 = 3.9$ μs, obtained at $T = 295$ K [4]. The two types of luminescence centres: Ho^{3+} (I) ($\tau_1 =$ 7.5 μs, relative amount – 57%) and Ho^{3+} (II) ($\tau_2 = 3.9$ μs, relative amount – 43%) in the $3CaO{-}Ga_2O_3{-}3GeO_2$ glass network have been proposed in [4]. The obtained experimental lifetimes have been compared and discussed with those calculated with the Judd-Ofelt theory.

The local structure of Ho^{3+} centres in the $3CaO{-}Ga_2O_3{-}3GeO_2$ glass network is determined utilizing the luminescence kinetics and EXAFS (Extended X-ray Absorption Fine Structure) spectroscopy results. The structural parameters (interatomic distances and coordination numbers to oxygen) for Ga and Ge atoms in the un-doped and rare-earth (Ho, Eu, Er) doped glasses with $Ca_3Ga_2Ge_3O_{12}$ garnet compositions have been obtained from the Ga and Ge K-edge EXAFS analysis [5, 6]. It has been shown that the introduction of rare-earth ions modifies the local structure around the Ga atoms in the glass network, whereas the Ge-subsystem in the glass structure remains completely unaffected by the presence of rare-earth dopants. On the basis of the obtained optical spectroscopy data and EXAFS spectra (L_3-edge) of the Ho, Er, and Eu analysis, the local structure of the rare-earth luminescence centres in the glass with $Ca_3Ga_2Ge_3O_{12}$ composition, it has been shown that Ho^{3+} and other luminescence centres occupy the glass network sites with the coordination number to oxygen $N = 6$ [7]. Because the EXAFS spectroscopy shows only one type of structural positions for rare-earth luminescence centres in the glass network, it has been assumed that two lifetime values correspond to two different ensembles of Ho^{3+} centres in the sites with $N = 6$, which are characterised by long and short average lengths of interatomic bonds.

The results of excited state absorption and up-converted emission spectra of Ho^{3+} centres in the examined glass have been presented and analysed. The observed ESA transitions have been assigned on the energy levels diagram of the Ho^{3+} ions. According to the ESA data the channels for an up-converted emission have been identified and the predicted up-converted emission bands have been registered under Ar ion laser excitation ($\lambda = 488$ nm) [8]. On the basis of the obtained results the scheme of

possible energy transfer and mechanism of up-converted transitions for Ho^{3+} centres in the investigated prototype material is proposed.

References

[1] Kaminskii A A, 1996 *Crystalline Lasers: Physical Processes and Operating Schemes* Boca Raton (FL), New York: TAYLOR & FRANCIS 592 p.
[2] Padlyak B V and Buchynskii P P 1998 *Patent of Ukraine* No UA 25235 A
[3] Padlyak B V, Kukliński B and Buchynskii P P 2003 *Opt. Appl.* **XXXIII** (1) 175
[4] Padlyak B, Vlokh O and Sagoo K 2005 *Ukr. J. Phys. Opt.* **6** (1) 33
[5] Chełstowski D, Witkowska A, Rybicki J, Padlyak B, Trapananti A and Principi E 2003 *Opt. Appl.*. **XXXIII** (1) 125
[6] Witkowska A, Padlyak B and Rybicki J 2006 *J. Non-Cryst. Solids* **352** (40–41) 4346
[7] Witkowska A, Padlyak B and Rybicki J 2008 *Opt. Mater.* **30** 699
[8] Padlyak B, Koepke Cz, Piątkowski D, Wioniewski K and Kuklinski B 2008 *J. Non-Cryst. Solids* (in press)

Magnetoresistance Relating to the Integer Hall Effect

G. J. Papadopoulos

Department of Physics, Solid State Physics Section, University of Athens, Panepistimiopolis, GR 157 84, Zografos, Athens, Greece

The formalism, developed earlier, for the magnetoresistance exhibited by a material, in the form of a rectangular parallelepiped, subjected to a perpendicular magnetic field is shown to apply in the case whereby the carriers are constrained in a way as to form a two dimensional gas. Utilizing parameters relating to the geometry of the carrier gas together with other parameters involved in our formulae such as temperature, mobility, and carrier density we are able to obtain the quantized magnetoresistance pertaining to the von Klitzing quantized Hall effect emerging at low temperature. The analysis shows that derivation of the magnetoresistance, in question, results from combination of the diffusion coefficient in terms of the magnetic field and the free field carrier mobility. Indeed, by varying the zero field mobility one can see that for fixed low temperature and given carrier density the almost zero resistance regions, characteristic to the integer Hall effect, do not appear. Increase in the mobility leads to the quantized magnetoresistance, and depending on the mobility value certain of the narrow resistance elevations at values of the magnetic field associated with the various filling factors may or may not become manifest. The case whereby such resistance elevations hide out has been observed in experiments. However, depending on the mobility value an uninterrupted succession of resistance elevations does appear. Furthermore, the height of resistance elevations depends on the mobility.

References

[1] G. J. Papadopoulos *J. Non-Cryst. Solids* **352** (2006) 4206
[2] G. J. Papadopoulos, *Rev. Adv. Mater. Sci.* **14** (2007) 187–192

Purification of Multi-Walled Carbon Nanotubes by Hydrogenation Method

I. Pełech, U. Narkiewicz, M. Podsiadły, D. Sibera

Institute of Chemical and Environment Engineering
Technical University of Szczecin
Pułaskiego 10, 70-322 Szczecin, Poland

Over the last year the catalytic growth of carbon nanotubes (CNTs) has been extensively studied using different methods: laser ablation, arc-vaporization or catalytic chemical vapor deposition [1–3]. These materials are produced together with a significant amount of other carbon products, such as amorphous carbon, carbon fibers and graphitic particles. In case of production of CNTs by catalytic methods, the catalyst particles remain in the product as an additional impurity. The separation of carbon nanotubes from catalyst traces and catalyst carriers is most often performed using hydrochloric [4], nitric [5] or hydrofluoric acids [6]. The oxidation method has been applied for purification of carbon nanotubes of carbon impurities. Amorphous carbon can be eliminated by oxidation in air flow [7] or by oxidation by potassium permanganate [8], hydrogen peroxide [9], ozone [8], perchloric acid [8]. In contradiction to detailed investigations concerning gasification of carbon by different oxidizing agents, some data is available with respect to the gasification of carbon by hydrogen.

This paper deals with the studies of nanocarbon materials formation using a doubly promoted (Al_2O_3, CaO) iron catalyst and ethylene as a carbon source. The carburisation processes were performed at 500°C and 550°C under atmospheric pressure. The increase in the carbon mass was controlled using a thermobalance (considered as an differential reactor). The samples after carburisation contained iron carbide (cementite) and carbon structures in the form of carbon nanofibers and nanotubes. The amorphous carbon can form as well and iron particles can be encapsulated by graphitic coating. In order to remove the amorphous carbon and the thick carbon nanofibers the samples were reduced with hydrogen in the range of temperatures from 460°C to 520°C. As a result of this treatment the cementite was decomposed to iron and methane. Amorphous carbon and thick carbon nanofibers were also removed and multiwalled carbon nanotubes about 10–30 nm in diameter remained. The samples after carburisation and hydrogenation were analyzed using the HRTEM (High Resolution Transmission Electron Microscopy) method (Jeol JEM 3010) and the X-ray diffraction method (Philips X'Pert).

The proposed method of reduction of nanocarbon materials with hydrogen can be applied for controlled purification of multiwalled carbon nanotubes of carbon impurities.

References

[1] Hernadi K, Fonseca A, Nagy J B, Bernaerts D and Lucas A A 1996 *Carbon* **34** 1249

[2] Venegoni D, Serp P, Feurer R, Kihn Y, Vahlas C and Kalck P 2002 *Carbon* **40** 1799
[3] Park C and Keane M A 2004 *J. Catal.* **221** 386
[4] Jeong T, Kim W Y and Hahn Y B 2001 *Chem. Phys. Lett.* **344** 18
[5] Takehira K, Ohi T, Shishido T, Kawabata T and Takaki K 2005 *Appl. Catal. A: General* **283** 137
[6] Colomer J F, Piedigrosso P, Fonseca A and Nagy J B 1999 *Synth. Met.* **103** 2482.
[7] Li W Z, Wen J G, Sennett M and Ren Z F 2003 *Chem. Phys. Lett.* **368** 299
[8] Hernadi K, Siska A, Thiên-Nga L, Forró L and Kiricsi I 2001 *Solid State Ionics* **141–142** 2003
[9] Ando Y, Zhao X, Inoue S and Iijima S 2002 *J. Cryst. Growth* **237–239** 1926

Dependence of Free Radicals/Magnetic Agglomerates Concentration on EPR/FMR Spectra

N. Guskos[1,2], G. Żołnierkiewicz[2], J. Typek[2],
A. Guskos[2], D. Petridis[3], P. Dallas[3]

[1] *Solid State Section, Department of Physics, University of Athens Panepistimiopolis, 15 784 Zografos, Athens, Greece*

[2] *Institute of Physics, Technical University of Szczecin Al. Piastów 17, 70-310 Szczecin, Poland*

[3] *NCSR "Demokritos", Aghia Paraskevi, Attikis, Athens, Greece*

Samples of an extended free radical network derived from condensation of cyanuric chloride with p-phenylenediamine have been used to obtain different concentrations of magnetic centres (free radicals and magnetic agglomerates). The iron nitrate has been used as an oxidant and the temperature dependent magnetic resonance spectra have been measured in the 290–90 K range. The magnetic resonance measurements at room temperature have shown a coexistence of two spectra arising from two different magnetic centers: one narrow line at the resonance field $H_r = 3374.48(3)$ Gs ($g_{eff} = 2.0031(1)$) with linewidth $\Delta H = 8.31(2)$ Gs, attributed to a free radical, and another broad line at $H_r = 2995(5)$ Gs ($g_{eff} = 2.254(1)$) with linewidth $\Delta H_{pp} = 1263(5)$ Gs, attributed to magnetic iron-oxide agglomerates. The investigated samples have been prepared in such a way that the broader line has been more intense. The temperature dependence of the magnetic resonance lines has shown significant changes. The integrated intensities have decreased with the decreasing temperatures in both spectra in a high temperature range.

This type of behavior is similar to that observed for magnetic nanoparticles in nonmagnetic matrixes. The resonance field of the broad line shifts to lower magnetic fields upon lowering the temperature with the gradient $\Delta H_r/\Delta T = 1.5(1)$ Gs/K, while the narrow line shifts towards higher magnetic fields with $\Delta H_r/\Delta T = 0.020(1)$ Gs/K. The linewidth of the broader line increases with the decreasing temperature while the narrow line remains almost constant. Magnetic iron-oxide clusters could produce an internal magnetic field which acts on free radicals. This field could induce free radicals to form a magnetic ordered state at high temperatures.

Electrophysical Properties of Thin Layers of Intermetallic Compounds

V. Prysyazhnyuk, S. Mudry, O. Mykolaychuk

Department of Physics, Ivan Franko National University of L'viv
8 Kyrylo and Mephodii str., 79005 L'viv, Ukraine

Influence of thickness and conditions of precipitation on electrophysical properties of Gd-Fe films was investigated. The films have been obtained by a thermal vacuum evaporation of a polycrystalline charge of the respective composition. Thickness of films has been determined with an optical interferometer (100–200 nanometers). The temperature of substrates carriers varied in the range of 300–500 K. Our investigations allowed us to conclude, that the value of electrical conduction, temperature coefficient of resistance and thermoelectromotive force depend on many factors: film thickness, preparation procedure and substrate temperature. Thermal annealing of films and subsequent ageing for 1–3 years under stable conditions did not result in significant changes of their electrophysical properties. This fact suggests that the character of scattering in the explored films remains invariable. Three mechanisms of current carriers dispersion, i.e. electron-phonon dispersion, dispersion due to the size effects (when the thickness of a film becomes comparable to a free path of electrons) and a dispersion of carriers at grain boundaries, contribute to the electrical conductivity of amorphous films. Furthermore, three different deposition modes resulted in amorphous, amorphous-crystalline and polycrystalline films.

Monte Carlo Simulations of Self-assembling in Block Copolymer Brushes

P. Romiszowski, A. Sikorski

Department of Chemistry, University of Warsaw
Pasteura 1, 02-093 Warszawa, Poland

We studied a simplified model of a polymer brush formed by linear chains, which positions were restricted to vertices of a simple cubic lattice. The macromolecules consisted of a sequence of hydrophilic and hydrophobic segments arranged in a specific sequence. The chains were grafted to an impenetrable surface, i.e. they were terminally attached to the surface with one end. The properties of this model system were determined by means of Monte Carlo simulations using a Metropolis-like sampling algorithm based on local changes of chain's conformations. The number of chains was varied from low to high grafting density. The model system was studied at different solvent quality from good to poor solvent. The structure and the dynamic properties of the brush were determined and discussed.

References

[1] Gelbart W M, Roux D, Ben-Shaul A (Eds) 1994 *Micelles, Membranes, Microemulsions and Monolayers* Springer Verlag, Berlin
[2] Zhao B and Brittain W J 2000 *Prog Polym Sci* **25** 677
[3] Romiszowski P and Sikorski A 2007 *J. Phys. Cond. Mat.* **19** 205137

Temperature Dependence of FMR Spectra of Low Concentration of Nickel Magnetic Nanoparticles in PBT-PTMO Polymer

N. Guskos[1,2], M. Maryniak[2], J. Typek[2], P. Podsiadły[3], U. Narkiewicz[3], E. Senderek[4], Z. Rosłaniec[4]

[1] *Solid State Section, Department of Physics, University of Athens Panepistimiopolis, 15 784 Athens, Greece*

[2] *Institute of Physics, Szczecin, University of Technology Al. Piastów 17, 70-310 Szczecin, Poland*

[3] *Institute of Chemical and Environmental Engineering Szczecin University of Technology Al. Piastów 17, 70-310 Szczecin, Poland*

[4] *Institute of Materials Science and Engineering Szczecin University of Technology Al. Piastów 17, 70-310 Szczecin, Poland*

Fine particles of a face-centered-cubic phase of Ni embedded in a PBT-*block*-PTMO polymer at a concentration of 0.1% have been prepared. The mean crystalline size of Ni has varied from 8 nm to 30 nm. The FMR investigations have been carried out in the 4–300 K temperature range (Fig. 1).

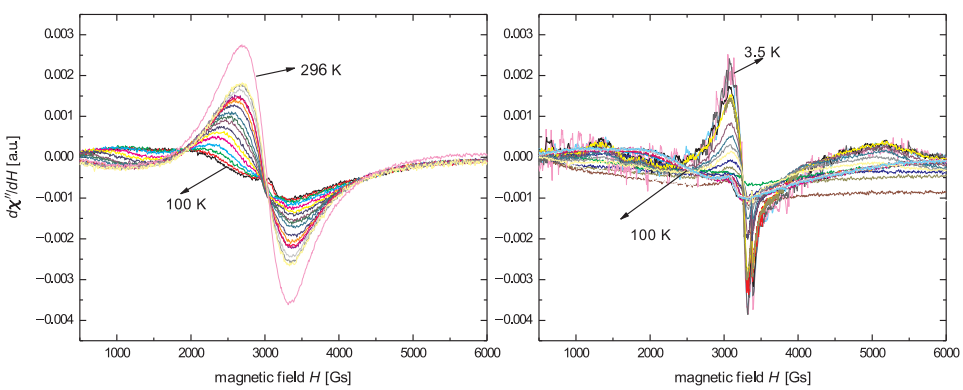

Figure 1: Temperature dependence of the FMR spectra of Ni magnetic nanoparticles in PBT-*block*-PTMO

An almost symmetrical and very intense magnetic resonance line has been recorded for all the investigated samples. The resonance line is centered at $g = 2.240(2)$ ($H_r = 2988(1)$ Gs) with linewidth $\Delta H_{pp} = 560(2)$ Gs and its integrated intensity increases with

a temperature increase. The resonance field ($\Delta H_r/\Delta T$) gradient strongly depends on the temperature with the following values in different temperature ranges:

- $\Delta H_r/\Delta T$(temperature range 295–172 K) = 1.1 Gs/K,
- $\Delta H_r/\Delta T$(172–75 K) = 8.5 Gs/K,
- $\Delta H_r/\Delta T$(75–40 K) = 0 Gs/K and
- $\Delta H_r/\Delta T$(40–17 K) = 70.7 Gs/K.

The internal magnetic field increases strongly at low temperature and shifts the resonance field to very a small field below 17 K. The linewidth increases with a temperature decrease and its strong change is registered below 40 K.

Features of Light Scattering by Surface Fractal Structures

O. Yu. Semchuk, D. L. Vodopianov, L. Yu. Kunitska

Institute of Surface Chemistry
National Academy of Sciences of Ukraine
03164, Kyiv, Ukraine

The average coefficient of light scattering by surface fractal structures in the frame of the Kirchhoff method has been calculated in this paper. A normalized band-limited Weierstrass function is presented for modeling 2D fractal rough surfaces. Scattering indicatrises diagrams for various surfaces and falling angles have been calculated on the basis of a numerical calculation of the average scattering coefficient. An analysis of the diagrams has resulted in the following conclusions: the scattering is symmetrical with respect to the fall plane; the picture becomes complicated with an increase in the surface calibration degree; the greatest intensity of a scattering wave is observed in a mirror direction; there are other directions in which bursts of intensity are observed.

Paramagnetic Centers in Oxide Nanopowders

V. N. Shevchuk[1a], Yu. N. Usatenko[2], D. I. Popovych[3], R. Ya. Serkiz[2]

[1] *Department of Electronics, L'viv Ivan Franko National University*
Dragomanova 50, 79005 L'viv, Ukraine
[a] *shevchuk@electronics.wups.lviv.ua*

[2] *Scientific and Technical Center of Low-Temperature Investigations*
L'viv Ivan Franko National University,
Dragomanova 50, 79005 L'viv, Ukraine

[3] *Yaroslav Pidstryhach Institute of Applied Problems of Mechanics and Mathematics NASU*
Naukova 3b, 79060 L'viv, Ukraine

Nanopowders SiO_2, ZnO and composites based on these materials are widely used in modern nanoelectronics, medical chemistry and other fields of science and technology. Moreover, nano-SiO_2 is used for modification of properties of other nanomaterials. Namely, the ZnO−SiO_2 nanocomposites luminescence is more intensive than in case of nano-ZnO. Luminescent sensors and high-effective displays are developed on the basis of these compounds. The characteristics of nano-SiO_2 are improved by the introduction of vanadium nanoclusters and the effect of V_2O_5-microphase formation has been observed for some V/Si ratios.

Scale factors, stability and reproductivity of nanomaterials characteristics rely on point defects. Vacancy type structural defects are more adequate for undoped nanopowders. If one (unpaired) electron is localized at such a defect, detection of EPR (electronic paramagnetic resonance) signal is possible. Thus, the EPR method is appropriate for the control of nanopowders with a paramagnetic impurities synthesis.

In this study, ZnO and $SiO_2-xV_2O_5$ ($x = 0$–10%) nanopowders obtained by the sol-gel method have been investigated by the EPR technique [1] at the liquid nitrogen temperature. Moreover, the luminescent properties of the samples have been studied. A raster electron microscope-analyzer has been applied for the investigation of the surface morphology and chemical element-wise composition of the samples.

As a result, complex EPR spectra with low-intense and relatively narrow lines (with 0.5–0.9 mT half-widths) for parent materials have been registered. For both nanomaterials, the most intensive EPR signal has been detected in the vicinity of the free electron g-factor (the isotropic g-factor assumption gives 2.001±0.001 and 1.998±0.001 for $SiO_2-V_2O_5$ and ZnO, respectively). The discovered paramagnetic centers are anticipated to be single-charged vacancies in an oxygen sublattice (oxygen vacancy with one captured electron). The fine structure of the $SiO_2-V_2O_5$ nanocomposite EPR line (eight equidistant components) is suggested to be due to an interaction between the unpaired electron and the nucleus V^{51}. The low-intense EPR signals for ZnO at higher magnetic fields with respect to the position of the major signal (g-factors are 1.975±0.001 and 1.960±0.001) are due to a shallow donor state and uncontrolled impurity, respectively. In this study, the influences of UV-irradiation and

high temperature treatments in various atmospheres on the EPR signals have been investigated. The existence of the "ion V−E′-center" complex as a probable defect in nano-SiO_2−V_2O_5 and other models of point defects in nanopowders are discussed.

References

[1] Shevchuk V. N., Popovych D. I., Usatenko Yu. N., Serkiz R. Ya. and Tsvetkova O. V. *Regional Science Seminar Modern Problems of Electronics. 31 Yanuary – 1 February, 2008, L'viv, Ukraine, L'viv Ivan Franko National University* Book of Abstr., L'viv Ivan Franko National University, 2008, pp. 68–69.

On the Photovoltaic Effect in a Hybrid Heterojunction Formed from Palladium Phthalocyanine and Titanium Dioxide Layers

R. Signerski, G. Jarosz, B. Kościelska

Faculty of Applied Physics and Mathematics
Gdansk University of Technology
G. Narutowicza 11/12, 80-952 Gdansk, Poland

Hybrid devices formed from titanium dioxide (TiO_2) and polymers as well as low molecular weight organic compounds exhibit interesting photovoltaic properties. In such kind of devices, TiO_2 constitutes an n-type semiconductor with a high light transmission and a good chemical and thermal stability. The organic materials should then exhibit the holes transport and high light absorption ability. The fundamental process of charge carrier photogeneration in these systems results from the dissociation of the excited state of an organic material at the TiO_2/organic interface, which leads to the electron transfer to the conduction band of TiO_2 and the hole moving in the organic material.

The work presents the results of research on photovoltaic properties of a system formed from tin oxide, titanium dioxide, palladium phthalocyanine and gold. TiO_2 films were deposited using a sol-gel method, PdPc and Au were subsequently evaporated under a high vacuum. In the dark the system exhibits a strong rectification effect, while an effective photogeneration of charge carriers within the TiO_2/PdPc junction is observed under illumination. The experimental relations of short-circuit current and open-circuit voltage versus light intensity suggest that interface states participate in generation-recombination processes.

This work has been supported by Polish Ministry of Science and Higher Education with a grant for 2006-2009 under Program No. 3T11B06530.

Characterization of Thin Conductive Polymer Films Deposited by Ionic Sputtering in Crossed Electromagnetic Field

P. Stakhira[1a], V. Cherpak[1], B. Tsizh[2], V. Belukh[3]

[1] *L'viv Polytechnic National University*
12 S. Bandera str., 79013 L'viv, Ukraine
[a] *stakhira@polynet.lviv.ua*

[2] *Kazimierz Wielki University*
Chodkiewicza 30, 85-064 Bydgoszcz, Poland

[3] *Ivan Franko L'viv National University*
50 Dragomanov str., L'viv, Ukraine

The technological conditions for conductive polymer thin films by ionic sputtering in argon atmosphere are considered. Ionic sputtering of polyaniline in crossed electromagnetic fields results in formation of conductive polymer films. The method allows to obtain chemically sensitive polymer films without additional doping.

On Weakly Dispersive Multiple-trapping Transport

W. Tomaszewicz

Department of Physics of Electronic Phenomena
Gdansk University of Technology
Narutowicza 11/12, 80-952 Gdansk, Poland
wtomasze@sunrise.pg.gda.pl

The equations for multiple-trapping carrier transport, corresponding to the time-of-flight (TOF) method, are approximately solved under assumption that the majority of carriers are in thermal quasi-equilibrium. The solutions show a Gaussian shape of the carrier packet. For a dispersive transport regime, the mean velocity of the carrier sheet decreases in time and its dispersion grows faster than the square time root.

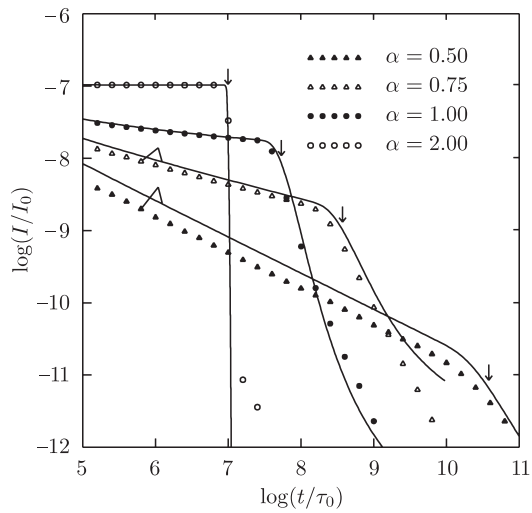

Figure 1: Current transients, calculated for the exponential trap distribution, $N_t(\varepsilon) \propto \exp(-\varepsilon/kT_c)$, and several values of the parameter $\alpha = T/T_c$. Solid lines and points denote analytical and numerical results, respectively, arrows indicate the effective carrier transit-times

The final formulas which determine the time dependence of current intensity, $I(t)$, and the effective carrier transit-time, τ_e, are:

$$I(t) = I_0 \Theta(t), \quad t < \tau_e,$$

$$\int_0^{\tau_e} \Theta(t')\,\mathrm{d}t' = \tau_0,$$

with

$$\Theta(t) \approx C_t \int_{\varepsilon_t^0}^{\varepsilon_0(t)} N_t(\varepsilon)\, \tau_r(\varepsilon)\, \mathrm{d}\varepsilon, \quad \Theta(t) \ll 1.$$

Here, I_0 is the initial current intensity, τ_0 – the free carrier time-of-flight, C_t – the carrier capture coefficient, ε – the trap depth, ε_t^0 – the minimum trap depth, $\varepsilon_0(t) = kT \ln(1.8\nu_0 t)$ – the demarcation level, $N_t(\varepsilon)$ – the trap density per energy unit, $\tau_r(\varepsilon) = \nu_0^{-1} \exp(\varepsilon/kT)$ – the mean carrier trapping time (with k – the Boltzmann constant, T – the temperature, ν_0 – the frequency factor).

The obtained formulas generalize those derived in [1, 2]. Their accuracy is verified by Monte Carlo calculations for exponential and Gaussian trap distributions. A satisfactory agreement is obtained up to the effective carrier transit-time, provided that the trap density falls-off sufficiently fast in the energy gap (Figure 1). The methods of determining the energetic trap profiles in disordered solids from TOF measurements are considered.

References

[1] Tiedje T and Rose A 1980 *Solid State Commun.* **37** (1) 49
[2] Orenstein J and Kastner M A 1981 *Phys. Rev. Lett.* **46** (21) 1421

Negative Poisson's Ratio of Two-dimensional Hard Cyclic Tetramers

K. V. Tretiakov[a], K. W. Wojciechowski[a]

Institute of Molecular Physics, Polish Academy of Sciences,
M. Smoluchowskiego 17, 60-179 Poznan, Poland
[a]*kvt@ifmpan.poznan.pl,* [b]*kww@ifmpan.poznan.pl*

Elastic properties of a two-dimensional model system of "tetramer" particles interacting through a site-site pure hard potential interaction are studied. The tetramers are composed of four identical hard "atoms" positioned at the corners of a square with the linear dimension equal to the disk diameter [1]. The elastic properties of a chriral tetramer crystal with square symmetry are investigated by constant pressure Monte Carlo simulations with a variable shape of the periodic box. It is found that the Poisson's ratio of this simple tetramer system is negative and equal to $-0.36\,(1)$. In addition to extending the known classes of auxetic systems, the tetramer system described here, when stretched along the crystalline axes, has significantly stronger auxetic properties [2, 3] than similar planar systems composed of either trimer [4] or hexamer particles [5, 6].

References

[1] K. W. Wojciechowski and A. C. Branka 1989 "Rotational Phase Transition and Melting in a Two-dimensional Hard-cyclic-tetramer System" *Phys. Rev. Lett.* **50** 846–7225
[2] R. S. Lakes 1987 Negative Poisson's Ratio Materials, *Science* **238** 551
[3] Ch. W. Smith and K. W. Wojciechowski 2008 Preface *Physica Status Solidi B* **245** 486–849 (see also other papers and references therein)
[4] K. W. Wojciechowski 2005 "Monte Carlo Simulations of Model Particles Forming phases of Negative Poisson Ratio" [in:] *Properties and Applications of Nanocrystalline Alloys from Amorphous Precursors* Eds. Bogdan Idzikowski, Peter Svec, and Marcel Miglierini, Kluwer Academic Publishers, Dordrecht 241–252
[5] K. W. Wojciechowski and A. C. Branka 1989 "Negative Poisson Ratio in a Two-dimensional 'Isotropic' Solid" *Phys. Rev. A* **40** 7222–7225
[6] K. V. Tretiakov and K. W. Wojciechowski 2005 "Monte Carlo Simulations of Two-dimensional Hard Body Systems with Extreme Values of the Poisson's Ratio" *Physica Status Solidi B* **242** 730–741

Obtaining and Dielectric Properties of Ferroelectric Materials on Chalcogenide Glasses Basis

V. M. Rubish[1], O. G. Guranich[1], V. V. Rubish[1], B. Tsizh[2a], P. P. Guranich[3]

[1] *Uzhgorod Scientific-Technological Center of the Institute for Information Recording NASU 4 Zamkovi Skhody Str., 88000 Uzhgorod, Ukraine*

[2] *Kazimierz Wielki University in Bydgoszcz Chodkiewicza 30, 85-064 Bydgoszcz, Poland*
[a] *tsizhb@ukw.edu.pl*

[3] *Uzhgorod National University N46 Pidhirna Str., 88000 Uzhgorod, Ukraine*

Chalcogenide glass materials on the base of SbSI arouse considerable scientific and practical interest, for the crystalline antimony sulphoiodide is a well-known quasi-one-dimensional ferroelectric semiconductor.

In this report the results of investigations of the structure and dielectric properties (ε and $\tan\delta$) of glassy SbSI and $(SbSI)_{100-x}(As_2S_3)_x$ glasses with a small content of As_2S_3 ($x = 3$, 5, 10) and their change during heat treatment are presented. Glassy alloys were prepared with the melt quenched technique in evacuated (≈ 0.01 Pa) quarts ampoules. The melts were hardened in cold (273 K) water. The Raman spectra of glassy, crystallized and crystalline materials were investigated at $\lambda = 6328$ Å with a resolution of 1–3 cm^{-1}. The investigations of diffractograms were carried out on a DRON-3 X-ray apparatus ($\lambda = 1.5418$ Å).

It has been shown that anomalies in the temperature dependences of ε and $\tan\delta$ are connected with a transition of glasses into a polar state during the structural relaxation and its subsequent crystallization. The polar state which arises during the softening is accompanied by breaking and switching of the chemical bonds Sb–S, As–S(Se), As–I, Sb–I in binary structural groupings which form a glass matrix and by forming ternary chain structural $(SbSI)_{100-x}(As_2S_3)_x$ groups with high polarizability.

The investigations of Raman spectra and diffractograms have shown that the phase structure arising in the $(SbSI)_{100-x}(As_2S_3)_x$ ($x = 0$, 3, 5, 10) glass matrix during its crystallization corresponds to the crystalline antimony sulphoiodide structure. The Raman spectra of crystallized glasses have sharp bands at 108–110, 138–140 and 318–320 cm^{-1}. The maxima of these bands for polycrystalline SbSI are at 108, 138 and 318 cm^{-1}. The position of lines on the diffractograms of crystallized glasses agrees well enough with the position of intensive lines on the polycrystalline SbSI diffractogram. The intensity of lines on the diffractograms and the Raman spectra bands of crystallized glasses is increasing while their half-widths are getting smaller

when the annealing time is increasing and the temperature is growing. It testifies to the growing size of SbSI crystals in a glass matrix and their structural ordering. The structural relaxation is followed by a change of the absorption edge's slope and position. Crystallization of glasses is accompanied by a sharp increase in the dielectric parameters.

The effect of heat and time related treatment modes on the structure and dielectrics properties of crystallized glasses of the SbSI$-As_2S_3$ system have been determined. It has been shown that ferroelectrics nanoceramics with grain sizes of 10–20 nm is obtained at the annealing temperatures near those noted at the beginning of crystallization and at shorter annealing times. The growing annealing temperature and time lead to the growing size of crystalline inclusions and dielectric permittivity. The value ε of crystallized glasses reaches 50–70 units and its temperature coefficient $\alpha = (1/\varepsilon)(d\varepsilon/dT)$ in 293–423 K interval is $(3–8) \cdot 10^{-4}$ K^{-1} in absolute figures. Moreover, depending on the heat treatment composition and mode, glass ceramics with both positive and negative α_ε can be obtained. The maxima confirming the presence of a smeared ferroelectric phase transition therein, the parameters of which depend on the chemical composition and heat treatment conditions have been found in the dependences of $\varepsilon(T)$ and $\tan\delta(T)$ in the region of 250–290 K.

Magnetic and EPR Study of $Zn_3Fe_4V_6O_{24}$

J. Typek[1], G. Żołnierkiewicz[1], N. Guskos[1,2], R. Szymczak[3], A. Błońska-Tabero[4]

[1] *Institute of Physics, Technical University of Szczecin Al. Piastów 17, 70-310 Szczecin, Poland*

[2] *Solid State Section, Department of Physics, University of Athens Panepistimiopolis, 15 784 Zografos, Athens, Greece*

[3] *Institute of Physics, Polish Academy of Sciences Al. Lotników 32/46, 02-668 Warsaw, Poland*

[4] *Department of Inorganic and Analytical Chemistry Szczecin University of Technology Al. Piastow 42, 70-065 Szczecin, Poland*

Compounds in the multicompent vanadates system $M-\mathrm{Fe}-\mathrm{V}-\mathrm{O}$ ($M=$ Zn, Mg, Ni, Cu) attract much interest because of their intricate magnetic properties due to a disorder in metal positions and oxygen deficiency [1–5]. They crystallize in a triclinic system and have a complicated structure with two subsystems of metal ions. Polycrystalline samples of $Zn_3Fe_4V_6O_{24}$ prepared by the solid-state reaction technique have been studied by magnetic and electron paramagnetic resonance (EPR) methods in the 4-300 K temperature range. Static magnetic susceptibility measurements have shown the presence of a strong antiferromagnetic interaction (Curie-Weiss temperature $\Theta=-101$ K) in the Fe^{3+} sublattice. The effective magnetic moment of a unit cell (about 11 μ_B for four iron ions) indicates significant presence of Fe^{3+} in a low-spin state. At low temperature (below 6 K) clear indications of the spin-glass state have been registered in the temperature dependence of susceptibility. EPR spectra have consisted of two components: a very broad line registered in high temperature (above 15 K) and a narrow line below 15 K. The EPR amplitude of the broad component has decreased with the temperature decrease while the opposite trend has been observed for the narrow line. On decreasing the temperature from RT, the broad line shifts slightly towards a higher magnetic field and its linewidth increases. Large changes of the g-factor and linewidth of this line are observed below 75 K. The temperature dependence of the EPR integrated intensity of the broad line has shown a marked anomaly at about 220 K in contrast to the static magnetic susceptibility where no such irregularity has been observed. The studied magnetic properties of $Zn_3Fe_4V_6O_{24}$ will be discussed in terms of inherent magnetic inhomogeneity of this compound with competing magnetic interactions and spin clusters.

References

[1] N. Guskos, J. Typek, G. Zolnierkiewicz, A. Błońska-Tabero, M. Kurzawa, M. Bosacka 2005 *Materials Science (Poland)* **23** 923

[2] N. Guskos, A. Beskrovnyj, J. Typek, N.Yu. Ryabova, A. Błońska-Tabero, M. Kurzawa, M. Maryniak 2005 *J. Alloys Compd.* **39** 20
[3] G. Żołnierkiewicz, N. Guskos, J. Typek, A. Błońska-Tabero 2006 *Acta Phys. Pol.* **A 109** 675
[4] G. Żołnierkiewicz, N. Guskos, J. Typek, A. Błońska-Tabero 2006 *J. Non-Cryst. Solids* **352** 4362
[5] G. Żołnierkiewicz, N. Guskos, J. Typek, E. A. Anagnostakis, A. Błońska-Tabero, M. Bosacka (to be printed in *J. Alloys Compd.*)

Growth Kinetics of HgTe and HgCdTe Thin Films Obtained by PLD

I. S. Virt[1,2], T. P. Shkumbatiuk[1]

[1] *Drogobych State Pedagogical University*
24 I. Franko Str., Drohobych, 82100, Ukraine

[2] *University of Rzeszow, Institute of Physics*
Rejtana 16A, Rzeszow, 35-959, Poland

Pulsed laser deposition (PLD) is successfully used to grow many different materials. We present the results of experimental and theoretical data on the electrophysical and photoelectrical properties of $Hg_{1-x}Cd_xTe$ ($x \approx 0.20$) thin films. The films were prepared by the PLD technique (Nd:YAG laser: $\lambda \approx 1064$ nm; $\Delta\tau \approx 10$ ns; $f \approx 0.5$ Hz) on glass and Al_2O_3substrates at different temperatures and pulse laser regimes.

The growth kinetics of films is investigated in the PLD process. A change of the resistive resistance of the grown $Hg_{1-x}Cd_xTe$ layer with the preliminary deposited Ag-contacts is measured by a METEX ohmmeter connected to a PC. According to the number of laser impulses, conductivity is derived from the film resistive resistance and its time dependence is found at $T_{sub} = 30°C$ and $T_{sub} = 200°C$. We have observed rather high specific conductivity of films with small thicknesses (less than 10 nm), and its significant decrease (by 100 times) with a minimum value at thicknesses of about 100 nm. At larger thicknesses slow growth of specific conductivity is observed. It indicates a prevailing process of metal atoms condensation (an increase in the adhesion coefficient), more likely of Cd atoms at the initial stages of film growth. The laser beam overlapping during growth has made it possible to find a real temperature of the film growth. The real temperature of the grown layers is estimated due to a concentration of proper charge carriers in a nondegenerate semiconductor model.

This temperature is 250°C higher than that of the substrate and results from the local heating of the film material by laser plasma. Radiation defects generated with laser plasma also influence the electroconductivity of the newly grown films. The process of annealing of such radiation defects takes a few hours at room temperature.

Electrical Properties of Pentacene Films Obtained by PLD

G. Wisz[1a], I. S. Virt[1], M. Kuźma[1], P. Sagan[1],
T. Ya. Gorbach[2], P. S. Smertenko[2]

[1] *Institute of Physics, Rzeszow University,*
Rejtana 16A, 35-309 Rzeszow, Poland
[a] *gwisz@univ.rzeszow.pl*

[2] *Institute of Semiconductor Physics*
National Academy of Sciences of Ukraine,
Prospect Nauki 45, Kiev 28, 03028 Ukraine

ITO covered glass was used as substrates for laser epitaxy of pentacene ($C_{22}H_{14}$) films. Different orientation of the substrate with respect to the pentacene plasma plume was applied. Thin pentacene films were deposited using a $YAG{:}Nd^{3+}$ laser with second harmonic ($\lambda = 532nm$). The electrical properties of the structures were analyzed on the basis of the current-voltage characteristics. The current- voltage characteristics are interpreted in relation to the molecular structure properties of the pentacene films and the pentacene/contact, pentacene/substrate interface. The carrier transport mechanisms for different interfaces and structures are presented.

Organic films fabrication offers a possibility of manufacturing low weight, mechanically flexible and low cost electronic devices. The material that is the subject of great interest is pentacene which is characterized by the largest carrier mobility $\left(1,5\ cm^2/Vs\right)$ [1, 2]. In the 2005 report, the authors tell about a new field mobility record in a Samsung transistor: 7 cm^2/Vs [3]. The molecular structure of pentacene layers affects strongly its functional properties, therefore, understanding the processes of growth which permit finding a way to control and optimize the structure, is the basis of the technology development. Structural properties strongly depend on the substrate type, on its surface properties, growth conditions and production method. We propose the pulse laser deposition (PLD) method as an alternative method of obtaining pentacene layers on a cold substrate [4–8]. This method provides a high degree of flexibility in the use of materials, their geometrical arrangements, and adjustment of growth parameters. The various growth conditions result in different layer growth mechanisms, different organic/inorganic interface properties and a different energy level alignment. In respect of organic material growth on inorganic substrates we have an additional possibility of forming different types of interfaces in respect of arranging molecules in the first monolayer [9].

In the case of a pentacene layer, different types of pentacene/substrate interfaces result not only in a different molecular structure, but lead to modifying the energy-band structure and the carrier transport mechanism, as well. In this work the influence of the ITO/glass substrate surface orientation with respect to the plasma

plume propagation direction on the pentacene films properties has been investigated by an analysis of the current voltage characteristics.

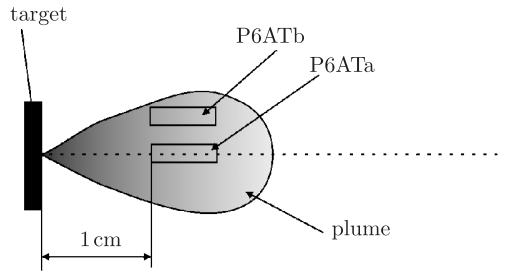

Figure 1: Sample orientation with respect to the plasma plume

Pentacene films were obtained by the PLD method using a $YAG{:}Nd^{3+}$ laser with the 532 nm (II harmonics) wavelength, 40 ns pulse time and fluence of the range of 930 mJ/cm^2. The layers were deposited in a vacuum chamber with a turbomolecular pump PFEIFFER TMH/U 071 which provides a 10^{-6} hPa vacuum. The Au top contact was prepared by thermal evaporation. The I-V characteristics were measured for two samples (P6ATa, P6ATb) obtained in one technological cycle for the geometrical arrangement presented in Fig. 1. The sample structure details, contact configuration and measurements setup were presented in Fig. 2. The measurements were performed for two-electrode configurations, sandwich and slit-like geometry (Fig. 2b, 2c, respectively).

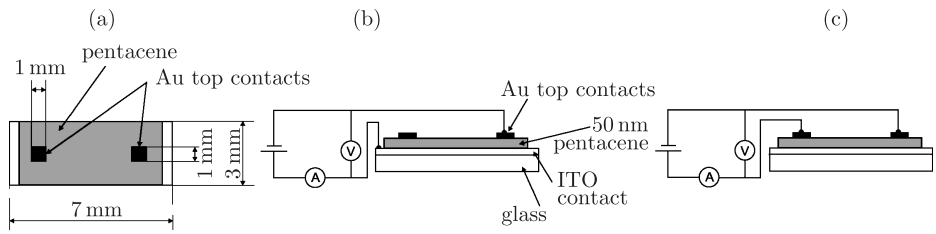

Figure 2: Sample structure and contact configuration: (a) top view; (b) sandwich configuration; (c) slit-like configuration

The properties of organic layers depend strongly on the deposition conditions, laser beam parameters and substrate properties. Figure 3 presents SEM images for samples P6ATa and P6ATb obtained in one technological cycle. The surface morphology for these samples has a few features: different thick, randomly distributed particles with a different shape and a different growth mode. A lower growth rate resulting from a lower plume flux density for P6ATb leads to a decrease in the number of inhomogeneities and the formation of a fractal-like surface structure which is characteristic for organic films.

The difference in electrical properties is recognized to be dependent on the substrate orientation with respect to the pentacene plasma plume. A fine structure of I-V

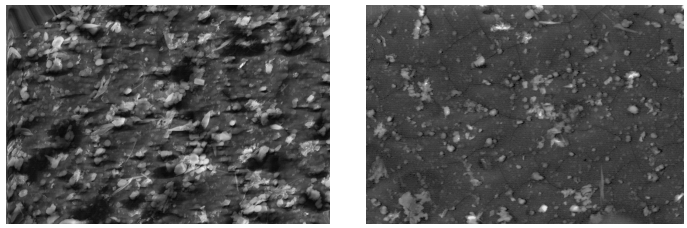

Figure 3: SEM images of P6ATa (left) and P6ATb (right) samples

characteristics determined by a differential approach includes the following peculiarities of the behavior of curves with the differential slope= 1; 1.25; 2; 0.5; −1; −2.

References

[1] W. J. E.Northrup 2002 *Phys. Rev.* **B 66** 121404
[2] A. R. Volkel, R. A. Street and D. Knipp 2002 *Phys. Rev.* **B 66** 195336
[3] M. Hong, B. S.Kim,Y. U. Lee 2005 *SID International Symposium*
[4] Y. Kawamura, K. Z. Toyoda, S. Namba 1982 *Appl., Phys. Lett.* **40** 374
[5] T. Ya. Gorbach, M. Kuzma, E. Sheregii, P. S. Smertenko, S. V. Svechnikov, G. Wisz 1996 *Appl. Surface Science* **96–98** 881–886
[6] J. M. Maud, A. J. Salih, J. M. Marshall 1999 *Synthetic Metals* **102** 986–989
[7] D. B. Chrisey, A. Pique, R. A. McGill, J. S. Horwitz, B. R. Ringeisen, D. M. Bubb, P. K. Wu 2003 *Chem. Rev.* **103** 553–576
[8] G. B. Blanchet, C. R. Fincher and I. Malajovich 2003 *J. Appl. Phys.* **94** 6181–6184
[9] F. Schreiber 2004 *Phys. Stat. Sol. (a)* **6** 1037–1054

Structural Changes in Pt Nano-crystalline Operating as Cathode Electrocatalyst in PEM FC: *in situ* XAFS

A. Witkowska[1,2], E. Principi[2], A. Di Cicco[2,3], S. Dsoke[4], R. Marassi[4]

[1] *Department of Solid State Physics, Gdansk University of Technology, Poland*

[2] *Department of Physics CNISM, CNR-INFM CRS SOFT, University of Camerino, Italy*

[3] *IMPMC-CNRS UMR 7590, University Pierre et Marie Curie, Paris, France*

[4] *Department of Chemistry, University of Camerino, Italy*

We present X-ray absorption fine structure (XAFS) investigation of the 20%Pt supported on Vulcan XC-72 operating as a cathode catalyst in a polymer electrolyte membrane fuel cell (PEM FC). XAFS spectroscopy has been performed *in situ* using a specially optimized for that measurement fuel cell [1]. High quality low-noise spectra have been obtained using transmission mode in a whole XAFS range, giving possibility to perform MS EXAFS data-analysis for Pt nano-crystalline system being under operation condition [2].

The results show the changes in the catalyst local structure induced by FC potential and working temperature. At a stable temperature condition and varying a potential value only in the cathode activation region slight changes in the Pt electronic structure are observed, while local geometric structure remains potential-independent. An increase in a structural disorder provoked by higher working FC temperature doesn't affect catalyst performance in the kinetically controlled region.

References

[1] E. Principi, A. Di Cicco, A.Witkowska, R. Marassi 2007 "Performance of a fuel cell optimized for *in situ* X-ray absorption experiments", *J. Synchrotron Rad.* **14**, 276–281

[2] A. Witkowska, A. Di Cicco, E. Principi 2007 "Local ordering of nano-structured Pt probed by multiple-scattering XAFS", *Phys. Rev.* **B 76**, 104110

Concentration Fluctuations in Liquid In-Sb and In-Bi Alloys

A. Yakymovych[a], V. Sklyarchuk, Yu. Plevachuk, S. Mudry

Faculty of Physics, Ivan Franko L'viv National University,
8 Kyrylo and Mephodii str., 79005 L'viv, Ukraine
[a] *yakymovych@online.ua*

Liquid alloys In-Sb and In-Bi systems are interesting from a technological point of a crystal grown from a liquid phase. InSb belong to covalent semiconductors and InBi and In_2Bi chemical compounds occur in solid In-Bi systems. Due to strong interactions between different sorts of atoms, influence on the structure of the liquid state in the precrystallization temperature region should be exerted. On the other hand, previous studies have indicated anomalous behavior in terms of the physical properties in liquid In-Sb and In-Bi systems. To better understand the mechanism of the crystal formation process an experimental investigation of viscosity has been conducted.

Following our previous paper, the viscosity of liquid In-Bi alloys shows anomalies in terms of the temperature dependence in the concentration region close to the In_2Bi chemical compounds. Some anomalous behavior of the viscosity in a liquid In-Sb has been in the study. An abnormal increase in the viscosity is connected with changes of the melt structure during cooling towards the melting point.

The viscosity data has been used for estimating the concentration fluctuations in molten alloys. A few theoretical models are applied by different research groups to connect the anomaly changes of viscosity with the fluctuation parameters. In this work the mode-coupling theory, connecting the viscosity with the correlation length has been used. The results obtained have confirmed the acceptability of this model for explaining some viscosity anomalies.

Temperature Dependence of EPR Spectra of $Cd_{2.34}Fe_{4.68}V_{5.35}O_{24}$

N. Guskos[1,2], G. Żołnierkiewicz[1], J. Typek[1], A. Błońska-Tabero[3]

[1] *Institute of Physics, Szczecin University of Technology*
Al. Piastów 17, 70-310 Szczecin, Poland

[2] *Solid State Physics, Department of Physics, University of Athens*
15 784 Zografos, Athens, Greece

[3] *Department of Inorganic and Analytical Chemistry*
Szczecin University of Technology
Al. Piastów 42, 71-065 Szczecin, Poland

A new multicomponent vanadate $Cd_{2.34}Fe_{4.68}V_{5.85}O_{24}$ has been synthesized and investigated by the Electron Paramagnetic Resonance (EPR) technique. The compound $Cd_{2.34}Fe_{4.68}V_{5.85}O_{24}$ is isostructural with previously studied $Mg_3Fe_4(VO_4)_6$ [1]. According to the nominal stoichiometry of $Cd_4Fe_8V_{10}O_{41}$ all ions, except for iron, are nonmagnetic. The registered EPR spectrum in the 4–300 K temperature range is dominated by the presence of a very wide and almost symmetrical resonance line which disappears below 20 K. The resonance line is centered at $g_{\text{eff}} = 2.017(1)$ with linewidth $\Delta B_{\text{pp}} = 77.3$ mT at room temperature. Its amplitude decreases with a decrease in temperature, and below 40 K, the linewidth strongly depends on temperature. Below 60 K, the resonance line shifts essentially with the decreasing temperature towards lower magnetic fields. It is suggested that a strong magnetic interaction leads to a magnetically ordered state. Replacement of non-magnetic cations by divalent cadmium ions seems to intensify the magnetic ordering processes in a low temperature region [2].

This scientific work is financed from the Polish budget resources allocated to science in 2005-2008 as Research Project (1311/TO9/2005/29).

References

[1] A Błońska-Tabero, *J. Therm. Anal. Cal.* (in press)
[2] N. Guskos, V. Likodimos, S. Glenis, G. Żołnierkiewicz, J. Typek, R. Szymczak, and A. Błońska-Tabero *J. Appl. Phys.* **101** (2007) 103922

EPR and FMR Study of $ZnO-Fe_2O_3-ZnFe_2O_4$ System

N. Guskos[1,2], G. Żołnierkiewicz[2], J. Typek[2],
D. Sibera[3], U. Narkiewicz[3]

[1] *Solid State Section, Department of Physics, University of Athens
Panepistimiopolis, 15 784, Greece*

[2] *Institute of Physics, Szczecin University of Technology
Al. Piastów 17, 70-310 Szczecin, Poland*

[3] *Institute of Chemical and Environmental Engineering
Szczecin University of Technology
Al. Piastów 17, 70-310 Szczecin, Poland*

Fine particles composed of $n(Fe_2O_3)/(1-n)ZnO$ ($n = 0.5$ to 0.95) powders are prepared by the wet chemistry method. According to the XRD analysis samples with $n = 0.95, 0.90, 0.80$ contain γ-Fe_2O_3 and $ZnFe_2O_4$ phases, while other samples contain only $ZnFe_2O_4$ and ZnO phases. The mean crystalline size of $ZnFe_2O_4$varies from 8 nm to 30 nm. The EPR/FMR investigations are carried out at room temperature. An almost symmetrical and very intense magnetic resonance line is recorded for all samples. For samples with $n \leq 0.60$ the resonance line is centred at $g = 2.005(2)$ with the integrated intensity increasing with the ferrite content, reaching a sample maximum of $n = 0.70$. For $n > 0.70$ the g parameter and the integrated intensity strongly depend on the ratio of iron in the form of γ-Fe_2O_3 to that in the form of $ZnFe_2O_4$, decreasing with an increased γ-Fe_2O_3 / $ZnFe_2O_4$ ratio. Below $n = 0.70$ the magnetic resonance study shows an EPR line originating from isolated iron(III) ions in zinc ferrite, and from magnetic nanoparticles γ-Fe_2O_3 (FMR lines) for higher concentrations.

INDEX OF AUTHORS